水和反応モデルに基づく膨張コンクリートの力学的性質及び中性化深さの予測に関する研究

Predicting Mechanical Properties and Carbonation Depth of Expansive Concrete Based on Hydration Reaction Model

水和反応モデルに基づく膨張コンクリートの力学的性質及び中性化深さの予測に関する研究

by

Nguyen Duc Van

A Dissertation Submitted in Partial Fulfillment
of the Requirements for the Degree of
Doctor of Philosophy

Division of Engineering

MURORAN INSTITUTE OF TECHNOLOGY

March 2021

Abstract

Although expansive additives have been widely used to efficiently reduce shrinkage cracking in concrete, little research has been undertaken to model the hydration reaction of cement and expansive additive blends and to predict the properties and durability of expansive concrete.

In this study, a numerical model to simulate the hydration reaction of cement paste containing expansive additive at an early age is proposed and then the compressive strength, carbonation depth, and expansion strain of expansive concrete are predicted based on the hydration reaction model. Additionally, the influence of restrained conditions on the mechanical properties and durability such as frost resistance and carbonation resistance are also investigated in this research. Using the proposed model, this study predicted the hydration degree, rate of heat evolution, gel/space ratio, amount of calcium silicate hydroxide (CSH), calcium hydroxide (CH), ettringite of hardening cement-expansive additive paste, and porosity of expansive concrete. For the experimental investigation, the rate of heat evolution test, under-water weighing test, length change ratio test, expansion strain test, compressive strength test, mercury intrusion porosimetry test, freezing-thawing test and accelerated carbonation test were performed to verify the proposed model and predicting equation. From the relationship between the gel/space ratio and compressive strength, an equation was deduced for the prediction of the development of compressive strength of expansive concrete. Considering the diffusion of CO_2 in a gaseous phase into the concrete pore and the reaction of CO_2 with CH and CSH, a mathematic model was proposed to predict the carbonation depth of expansive concrete. A hypothesis was described to predict the expansion strain through a model of the volumetric change of expansive concrete calculated by combining the formation of ettringite, influence coefficient of shrinkage, and restraint degree coefficient.

For verification of the model and predicting equation, the results indicated good agreement of the calculated data with the measured data. Furthermore, this work also found that the model parameters (in the hydration reaction model) can be represented as a function of the mineral composition of the cement. A coefficient was deduced to find the satisfactory value for predicted results (in predicting compressive strength). A restraint degree coefficient was found to build an equation for predicting the expansion strain of expansive concrete under restrained conditions. The results demonstrate that the proposed model and equation are effective and useful in predicting the hydration, mechanical properties, and carbonation depth of expansive concrete.

Table of Contents

List of Tables

List of Figures

List of Chemical Notations

Compounds	Notation
Calcium dioxide (CaO)	C
Silicon oxide (Si_2O)	S
Alumina oxide (Al_2O_3)	A
Iron oxide (Fe_2O_3)	F
Sulfur oxide (SO_3)	$\bar{S}$
Water (H_2O)	H
Carbon dioxide (CO_2)	$\bar{C}$
Tricalcium silicate ($3CaO.SiO_2$)	C_3S
Dicalcium silicate ($2CaO.SiO_2$)	C_2S
Tricalcium aluminate ($3CaO.Al_2O_3$)	C_3A
Tetracalcium aluminate ($4CaO.Al_2O_3\,Fe_2O_3$)	C_4AF
Calcium sulfoaluminate (Ye'elimite) ($4CaO.Al_2O_3.3SO_3$)	$C_4A_3\bar{S}$
Anhydrite ($CaSO_4$)	$C\bar{S}$
Gypsum ($CaSO_4.2H_2O$)	$C\bar{S}H_2$
Calcium silicate hydrate ($3CaO.SiO_2.H_2O$)	CSH
Calcium hydroxide $Ca(OH)_2$	CH
Ettringite ($6CaO.Al_2O_3.3SO_3.32H_2O$)	$C_6A\bar{S}_3H_{32}$
Monosulfate ($4CaO.Al_2O_3.SO_3.10H_2O$)	$C_4A\bar{S}H_{10}$

CHAPTER 1

INTRODUCTION

CHAPTER 1 INTRODUCTION

1.1 Background

Concrete is one of the construction materials and is the single most widely used throughout the work due to its unique advantages such as high durability, high resistance to nature, and low cost. However, there are many factors that affect the quality of concrete, where drying shrinkage is one of the unfavorable properties of concrete. Under the restrained conditions, the drying shrinkage causes an increase in tensile stress leading to cracking, which dramatically affects the durability, architectural aesthetics, and service lifetime of the building. Using the admixtures as one solution to prevent the crack caused by the drying shrinkage such as expansive additive, shrinkage reducing agent, and limestone powder.

Nowadays, expansive concrete is widely used as an efficient way to either reduce and eliminate shrinkage cracking. Expansive concrete is made by mixing the expansive additive with cement, water, aggregate (coarse and fine), and other admixtures, which increases the volume of concrete. The action of expanding concrete is due to the production of ettringite or calcium hydroxide from the hydration reaction of expansive additive with water [1.1]. In order to investigate the effect of expansive additive on the quality of concrete, most previous studies have been carried out based on the experimental investigations. Thus, a question is posed here that is possible through a certain factor to build up a model to predict the change as well as the development of expansive concrete properties. From there, it is possible to evaluate the quality of the concrete.

There are lots of researches [1.2-1.5] reported that hydration reaction of ordinary Portland cement (OPC) (or cement-based materials) is very important to be estimated since there is a great relation of hydration with the microstructure of hardening cement-based materials, the development of strength, the carbonation, the volumetric change and the expansion strain of concrete as well. It also means these properties of concrete could be predicted based on the hydration reaction of cement (or cement-based materials). Therefore, in this study, a numerical model was proposed for simulation of the hydration reaction of cement paste containing the expansive additive and then predicting the mechanical properties and carbonation depth of expansive concrete based on its relationship with the hydration reaction of cement-expansive additive (cement-EX) blends.

1.2 Expansive additive

1.2.1 Type of expansive additive

According to JIS A 6202 [1.7], an expansive additive (EX) is an admixture mixed with OPC and water, producing the ettringite and calcium hydroxide (CH) from hydration reaction, which makes the concrete or mortar expand. In Japan, the expansive additive has been made with the use of expansive cement, which is manufactured by mixing expansive admixtures with concrete [1.8]. Therefore, expansive concretes of the Japanese type are widely used not only in shrinkage-compensating concrete but also in chemical prestressed concrete which positively utilizes the expansibility of them. The expansive additive is divided into the ettringite type and limestone type. Recently, the expansive additive combining ettringite type and limestone type has been used.

Unlike the expansive concrete that developed in Japan. According to ACI standards [1.9], the expansive cement is divided into four types as given in Table 1.1.

Table 1.1 Type of expansive additive according to ACI standards [1.9]

Type	Compounds	Hydration products
K Type	Calcium sulfoaluminate ($4CaO.3Al_2O_3.SO_3$)	Ettringite
	Gypsum ($CaSO_4$)	
	Lime (CaO)	
S Type	Tricalcium aluminate ($3CaO.\ Al_2O_3$)	Ettringite
	Gypsum ($CaSO_4$)	
M Type	Aluminous cement $CaO.Al_2O_3$	Ettringite
	Gypsum ($CaSO_4$)	
O Type	Lime (CaO)	Calcium hydroxide

1.2.2 Hydration of expansive additive

The main hydration products of expansive additive are the ettringite and CH [1.10]. The chemical reactions of the expansive additive are described as shown in Eqs. (1.1a) and (1.1b).

$$C + H \rightarrow CH \qquad \text{Eq. (1.1a)}$$

$$6C + C_4A_3\bar{S} + 8C\bar{S} + 96H \rightarrow C_6A\overline{S_3}H_{32} \qquad \text{Eq. (1.1b)}$$

However, by the XRD quantitative analysis, Morioka et al. [1.11, 1.12] reported that the hydration products of EX are not only Ettringite and CH, but also calcium sulfate ($CaSO_4.2H_2O$) and monosulphate (AFm) were observed. The results indicated that in the early stage of the reaction, the free-lime reacted faster than the hydration of Hauyne anhydrite. The results were also found that 2-2.5 molar of ettringite and gel were produced by 1 molar of Hauyne.

1.2.3 Mechanism of reduction in shrinkage crack using expansive additive

Figure 1.1 shows the mechanism of reduction in shrinkage crack using the expansive additive. In the case of Portland cement concrete, tensile stress is generated by restraining shrinkage and cracks develop if tensile stress exceeds tensile strength.

For expansive concrete, concrete mixed with an expansive additive that expands on the early age by the formation of ettringite and calcium hydroxide. The compressive force is introduced into the concrete by the restrained condition during expansion. Subsequent tensile stress caused by the drying shrinkage will reduce these stresses. A residual compression will remain in the concrete, minimizing the risk of shrinkage cracking.

M. Morioka [1.13] reported that to provide expansion effectively, the expansive additive should react in the effective expansion periods which are periods II and III. The expansion is not useful with period I in the fresh state, while expansive strain becomes small in period IV once sufficient strength has developed. Figure 1.2 shows the relationship between mortar strength and expansion of expansive additive.

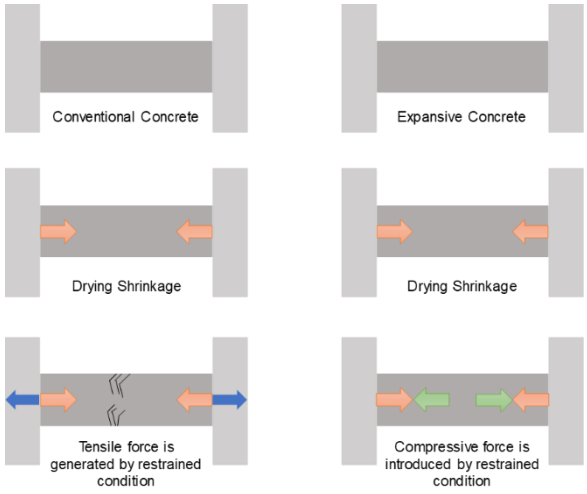

Figure 1.1 Mechanism of reduction in shrinkage cracking using the EX.

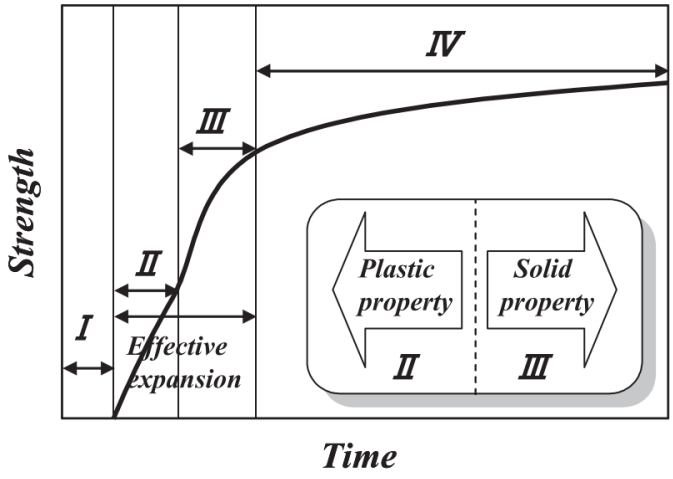

Figure 1.2 Schematic of relationship between mortar strength and expansion of the EX [1.13]

1.3 Previous research

1.3.1 Influence of restrained condition on properties of expansive concrete

In concrete structure, the restrained condition divided into two types (see Figure 1.3): Internal restraint due to either reinforcement or aggregate; External restraint by some adjacent structural elements such as beam, column, etc.

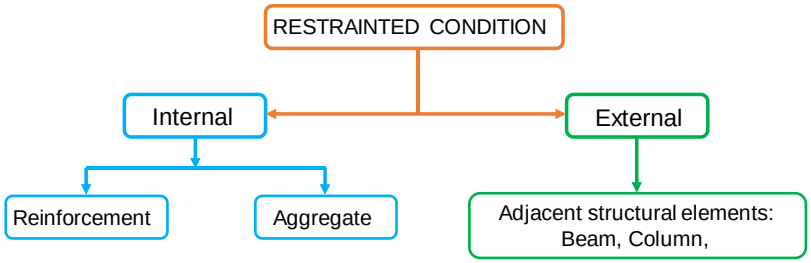

Figure 1.3 Type of restrained condition

In order to evaluate the effect of restrained conditions on the properties of expansive concrete, Nguyen et al. [1.14] reported that the compressive strength of expansive concrete was enhanced by the restrained conditions. However, the authors have mostly focused on the horizontal restrained condition (it called uniaxial), as shown in Figure 1.4. In an actuarial concrete structure, the concrete could be restrained by three directions (triaxial). Therefore, it is interesting to consider the effect of the restrained condition in three directions.

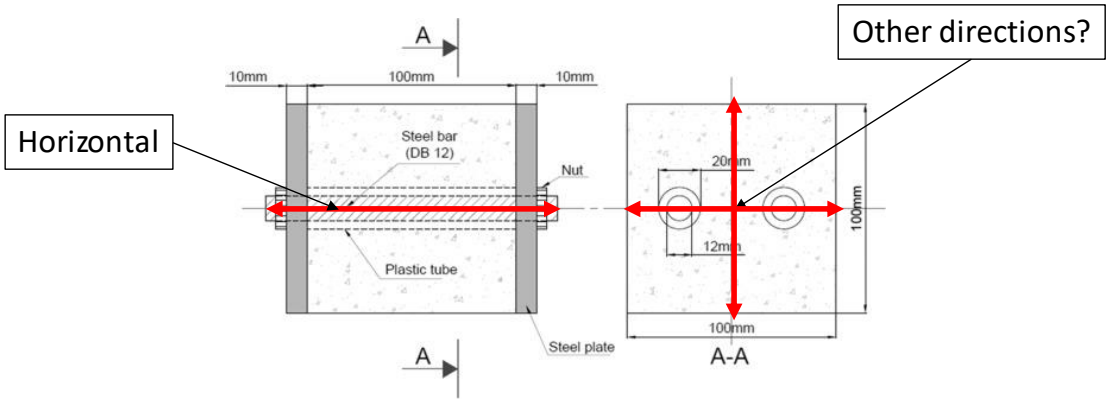

Figure 1.4 Schematic of restrained condition [1.14]

Tsuji et al. [1.15] have studied the effect of the triaxial restrained condition on the properties of expansive additive. The results showed that the compressive strength of expansive concrete higher than that of cement concrete around 30%-50% under triaxial restrained conditions. However, the dosage of EX was a high level about 80 and 90 kg of 1 m^3 of concrete. Meanwhile, 20 kg of 1 m^3 of concrete is as a standard amount of expansive additive [1.16].

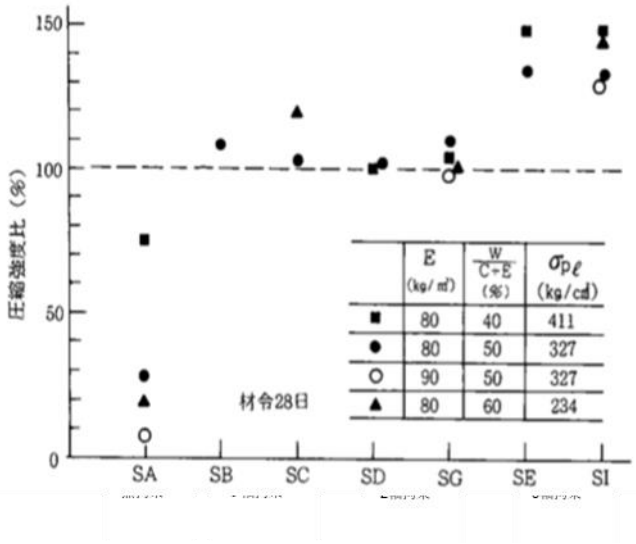

Figure 1.5 Compressive strength ratio of expansive concrete by restraining [1.15]

Also, consider the effect of the confinement, Harada [1.17] found that the frost resistance of concrete could be enhanced by the confinement. It concluded that under the restrained condition the mechanical properties of expansive concrete could be improved.

1.3.2 Hydration reaction model

Over the past few decades, several models have been built and developed to simulate the hydration reaction of cement or cement-based materials using various approaches, as shown in Table 1.2.

Table 1.2 Hydration Reaction Model

Hydration Reaction Model	Authors
TOMOSAWA'S MODEL (1997)	Fuminori Tomosawa, The University of Tokyo
HYMOSTRUC (1991)	K. van Breugel, Delft University of Technology
DUCOM (1996)	Koichi Maekawa, The University of Tokyo
CEMHYD3D	Bentz and Garboczi, National Institute of Standards and Technology
C-CBM (2003)	Ippei Maruyama, The University of Tokyo

In 1974, Tomosawa [1.18] proposed a kinetic model of Portland cement hydration. Based on Tomosawa's model, Maruyama [1.19] has developed and proposed a model of Portland cement hydration. In this model, the volumetric changes of the cement particle, the chemically bound, and physically bound water were

considered. Figure 1.6 shows the C-CBM model [1.19, 1.20] with three types of mode, “Mode 1” is the state that the cement particle does not make contact with the surfaces of the cell, “Mode 2” is the state that the cement particle starts to make contact with surfaces of cell and the contacted parts have a circular shape, and “Mode 3” is the state that the cement particle makes contact with the surface of cell widely and the contacted parts are connected each other.

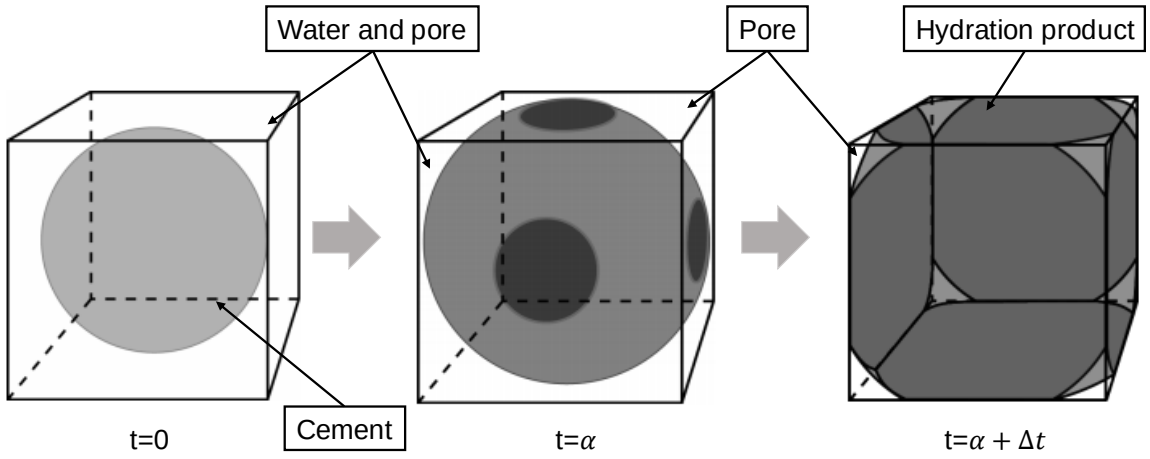

Figure 1.6 C-CBM model [1.19, 1.20].

Park [1.21] designed a microstructural hydration model of Portland cement that considered the reduction in the hydration rate that occurs due to the interfacial area of contact between the free water and the hydration products. A hydration model of slag-cement blends was proposed by Wang [1.22], this model has considered the production of calcium hydroxide in cement hydration and its consumption in the slag reaction.

Mongkhon Narmluk et al. [1.23] investigated the effect of fly ash on the hydration kinetics of cement in low water to binder (w/b) fly ash-cement at different curing temperatures using the modified shrinking-core model. The results show that, at 20℃ and 35℃, the fly ash retards the hydration of cement in the early period, but accelerates the hydration of cement in the later period. However, at 50℃, the fly ash retards the hydration of the cement at a later period when using high replacement ratios.

K. van Breugel [1.2] built a computer-based model, called HYMOSTRUC, the acronym for HYdration, MOrphology and STRUCture formation as shown in Figure 1.7, where grey color is unhydrated cement, the red color is inner hydration products, and the yellow color is outer hydration products. This model has been presented for the kinetics of hydration and structural formation of cement-based materials. The hydrating cement particles are represented as expanding spheres to be shown in Figure 1.8. The model can simulate the development of properties of cement-based materials such as the development of hydration and microstructure, the volume changes of the hardened cement pastes, and the effect of geometrical changes of the microstructure on the creep of the hardened concrete.

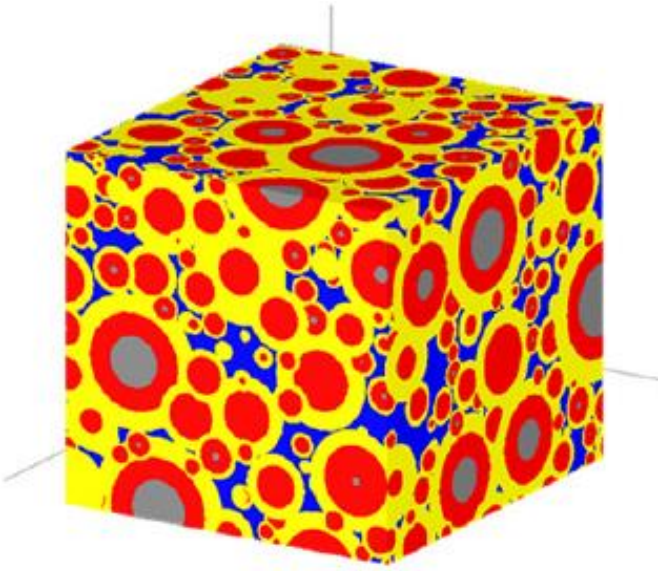

Figure 1.7 HYMOSTRUC model [1.2].

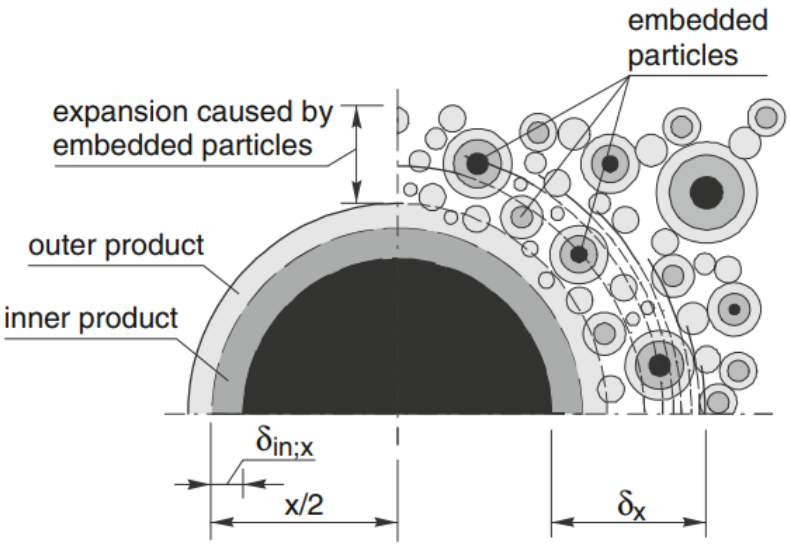

Figure 1.8 Embedding of particles in the outer shell of hydrating particles [1.24].

Based on the HYMOSTRUC model, Xian Liu et al. [1.25] have developed a computational materials model to simulate the formation of microstructure in materials containing limestone powder. He reported that with the proceeding of hydration the limestone powder has a decreasing influence on the microstructure and could obstruct somewhat the formation of a denser microstructure at later hydration stage.

Maekawa et al. [1.26] have modeled the concrete performance that covers microstructure, hydration, temperature, moisture content, state of equilibrium, mechanical strength, and volumetric change through a computational simulation model called DuCOM (Durability of Concrete Model).

P. Navi and C. Pignat [1.27] developed a 3-D computer model for simulating the hydration and microstructure development of C_3S pastes with or without small inert grains during hydration based on "Integrated Particles Kinetics Model". In this research, the pore volume and the contact surfaces between

the hydrated particles and the inert grains are calculated. The influences of the inert grains on the overall degree of hydration and the total contact surfaces, and on the setting time of the hydrated cement are shown. He reported that when 1 cm^3 C_3S dissolves, it produces 1.7 cm^3 CSH and 0.6 cm^3 CH. The part of CSH is divided into two parts: 1 cm^3 inner CSH and 0.7 cm^3 outer CSH as shown in Figure 1.9.

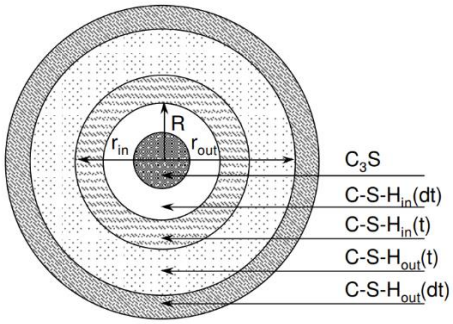

Figure 1.9 The hydrating C_3S particle at time t (Navi and Pignat model [1.27]).

The computer model CEMHYD3D was originally developed in NIST by Bentz and Garboczi to represent the hydration process of Portland cement two-dimensionally. D.P. Bentz [1.28] has simulated the Portland cement hydration and microstructure development using a three-dimensional computer model as shown in Figure 1.10. The computer model was used to simulate the development of microstructure, hydration degree, and to predict the compressive strength. Based on CEMHYD3D, D.P. Benzt [1.29] modeled the influence of limestone filler on cement hydration. In this paper, the CEMHYD3D computer model has been modified to consider the influence of limestone substitutions, the effects of various limestone substitutions on achieved a degree of hydration, microstructure, and strength development was predicted.

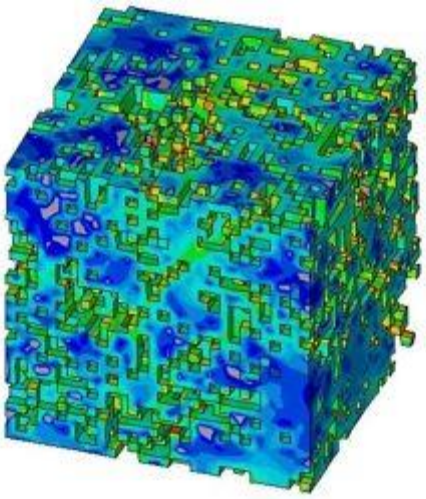

Figure 1.10 CEMHYD3D model [1.28].

Chen Wei [1.30] simulated the hydration of Portland cement paste using Van Eijk's Model. In this research, the computer model CEMHYD3D is extended based on the version developed by Van Eijk for simulating the hydration of slag cement. The author reported that the extended model is able to simulate the hydration process of slag cement paste in a precise way and can be used to predict various properties of the hydrating paste. In addition, the simulated microstructure can be used to evaluate some durability-related properties of slag cement concrete.

1.3.3 Predicting the compressive strength

In general, there exists a fundamental inverse relationship between porosity and strength of solids [1.31]. This relationship can be described by the expression.

$$S = S_0 \cdot e^{-kp} \qquad \text{Eq. (1.2)}$$

where

S is strength of the material which has a given porosity p;

S_0 is intrinsic strength at zero porosity;

k is constant.

In addition, many studies also have reported the relationship between the gel/space ratio and strength [1.31, 1.32]. A gel/space ratio is defined as the ratio of the volume of the hydrated cement paste to the sum of the volumes of hydrated cement and of the capillary pore, also called the amount of solid fraction in the system, which is therefore equal to 1-porosity [1.31]. Powers [1.31] found that the 28-day compressive strength f_c of three different mortar mixture was related to the gel/space ratio. Figure 1.11 shows the relationship between the compressive strength and gel/space ratio. From this figure, he suggested a compressive strength equation as a function of gel/space ratio as shown in Eq. (1.3).

$$f_c = 243x_C^3 \qquad \text{Eq. (1.3)}$$

where

x_c is the gel/space ratio, 243 is the value of intrinsic strength of mortar at zero porosity.

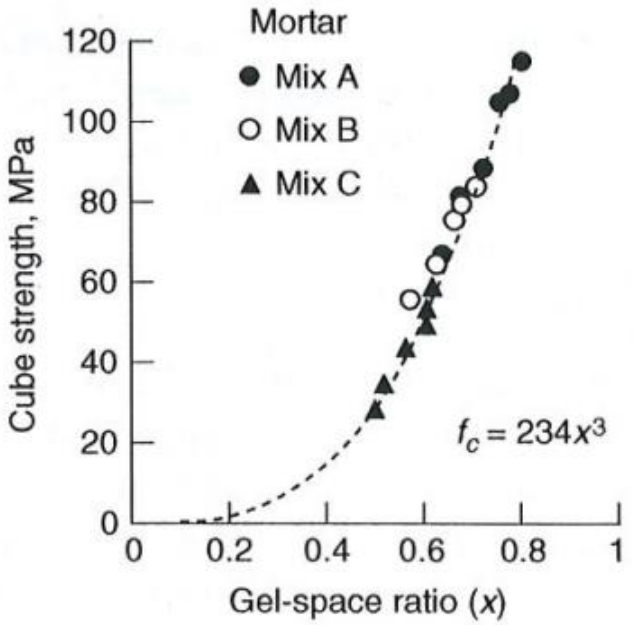

Figure 1.11 Relationship between strength and gel/space ratio with different mix proposition [1.31].

Ryshkewitch [1.33] and Schiller [1.34] have suggested an equation as shown in Eqs. (1.4) and (1.5) that show the relationship between the strength and porosity of low porosity case.

$$f_c = f_0 \cdot e^{-BP} \quad \text{Eq. (1.4)}$$

$$f_c = C \cdot \ln (P_{cr}/P) \quad \text{Eq. (1.5)}$$

where,

f_c is the compressive strength of a hardened cement paste;

P is the porosity;

f_0 is the strength of the hardened cement paste at zero porosity;

P_{cr} is the porosity of the hardened cement paste at zero strength;

B and C are material constants.

Based on the equation of Ryshkewitch and Schiller, Choi et al. [1.16] have assumed that the development of compressive strength of cement paste with an expansive additive was closely related to the pore volume based on the results of the existing studies as shown in equation (1.6) and (1.7). The coefficient of each porosity was referred to the existing studies of Maruyama [1.19] and Katsura [1.35].

$$f_c = 182 \cdot e^{-5.215P} : 0.3 > P \quad \text{Eq. (1.6)}$$

$$f_c = 73 \cdot \ln (0.523/P) : 0.3 \leq P \quad \text{Eq. (1.7)}$$

Similar to the suggestion of Powers, Wang X.Y. [1.36] evaluated the compressive strength of Portland-Limestone cement by using the gel/space ratio, x_{fc}, of concrete can be calculated as follows:

$$x_C = \frac{2.06(1/\rho_C)\alpha_C C_0}{(1/\rho_C)\alpha_C C_0 + W_0} \quad \text{Eq. (1.8)}$$

where

ρ_C is specific gravity of cement;

α_C is hydration degree;

C_0 and W_0 are the mass fractions of OPC and water in the mix proportions, respectively.

2.06 is the volume increase rate of OPC paste or also known that 1 ml of hydrated cement occupies 2.06 ml [1.37].

Lam L. et al. [1.32] introduced a model to describe the relationship between the w/c ratio and the degree of hydration and the gel/space ratio of high-volume fly ash/cement systems. The gel/space ratio of Fly ash – Cement (FC) paste, evaluated based on the proposed model, were found to be consistent with the gel/space ratio of Portland cement (PC) paste in terms of the relationship with compressive strength. However, the hydration degree of FC and PC paste was obtained by determining the non-evaporable water content.
The relationship between compressive strength and porosity for porous concrete was investigated by Lian C. et al. [1.38] through a new model, which was derived from Griffith's theory. The predicted results show a better agreement with the experimental data for porous concrete.

1.3.4 Predicting the carbonation depth

Papadakis et al. [1.39, 1.40] described the physicochemical processes of concrete carbonation, then proposed and developed a simple mathematical model for the evolution of carbonation in time. The chemical reaction of carbonation and parameters such as the ambient concentration of CO_2, the molar concentrations of the carbonate constituents (CH and CSH), and the effective diffusivity of CO_2 in carbonated concrete were considered in the mathematical model, as described in Eq. (1.9) and (1.10).

$$x_c = \sqrt{\frac{2D_{e,CO_2}[CO_2]^0}{[CH] + 3[CSH]}} \cdot \sqrt{t} \quad \text{Eq. (1.9)}$$

$$D_{e,CO_2} = A\left(\frac{\varepsilon_c}{\frac{C}{\rho_c} + \frac{P}{\rho_p} + \frac{W}{\rho_w}}\right)^a \left(1 - \frac{RH}{100}\right)^b \quad \text{Eq. (1.10)}$$

where,

x_c (cm) is the carbonation depth;

t (week) is the time to expose specimen in carbonation condition;

D_{e,CO_2} (m^2/s) is the effective diffusivity of CO_2 in carbonated concrete;

$[CO_2]^0$ (%) is the CO_2 content in the ambient air at the concrete surface, $[CO_2]^0$ = 5%;

[CH] and [CSH] (mol) are the molar concentrations of Portlandite and Calcium silicate hydrate;

RH (%) is the ambient relative humidity;

ρ_c, ρ_p, and ρ_w (kg/m^3) are the density of cement, supplementary cementing materials, and water, respectively;

C, P, and W is the cement, supplementary cementing materials (silica fume or fly ash) and water content in 1 m^3 of fresh concrete;

ε_c (%) is the porosity of concrete.

Based on the mathematical model for the evolution of concrete carbonation and combined the numerical model for the hydration reaction, X-Y Wang et al. [1.41] proposed a numerical model that can predict the carbonation of concrete containing the low-calcium fly ash. In this model, the parameters were calculated by considering the time dependence of the hydration reaction of cement.

1.3.5 Predicting the expansion strain

Choi et al. [1.5] modeled the volumetric change of concrete mixed with an expansive additive by the balance between the shrinkage of OPC and the expansion of the expansive additive, as shown in Figure 1.12. By assuming that the shrinkage of cement is caused by the capillary tension and taking into account the behavior of the moisture inside the pore structure and the pore size distribution of hardened cement paste, the shrinkage of cement was modeled. Meanwhile, the expansion of the EX was modeled by considering the volumetric change of the EX-particles caused by an increase in the outermost layer of particles of the hydration products that were formed at an early age.

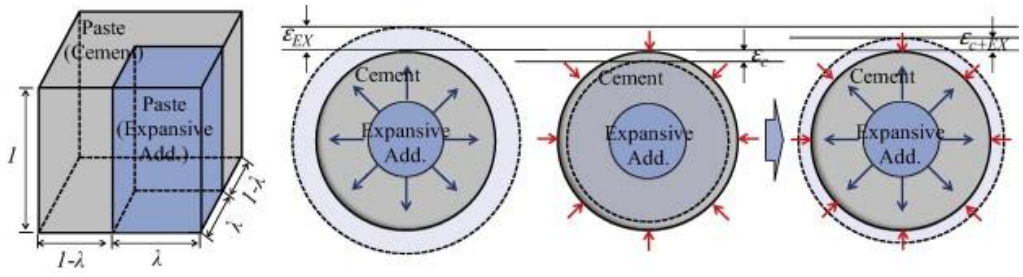

Figure 1.12 Schematic of volumetric change of cement paste containing expansive additive [1.5].

Similar to the assuming of Choi et al. [1.5], Miyazawa [1.42] reported that the expansion strain of expansive concrete was modeled by considering the expansion strain of the expansive additive and autogenous shrinkage of cement, as described in Figure 1.13.

Commentary

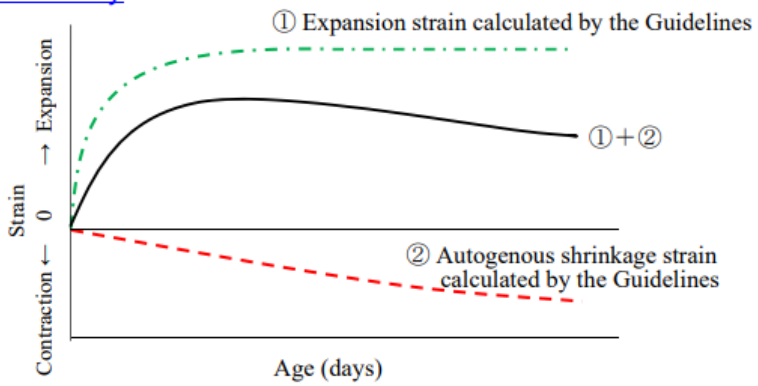

Figure 1.13 Schematic of expansion strain and autogenous shrinkage strain [1.43].

1.4 Objective of Research

The aim of the research is to model the hydration reaction of cement paste mixed with an expansive additive at an early age and then predict the mechanical properties and carbonation of expansive concrete based on the hydration reaction model.

From these aims, the objectives of the research in this thesis can be listed as follows:

- To propose a numerical model to simulate the early age hydration reaction of cement paste mixed with expansive additive.
- To propose an equation for the prediction of the development of compressive strength of expansive concrete.
- To predict the expansion strain of expansive concrete.
- To predict the carbonation depth of expansive concrete.

1.5 Outline of thesis

The research framework of this thesis is presented in Figure 1.14. The thesis is organized into 7 chapters, and the contents are briefly summarized as follows:

Chapter 1 covers the introduction, including the background of the research, information of expansive additive, previous researches, and the objective of the research.

Chapter 2 contains materials used and experimental investigation in this work. The results of this chapter will be used to verify the results of the proposed model and predicting equation in this research. Especially, the effect of restrained conditions on the mechanical properties, carbonation resistance, and frost resistance of expansive concrete is also presented in this chapter.

Chapter 3 presents a hydration model that describes the hydration reaction that occurs when the expansive additive is mixed with cement at an early stage. The effect of curing temperature on the model parameters is considered. Besides, the relationship between the model parameters and the compound of cement is deduced and explained in detail.

Chapter 4 presents an equation to predict the compressive strength of expansive additive by considering the gel/space ratio and compressive strength. The relationship between the compressive strength of cement pastes and concrete is discussed. A conversion coefficient is deduced to find a satisfactory value for predicted data.

Chapter 5 deals with the mathematical model for predicting the carbonation depth of cement concrete and expansive concrete. The value of parameters in this model will be calculated based on the hydration reaction model.

Chapter 6 focuses on the production of ettringite and calcium hydroxide from the hydration reaction of both cement and expansive additive. This is the main key for predicting the expansion strain of expansive concrete. Besides that, the balance between the shrinkage of cement and the expansion of expansive additive is considered. The coefficient of the restraint degree is discussed and used as a parameter in this model.

Chapter 7 summarizes the main findings of the research and suggestion for future works are presented.

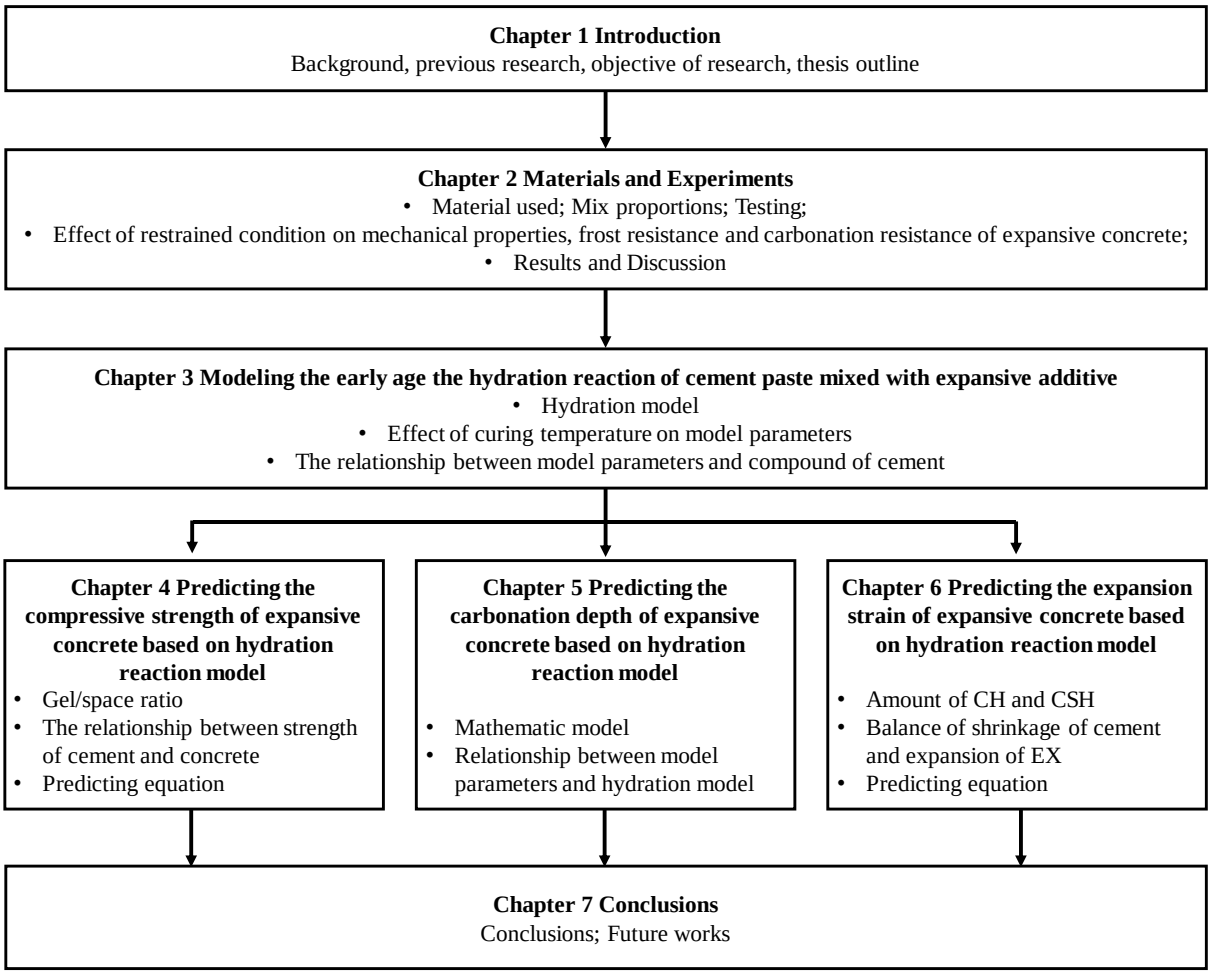

Figure 1.14 Framework of this thesis

References

[1.1] Recommended practice for expansive concrete, Concrete library of JSCE No.23 (1994).

[1.2] K. van Breugel, Simulation of hydration and formation of structure in hardening cement-based materials. Doctoral thesis, Delft University of Technology (1991).

[1.3] X. Liu, G. Ye, G. De Schutter, Simulation of the microstructure formation in hardening self-compacting cement paste containing limestone powder as filler via computer-based model, Materials and Structures 46 (2013) pp 1861-1879.

[1.4] X-Y. Wang, H-S. Lee, Model for predicting the carbonation depth of concrete containing low-calcium fly ash, Construction and Building Materials 23 (2009) pp 725-733.

[1.5] Choi H., Choi H., Lim M., Noguchi T., Kitagaki R., Modeling of volume changes of concrete mixed with expansive additives, Construction and Building Materials 75 (2015), pp 266-274.

[1.6] Choi H., Noguchi T., Modeling of Mechanical Properties of Concrete Mixed with Expansive Additive. International Journal of Concrete Structures and Materials, Vol.9, No.4, pp.391-399, December 2015.

[1.7]. JIS A 6202, Expansive Additive for Concrete (Amendment 1), Japanese Industrial Standard Committee (2008).

[1.8] Nagataki S., Gomi H., Expansive admixtures (mainly etrringite), Cement and Concrete Composites, 20, pp 163-170, 1998.

[1.9] ACI Committee 223: Expansive cement concretes - Present state of knowledge. ACI Journal, pp. 583-610, August 1970.

[1.10] Hyeonggil Choi, A study on the macro prediction of shrinkage-reduction behavior in concrete using expansive additive. Doctoral thesis, The university of Tokyo (2013). (in Japanese)

[1.11] M. Morioka, H. Hagiwara, E. Sakai, M. Daimon, Hydration reaction of the calciumshulphoaluminate-type expansive additive, Cement and Science and Concrete Technology 52 (1998) pp 2-7. (in Japanese).

[1.12] M. Morioka, H. Hagiwara, J-K. Kang, Y. Ohba, E. Sakai, M. Daimon, Hydration of Calciumsulphoaluminate type expansive containing excess free-lime, Journal of the society of inorganic material, Japan 7 (2000) pp 99-106.

[1.13] T. Higuchi, M. Eguchi, M. Morioka, E. Sakai, Hydration and properties of expansive additive treated high temperature carbonation. Cement and Concrete Research. 64 (2014), pp.11-16.

[1.14] Nguyen T.B.T.; Chatchawan R.; Saengsoy W.; Tangtermsirikul S.; Sugiyama T. Influences of different types of fly ash and confinement on performances of expansive mortars and concretes, Constr. Build. Mater. 2019, 209, 176-186.

[1.15] Y. Tsuji, H. Maruyama, A fundamental study on effect of restraint method on mechanical properties of expansive concrete. Proceedings of the 6th Annual Conference on Concrete Engineering, 1984, 86, 341-344.

[1.16] H. Choi, T. Noguchi, Modeling of Mechanical Properties of Concrete Mixed with Expansive Additive, International Journal of Concrete Structure and Materials, Vol.9, No.4, December 2015, pp.391-399.

[1.17] A. Harada, Effect of rebar restraint on the length change of freeze-thaw behavior and deterioration of frost damage of concrete structure. Master's thesis (2007), Muroran Institute of Technology.

[1.18] Tomosawa F., Hydration Model of Cement, Cement Technology Annual Report 28 pp.53-57, 1974.

[1.19] Maruyama I., Time dependent property of cement-based materials on the basis of microstructure mechanics, Doctorate Thesis University of Tokyo, Japan, March 2003 (in Japanese).

[1.20] Maruyama I., Matsushita T., Noguchi T., Numerical modeling of Portland cement hydration. International RILEM symposium on concrete modelling- CONMOD'08 (2008) Delft, the Netherlands.

[1.21] Park, K.B., Jee, N.Y., Yoon, I.S., Lee, H.S., Prediction of Temperature Distribution in High-Strength Concrete Using Hydration Model, ACI Materials Journal (2008) 105:180-186.

[1.22] Wang, X.Y., Lee, H.S., Park, K.B., Kim, J.J., Golden, J.S., "A Multi-Phase Kinetic Model to Simulate Hydration of Slag-Cement Blends," Cement and Concrete Composite 32 (2010).

[1.23] Narmluuk, M., Nawa, T., Effect of Fly Ash on the Kinetics of Portland Cement Hydration at Different Curing Temperatures, Cement and Concrete Research 41 (2011) 579-589.

[1.24] Lossier, H., The self-stressing of concrete by expanding cements, 1948.

[1.25] Xian Liu, Guang Y., Geert D. S., Yong Y., Simulation of the microstructure Formation in Hardening Self-Compacting Cement Paste Containing Limestone Powder as Filler via Computer-Based Model. Materials and Structures, 46 (11), pp. 1861-1897, 2013.

[1.26] Maekawa et al., Koichi Maekawa, Rajesh Chaube and Toshiharu Kishi. Modelling of Concrete Performance: Hydration, Microstructure Formation and Mass Transport, 1999.

[1.27] P. Navi, C.Pignat, Simulation of cement hydration and the connectivity of capillary pore space, Advanced Cement Based Material 4 (2) (1996) 58-67.

[1.28] D.P. Bentz, Three-dimensional computer simulation of cement hydration and microstructure development J Am Ceram Soc, 80 (1) (1997), pp. 3-21.

[1.29] D.P. Benzt, Modeling the influence of limestone filler on cement hydration using CEMHYD3D, Cement and Concrete Composites, Vol. 28, Issue 2, Feb 2006, pages 124-129.

[1.30] Chen Wei, Hydration of slag cement: Theory, Modeling and Application, (Doctorate thesis) The University of Twente, January 2007.

[1.30] [1.31] P. Kumar Mehta, Paulo J. M. Monteiro, "Concrete: Microstructure, Properties, and Materials," Fourth Edition.

[1.32] Lam L., Wong Y.L., Poon C.S., Degree of hydration and gel/space ratio of high-volume fly ash/cement systems. Cement and Concrete Research 30 (2000) 747-756.

[1.33] Ryshkewitch, E. (1953). Composition and strength of porous sintered alumina and zirconia. Journal of the American Ceramic Society, 36, 65–68.

[1.34] Schiller, K. K. (1958). Mechanical properties of non-metallic materials (pp. 35–50). London, UK: Butterworths

[1.35] Katsura O., Morimoto J., Nawa T., A Model of Strength development considering hydration of cement. Proceeding of the Japan Concrete Institute, 39, 109-114.

[1.36] Wang, Modeling of Hydration, Compressive Strength, and Carbonation of Portland-Limestone Cement (PLC) Concrete. Materials, 10, 115, 2017.

[1.37] A. M. Neville, "Properties of Concrete", Fourth Edition.

[1.38] Lian C., Zhuge Y., Beecham S., The Relationship Between Porosity and Strength for Porous Concrete. Construction and Building Materials, 25, pp 4294-4298, 2011.

[1.39] V.G. Papadakis, M.N. Fardis, C.G. Vayenas, Effect of composition, environmental factors and cement-lime mortar coating on concrete carbonation. Materials and Structures 25 (1992) pp 293-304.

[1.40] V. G. Papadakis, Effect of supplementary cementing materials on concrete resistance against carbonation a chloride ingress. Cement and Concrete Research Volume 30, (2000) pp 291-299.

[1.41] X.Y. Wang, H.S. Lee, A model for predicting the carbonation depth of concrete containing low-calcium fly ash. Construction and Building Materials 23 (2009) pp 725-733.

[1.42] Shingo Miyazawa, JCI-RILEM International Workshop, Concrack5, April 24-26, 2017, Japan

CHAPTER 2

MATERIALS AND EXPERIMENTAL INVESTIGATION

CHAPTER 2 MATERIAL AND EXPERIMENTAL INVESTIGATION

2.1 Introduction

Concrete has a major unfavorable property, which is drying shrinkage [2.1]. The cracks caused by drying shrinkage leads to reduced strength and durability and increased risk of corrosion. To address this problem, expansive concrete is widely used to efficiently prevent the shrinkage cracks. Expansive concrete is nowadays made in two ways. The first method is using expansive cement to make expansive concrete. The second approach is using an expansive additive as a cement replacement material to make expansive concrete. The latter method has been widely used in Japan and Thailand [2.2]. According to the American Concrete Institute standard [2.3], three kinds of expansive cement are available: K, M, and S types. According to the JIS A 6202 [4], an expansive additive is an admixture that reacts with water and makes the concrete expand due to the production of ettringite and calcium hydroxide from the hydration reaction. Expansive concrete has been applied to slabs, pavements, shrinkage-compensating concrete structures, etc. [2.5]. Considerable laboratory research on the mechanical properties and durability of expansive concrete has been undertaken. However, these experiments were performed under unrestrained (free) conditions (e.g., compressive strength, accelerated carbonation, and freezing–thawing tests). In an actual concrete structure, the expansive concrete is usually restrained by reinforcement, connecting members, foundation, etc. Therefore, the behavior of expansive concrete under restrained conditions must be investigated in a laboratory.

Several studies were conducted to investigate the effect of restrained conditions on the expansive concrete properties. Tsuji et al. [2.6] reported that the compressive strength of expansive concrete was higher than that of cement concrete by approximately 30%-50% under a restrained condition. The amount of expansive additive (EX) was used at a high level, which was approximately 80 kg/m^3 of concrete. However, as a standard amount in Japan, EX is known as 20 kg/m^3 of concrete. Similar to the results reported by Nguyen et al. [2.2], Tsuji et al. [2.6] also reported that the compressive strength of expansive concrete could be improved by confinement. However, the expansive concrete confinement was only restrained by the horizontal directions and did not consider the vertical directions. Considering the effect of restrained conditions, Harada [2.7] found that the frost resistance of the restrained concrete was enhanced compared to that of the unrestrained conditions for cement concrete. Furthermore, Colin et al. [2.8] found a decrease in the size of the large pores of expansive cement paste under uniaxial restrained conditions. Note that most of these works only focused on the mechanical behavior of expansive concrete under uniaxial restrained conditions. Meanwhile, an experimental study on the effect of both uniaxial and triaxial restrained conditions on the mechanical properties and durability of expansive concrete has not yet been established.

The aim of this chapter are: firstly, to presents the information of materials, mix proportions of pates and concrete, and test method, which were used in this study; secondly, to understand the effect of expansive additive on the properties of paste and concrete and use the results of this chapter as a way to verify the calculated data that will be presented in Chapter 3, Chapter 4 and Chapter 5; finally, to investigate the effect

of a restrained condition on the mechanical properties, carbonation depth, and frost resistance of expansive concrete at different water-binder (w/b) ratios and grasp these effects to obtain a correct assessment of the experiments on expansive concrete in a laboratory.

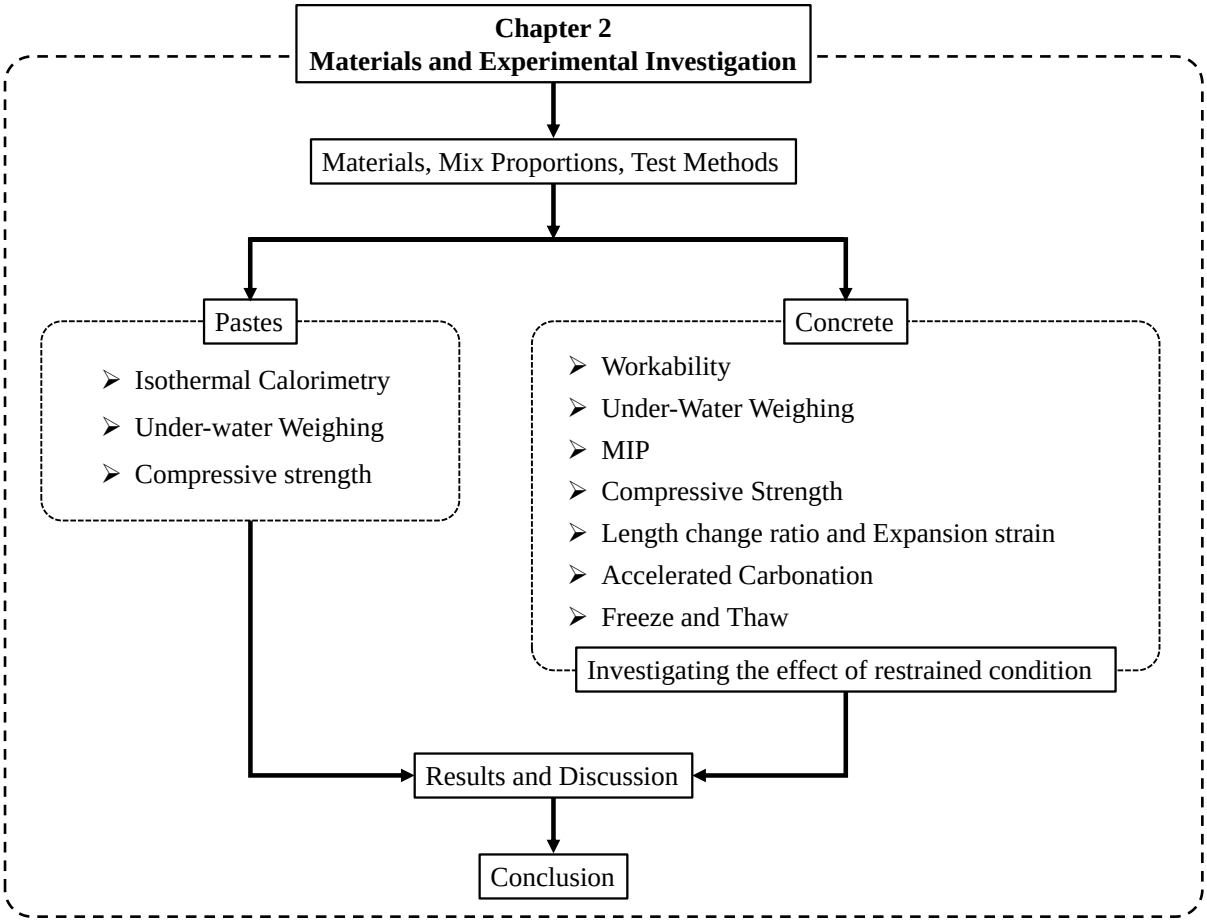

Figure 2.1 Plan process of Chapter 2

2.2 Material

2.2.1 Ordinary Portland Cement

In this study, Ordinary Portland Cement (OPC) was used as compliance with Japanese Industrial Standards (JIS) and was introduced into the matrix in pastes and concrete. Table 2.1 shows the chemical compositions and physical properties of OPC. Table 2.2 shows the mineral composition of OPC. The composition of OPC were calculated using the Bogue equation [2.9], as shown in Eqs. (2.1a) - (2.1d).

$$C_3S = 4.07(CaO) - 7.60(SiO_2) - 6.72(Al_2O_3) - 1.43(Fe_2O_3) - 2.85(SO_2) \quad \text{(Eq. 2.1a)}$$

$$C_2S = 2.87(SiO_2) - 0.75(3CaO.SiO_2) \quad \text{(Eq. 2.1b)}$$

$$C_3A = 2.65(Al_2O_3) - 1.69(Fe_2O_3) \quad \text{(Eq. 2.1c)}$$

$$C_4AF = 3.04(Fe_2O_3) \quad \text{(Eq. 2.1d)}$$

Table 2.1 Chemical composition and physical properties of materials

Material	Chemical composition (mass, %)						Density (g/cm^3)	Blain (cm^2/g)
	SiO_2	Al_2O_3	Fe_2O_3	CaO	MgO	SO_3		
OPC	21.4	5.5	2.9	64.3	1.5	2.0	3.15	3490
EX	1.8	5.4	0.9	67.0	-	19.6	3.05	3260

Table 2.2 Composition of materials

Material	Composition, (mass,%)						
	C_3S (%)	C_2S (%)	C_3A (%)	C_4AF (%)	f-CaO	Ye'elimite	$CaSO_4$
OPC	50.33	23.41	9.51	8.92	-	-	-
EX	-	8.0	-	3.3	45.4	9.2	31.4

2.2.2 Expansive Additive

Calcium Sulphoaluminate (CSA) – type expansive additive (EX) was used in this study. The chemical composition and physical properties, and composition of expansive additive are given in Table 2.1 and Table 2.2, respectively. The composition of EX (see Table 2.2) were obtained from the report made by Takayuki Higuchi et al. [2.10].

2.2.3 Aggregate

For concrete mixes, the JIS standard aggregate (coarse and fine aggregates) was used in this research. The properties of the fine and coarse aggregates are given in Table 2.3.

2.2.4 Admixtures

An AE water-reducing agent (Master Pozzolith No. 70), high-performance water-reducing agents, and an AE agent (Master Air 404) were used to control the concrete workability and air content.

2.2.5 Water

Tap water of Muroran Institute of Technology was used as the mixing water for paste and concrete in this work.

Table 2.3 Properties of Aggregates

Tests	Aggregates	
	Fine	Coarse
Sieve Analysis		
% Passing		
No. of Sieve (mm)		
5	100	
2.5	93	Maximum size: 20 mm
1.2	72	
0.6	46	
0.3	20	
0.15	3	
Fine Modulus	2.5	-
Density (g/cm^3)	2.68	2.68
Absorption (%)	1.78	2.17

2.3 Experimental Design

2.3.1 Design of Paste

For cement and cement-expansive additive (cement-EX) paste, two series of the sample were considered. The mixture proportions for each were summarized in Table 2.4. In series 1, the EX replacement levels were 0%, 5%, 10%, 15%, 20%, and 100%. The water-to-binder (w/b) ratios were 0.3 and 0.5. The energy generated during the hydration of OPC and cement–EX was measured using a multi-micro calorimeter (MMC-511 SV) at 20 °C for 72 h and these values were used to determine the hydration reaction rate. In order to evaluate the effect of the curing temperature on the hydration reaction model, the energies generated during the hydration of OPC100, EX5, and EX10 were also measured at different curing temperatures (5, 20, and 40 °C) at w/b 0.5. In series 2, the blended cement mixes contained 0% and 5% EX cement replacement by weight; the w/b ratios were 0.3, 0.4, and 0.5. The gel/space ratio was calculated from the porosity of OPC and the cement–EX paste, wherein the porosity was determined by underwater weighing. A compressive strength test was conducted to determine the compressive strength of the cement paste and the cement–EX paste.

Table 2.4 Mix Proportions

Samples		OPC (%)	EX (%)	w/b	Curing Temperature (℃)	Experiments
Series 1	EX0*	100	0	0.3, 0.5*	5*, 20, 40*,	Isothermal calorimetry
	EX5*	95	5			
	EX10*	90	10			
	EX15	85	15			
	EX20	80	20			
	EX100	0	100			
Series 2	EX0	100	0	0.3, 0.4, 0.5	20	Under-water weighing Compressive strength
	EX5	95	5			

Note: * denotes the heat evolution of OPC100, EX5, and EX10 were determined at curing temperatures of 5 and 40℃ for w/b 0.5.

2.3.2 Design of Concrete

For cement concrete and expansive concrete, the mix concrete proportions are given in Table 2.5. Cement concrete and expansive concrete were prepared with water-binder ratios (w/b) of 0.3 and 0.5, which was divided into two series, respectively. The amount of EX replacing the binder was 0, 20, and 40 kg/m^3. For concrete mixes with w/b 0.3, in order to control the slump, flow, and air content, the high-performance

water-reducing agents, and an AE agent (Master Air 404) were used with the dosage of 1.2% and 0.001% by weight of binder, respectively. The concrete samples were used for the tests on the length change ratio, expansion strain, underwater weighing, compressive strength, accelerated carbonation and freeze-thaw. The mortar samples were used to determine the pore size distribution using the MIP test, which were obtained by separating the coarse aggregates from the fresh concrete by wet sieving (5 mm sieve).

Table 2.5 Mix proportions

Series	Sym.	w/b	Unit weight, kg/m^3					Admixtures	Experiments
			W	C	EX	S	A		
Series 1	OPC	0.3	175	583	-	616	981	SP8SV (Bx1.2%) Master air 404 (Bx0.001%)	Workability, Length change ratio, Expansion strain, Under-water weighing, Compressive strength, Accelerated carbonation, Freeze-thaw
	EX20			563	20				
	EX40			543	40				
Series 2	OPC	0.5	185	370	-	855	959	No. 70 (250 ml/B = 100 kg)	
	EX20			350	20				
	EX40			330	40				

2.4 Experimental Method

2.4.1 Cement Paste and Cement Paste mixed with Expansive Additive

2.4.1.1 Calorimetry Test

The hydration of cement-based materials is an important characteristic. To investigate the hydration process of cement-based materials, isothermal calorimetry, semi-adiabatic calorimetry, or solution calorimetry method can be used for different purposes. Isothermal calorimetry is a useful method for determining the heat production rate and the developed heat during cement hydration. It may be used for different purposes: to determine the total heat of hydration; to determine the rate of heat evolution; as a general tool to investigate the hydration process of cement.

In this study, an isothermal calorimeter (MMC-511SV6) from TOKYO RIKO as shown in Figure 2.2 was used to measure the rate of heat evolution of OPC paste and Cement-EX paste at 30-second intervals. The specification of MMC-511SV6 is shown in Table 2.6.

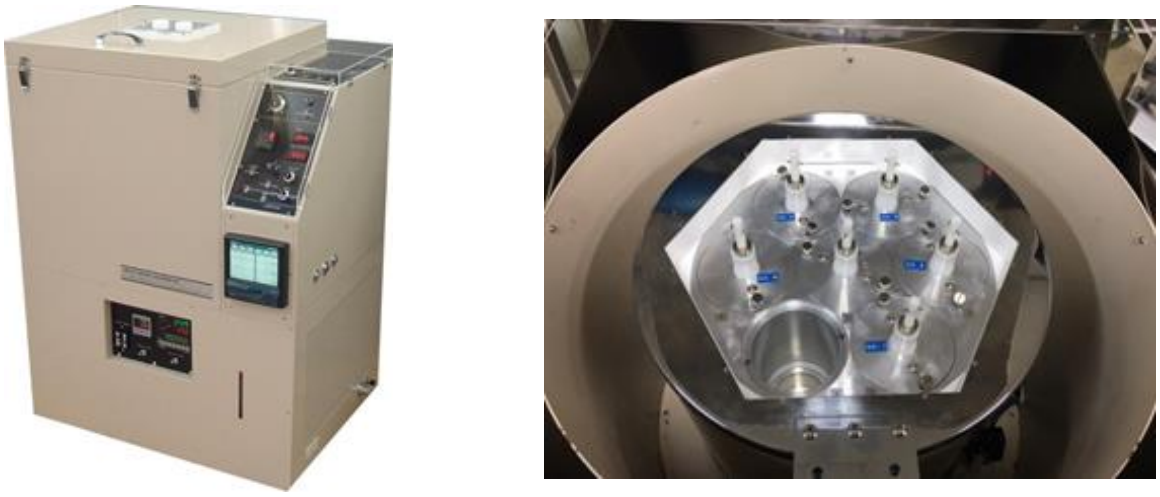

Figure 2.2 Isothermal Calorimetry Apparatus (MMC-511SV6)

Table 2.6 Specification of MMC-511SV6

	Specifications
Measurement temperature ranges	5°C~60°C
Detector	Thermo-module approximately 52mV/°C
Calorimetric detection sensitivity	Approximately 0.16μV/μW
Measurement channel	1~6 点
Baseline drift	±1μV/5°C・24h（8.5μW）
Calibrated calorie supply	25μW~0.8W Continuously variable supply
Stirring	0~114r.p.m. Continuously variable stirring
Data Measurement	Analyze the data recorded on the graphic recorder card using a computer

2.4.1.2 Under-Water Weighing Test

Many studies [2.2], [2.11], [2.12] used the MIP test to determine the total porosity of mortar and concrete. However, the MIP test cannot measure a pore size (diameter) smaller than 3 nm [2.8, 2.13]. Meanwhile, the gel pore diameter ranges from 1 nm to 10 nm [2.13]. Therefore, the underwater weighing (Figure 2.3) test was used herein to determine the satisfactory value of the total porosity of concrete. The preparation of the total-porosity test samples was similar to that for the MIP sample test. After being vacuum freeze-dried for 24 h, the cube samples were immersed in water and continued to be kept in a vacuum chamber for 24 h. The masses of the cube samples were determined under the water in a saturated surface-dry condition and after drying at 105 ℃ for 24 h. The total porosity was calculated as follows:

$$V_t = \left(1 - \frac{\rho_b}{\rho_{tr}}\right) \times 100\% \quad \text{(Eq. 2.2)}$$

$$\rho_b = \frac{m_{oven}}{m_{float}} \quad \text{(Eq. 2.3)}$$

$$\rho_t = \frac{m_{oven}}{m_{oven} - m_{water}} \quad \text{(Eq. 2.4)}$$

where V_t is the total porosity (%); ρ_b is the bulk density (g/cm^3); ρ_{tr} is the true density (g/cm^3); m_{oven} is the sample mass after drying at 105 ℃; m_{float} is the sample mass in the floating condition (g); $m_{water} = m_t - m_{ap}$ is the mass of sample under water (g); m_t is the mass of the equipment and sample under water (g); and m_{ap} is the mass of the equipment under water (g).

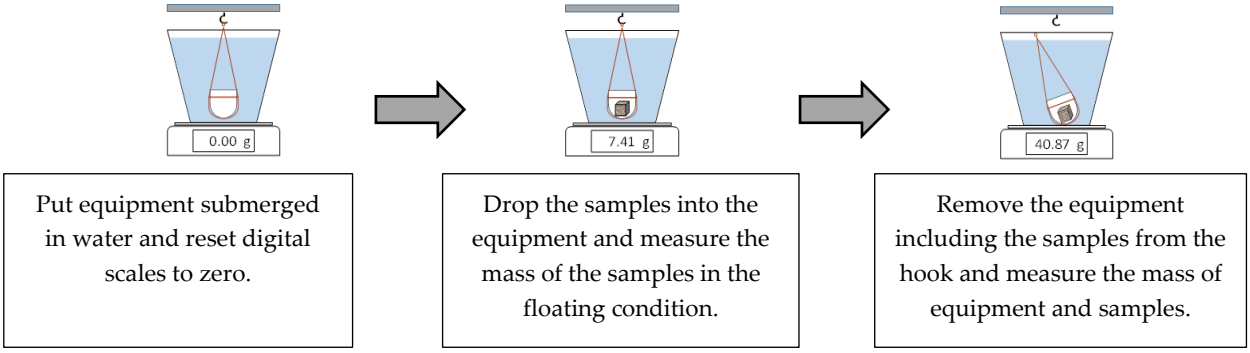

Figure 2.3 Schematic of the underwater weighing test

The ages and curing condition were 1-day, 3-day, 7-day, 14-day and 28-day, and under-water curing condition.

2.4.1.3 Compressive Strength

Compressive strength tests were conducted on paste samples according to JIS A 1108 [2.14] with dimensions 40×40×160 mm^3 at 1-day, 3-day, 7-day, 14-day, and 28-day of under-water curing condition.

2.4.2 Cement Concrete and Expansive Concrete

2.4.2.1 Workability Test

For workability of concrete mixes, the slump, slump flow and air content of concrete were carried out according to JIS A 1101 [2.15], JIS A 1150 [2.16], and JIS A 1128 [2.17], respectively.

2.4.2.2 Mercury Intrusion Porosimetry Test

The interfacial transition zone is well known to have a significant effect on the pore size distribution of the hardened concrete. The MIP test was conducted on the mortar samples herein to address this problem. The samples were obtained by separating the coarse aggregates from the fresh concrete by wet sieving (5 mm sieve). The unrestrained mortar was cast in prism molds measuring 40×40×160 mm^3 and demolded after 1 day. Sealed curing was then performed in a room at a temperature of 20℃ and relative humidity of 60%. On the contrary, the restrained mortar was cast into the designed molds (Figure 2.4). At the test ages, the mortars were cut into small 5×5×5 mm^3 cubes and soaked in ethanol for 1 week prior to being vacuum freeze-dried for 24 h to stop the hydration. The mortar samples for this test were randomly selected.

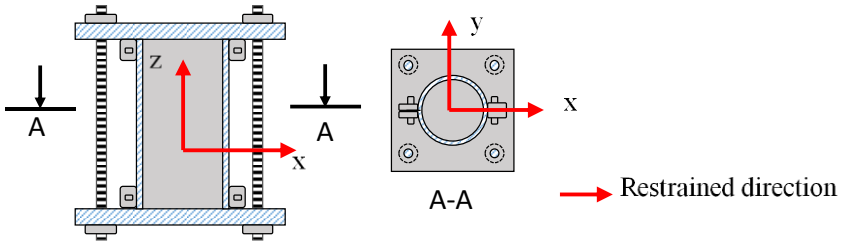

Figure 2.4 Schematic of the restrained mold for testing the pore structure and restrained compressive strength

2.4.2.3 Compressive Strength Test

The compressive strength was measured on Ø100 × 200 mm cylinders at different conditions (i.e., unrestrained and restrained conditions) to evaluate the effect of the restrained condition on the compressive strength of concrete. The unrestrained concrete was demolded 24 h after casting and covered by a plastic sheet to cure at 20℃ and 60% relative humidity until the time of the test. For the restrained condition, Nguyen et al. [2.2] designed a cube mold measuring 100×100×100 mm^3, which was restrained using two steel bars to connect with a steel plate at the specimens' ends. However, these molds could only confine the concrete in one direction (i.e., horizontal direction) and did not consider the vertical direction. To address this limitation, the concrete was cast in the steel molds to restraint three directions. The vertical direction was restrained by connecting the two-steel plate using four steel bars (Figure 2.4). Both the unrestrained and restrained compressive strengths were tested in accordance with JIS A 1108 [2.14] at 3, 7, and 28 days.

2.4.2.4 Length Change Ratio and Expansion Strain Test

The length change ratio and expansion strain of concrete tests were performed under both free and restrained conditions. For the free condition, the free expansion of concrete was conducted in accordance with the JIS A 1129 [2.18]. For this test, steel prisms measuring 100×100×400 mm^3 and 75×75×400 mm^3 were used. The specimens were demolded at 24 h after casting to avoid steel mold confinement. An embedded strain gauge was installed into the center of the unstrained specimens to measure the expansion strain for the free condition (Figures 2.5a and 2.6a). For the restrained condition, the concrete was cast into the restrained molds according to the JIS A 6202 [2.4] (Figure 2.5b). A strain gauge was attached on the top and bottom surface of the rebar at the center of the specimen. A data logger was used to immediately record the strains of the unrestrained and restrained concrete after casting.

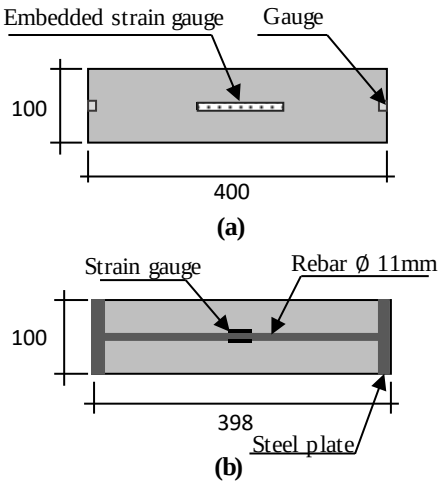

Figure 2.5 Schematic of the specimens measuring 100 × 100 × 400 mm^3: (a) free condition and (b) restrained condition according to the JIS A 6202.

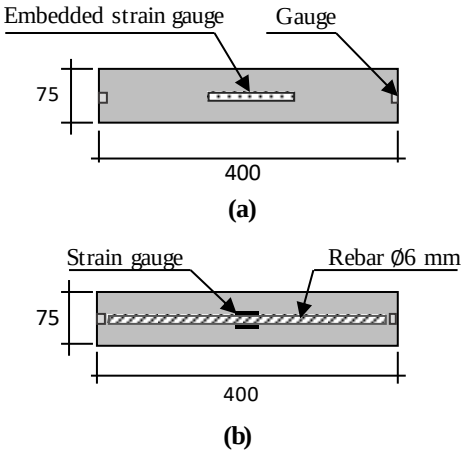

Figure 2.6 Schematic of the specimens measuring 75 × 75 × 400 mm^3: (a) free condition and (b) restrained condition.

2.4.2.5 Underwater Weighing Test

The total porosity of mortar and concrete were carried out at 28 days with the same as method in section *2.3.1.2.*

2.4.2.5 Accelerated Carbonation Test

The accelerated carbonation test was conducted in accordance with JIS A 1153 [2.19] to measure the carbonation depth of all the concrete mixtures measuring 100×100×400 mm^3. The carbonation depth was measured by spraying a phenolphthalein solution on the test surface after 13 weeks of exposure to an accelerated carbonation condition (ambient temperature: 20±2℃; CO_2 concentration: 5±0.2%; and relative humidity: 60±5%). Figure 2.7 shows the accelerated carbonation chamber.

Figure 2.7 Accelerated Carbonation Chamber

2.4.2.6 Freezing - Thawing Test

In this test, the frost resistance of concrete was determined according to the JIS A 1148 [2.20] with dimensions of 75×75×400 mm^3. The fundamental transverse frequency and the mass loss change of the specimens were measured within 300 cycles. The resistance of concrete to freeze–thaw was evaluated by calculating the value of the relative dynamic modulus of elasticity (RDM), as given in Eq. (4). The specimens are often considered as frost damage when the RDM value is less than 60%. Figure 2.8 shows the testing freezing-thawing system.

$$P_n = \left(\frac{f_n^2}{f_0^2}\right) \times 100\% \qquad \text{(Eq. 2.5)}$$

Figure 2.8 Freezing-Thawing chamber

2.5 Results and Discussion

2.5.1 Heat Evolution and Hydration Degree

Figure 2.9, Figure 2.10 show the rate of heat evolution and degree of hydration of the OPC paste and the cement–EX paste with diffident of w/b ratio 0.3 and 0.5 cured at 20 °C, respectively. According to these figures, the rate of heat evolution for EX100 at all ages were higher than those of the OPC paste and cement–EX paste. The degrees of hydration were approximately 0.5, 0.6 and 0.78, 0.8 for OPC100 and EX100 for w/b 0.3 and w/b 0.5, respectively. For the cement–EX paste, the degree of hydration increased with increasing EX replacement. The results demonstrated that the presence of the expansive additive contributes to increase in the heat of hydration, consistent with the results reported by Choi et al. [2.21]. This phenomenon arose due to the contribution C_4AF and free lime (frC) to the heat of hydration.

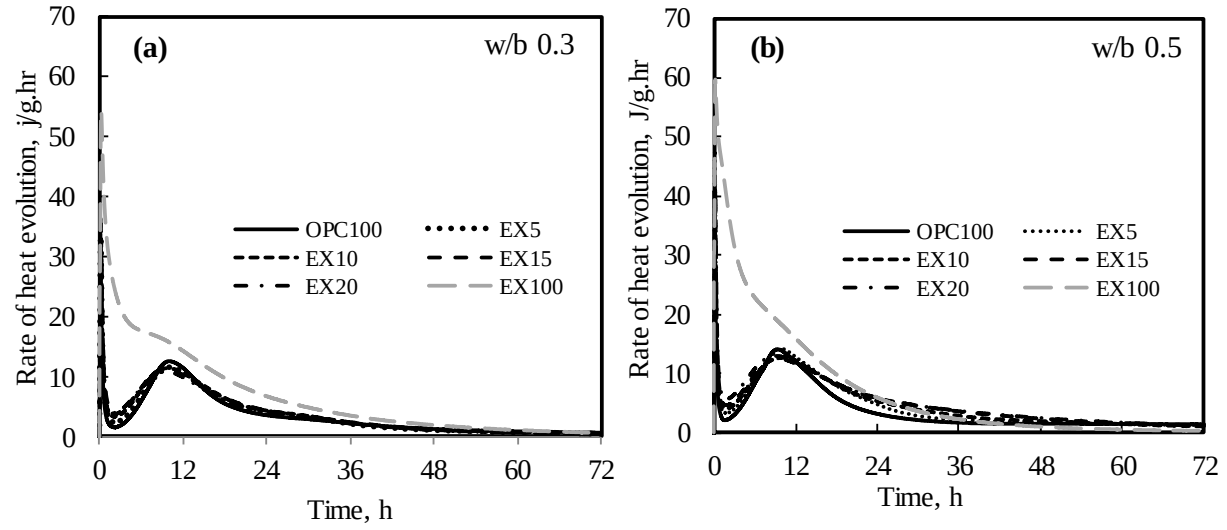

Figure 2.9 Heat evolution: (a) w/b 0.3 and (b) w/b 0.5

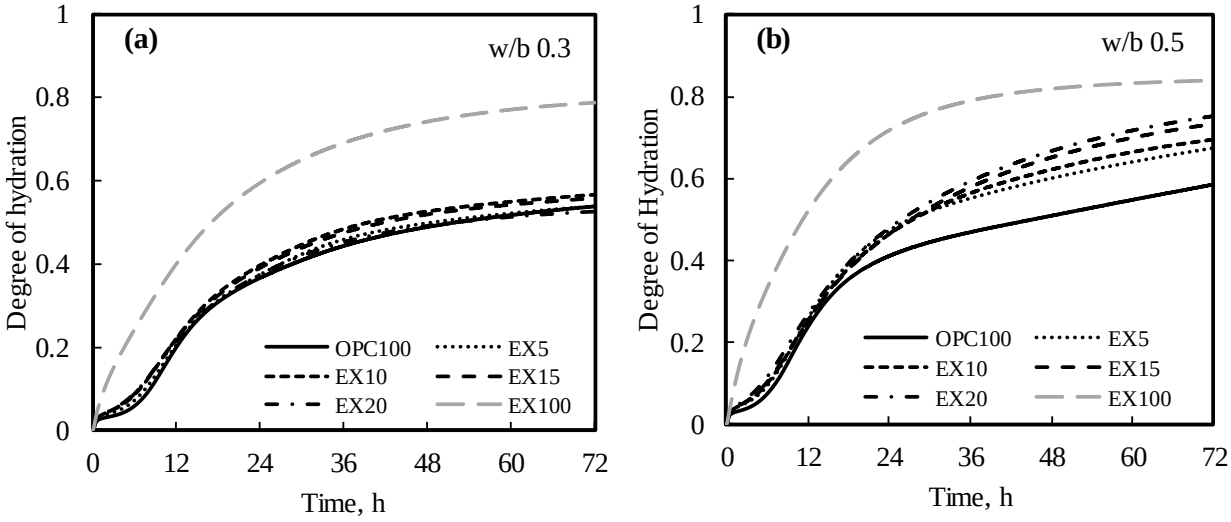

Figure 2.10 Degree of hydration: (a) w/b 0.3 and (b) w/b 0.5

The results for the rate of heat evolution for OPC100, EX5, and EX10 paste at 5℃ , 20℃, and 40℃ are presented in Figure 2.11. A higher curing temperature leads to faster heat evolution for all samples. The total heat evolution of the EX10 was higher than that of EX5 and OPC100.

Our experimental results demonstrate that the curing temperature had a significant effect on the hydration reaction of cement and cement–EX blends. This is similar to the results reported by Maruyama [2.22], who showed the results of the heat liberation rate of cement in isothermal conditions. In addition, because of the formation of more ettringite, highly exothermic properties (high and broadened first peak, shorter induction period, and lower second peak) were observed. This observation is consistent with the finding of W. Nocun-Wczelik [2.23]. However, this may also be explained by the hydration reaction of the mineral content. Specifically, give a certain curing temperature, the second peak becomes lower with increasing amounts of EX (see Fig. 2.11a-c). This is due to a decrease in the amount of C_3S phase, which leads to lower heat evolution for the cement-EX paste in the acceleration period. The effect of the phase composition of the OPC at different periods of OPC hydration is presented in Chapter 3.

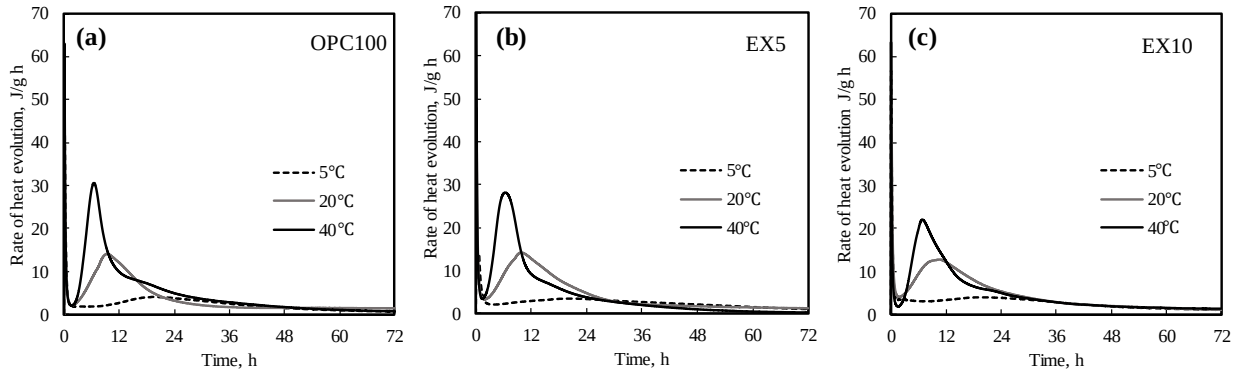

Figure 2.11 Rates of heat evolution of cement with and without EX against time at different curing temperatures: (a) OPC100, (b) EX5, and (c) EX10.

2.5.2 Workability of concrete

Table 2.7 presents the test results of the fresh non-expansive and expansive concrete. The slump, flow, and air content results were obtained in accordance with the JIS A 1101 [2.15], JIS A 1150 [2.16], and JIS A 1128 [2.17], respectively. Table 1 shows that the slump and the flow of concrete were almost the same for all samples in the two series. The tendency was also seen in the air content results for concrete with w/b 0.5. Meanwhile, the air content of the fresh concrete with w/b 0.3 slightly increased when the amount of expansive additive was increased. These tendencies were similar to those reported by M. Tsuji et al. [2.6], who showed the results of a new test method for the restrained expansion of expansive concrete.

Table 2.7 Test results of fresh concrete

	Sample	w/b	Slump (cm)	Flow (cm)	Air content (%)
Series 1	OPC	0.3	-	66	4.7
	EX20		-	65.5	5.5
	EX40		-	66	5.8
Series 2	OPC	0.5	20	-	4.8
	EX20		19.4	-	4.9
	EX40		19.5	-	4.9

2.5.2 Porosity

2.5.2.1 Paste

Figure 2.12 compares the results of total porosity of the hardened cement paste containing the expansive additive with the w/b ratio of 0.3, 0.4, and 0.5. The results indicated that the total porosity for all sample slight decreases with time. This is due to the formation of hydration products (C-S-H, ettringite) fills into the pore in the paste. It means the pore structures of the pastes are dense with the hydration process. Additionally, the results also showed that the total porosity is lower with the lower w/b ratio. This may explain why decreasing the w/b ratio increases the compressive strength of hardened paste.

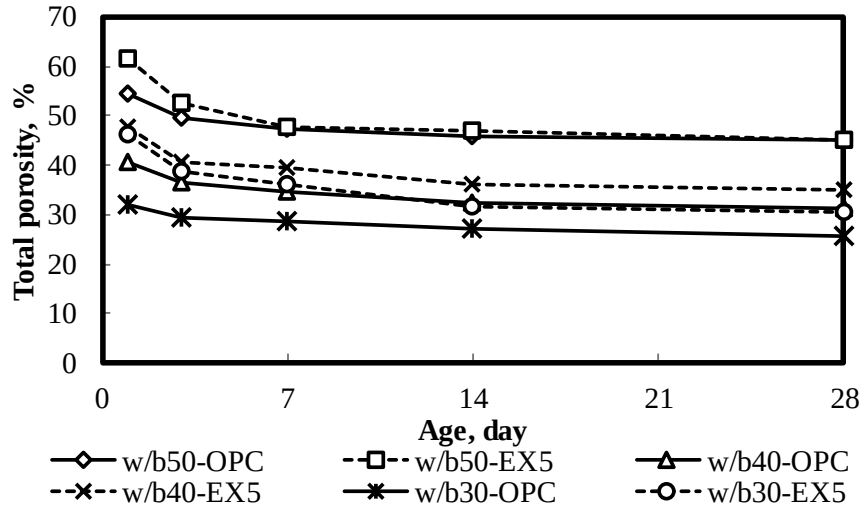

Figure 2.12 Total porosity of hardened paste with different w/b ratios

2.5.2.2 Concrete

a) Pore structure

Figure 2.13 shows the test results of the pore size distribution of the cement mortar (OPC sample) and the expansive mortar (EX20 and EX40) with w/b 0.3 and 0.5 obtained by the MIP test at 28 days. The pore

size distribution curves of the control mortar sample (OPC sample) typically exhibited at least two sharp peaks for w/b 0.3 and 0.5. The first one laid less than 10 nm, while the second corresponded to a diameter of approximately 20–50 nm. The first peak that laid less than 10 nm was difficult to observe in the expansive mortar. The results showed that the pore diameter corresponding to the highest peak in the differential curve slightly decreased with the addition of the expansive additives for both w/b 0.3 and 0.5. When comparing different w/b ratios, these pore diameters increased with a higher w/b ratio. For the EX40 sample with both w/b 0.3 and 0.5, the rounded peak appeared in the pore size ranging from 100 to 1000 nm, indicating that the EX-addition affected the pore diameter of 100–1000 nm. However, the effect of the restrained condition on this pore diameter range was not observed.

The concept of a critical pore entry diameter was considered to evaluate the influence of the restrained condition on the pore size distribution of the control and expansive mortar samples. Scrivener et al. [2.24] reported that the critical pore entry diameter is the pore diameter, where the steepest slope of the cumulative curve is recorded. The critical pore entry diameter is the pore diameter that corresponds to the highest peak of the differential curve. Table 2.8 shows the test results of the critical pore entry diameter. Under the same w/b ratio, the critical pore entry diameter increased with the increasing amount of EX. The critical pore entry diameter was decreased by the restrained condition. In other words, under the restrained conditions, the pore diameter tended to become finer, which may be explained by the hypotheses below.

The first hypothesis is relevant to the formation of the ettringite crystal when the expansive additive reacts with water, which will fill the microspore in the cement–expansive paste matrix. This phenomenon leads to a denser pore structure. This hypothesis was also reported by Van et al. [2.25] and Nguyen et al. [2.2].

For the second hypothesis, the pore size distribution of the restrained sample shifts to a finer region because of the chemical stress effect [2.6]. The expansive force is caused by the EX hydration that makes the pore diameter become smaller by the constraining pressure of the external constraining restrained mold (e.g., framework) (Figure 2.14).

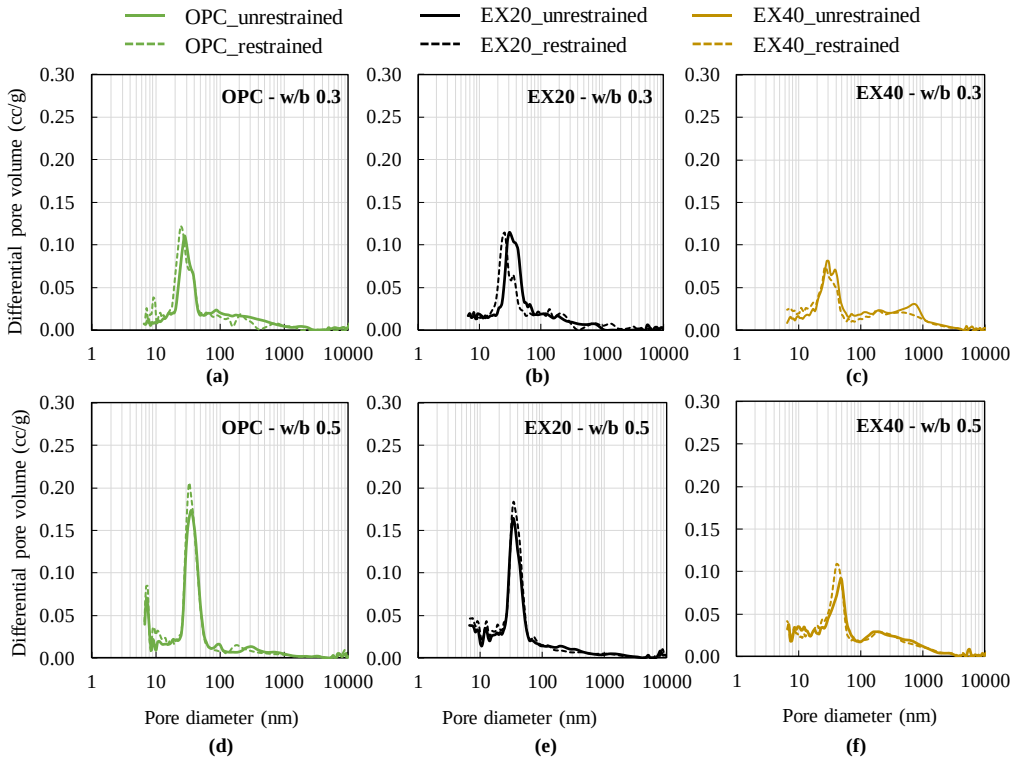

Figure 2.13 Effect of the triaxial restrained condition on the pore size distribution of the cement and expansive mortar under the restrained and unrestrained conditions with different w/b ratios: (a, b, c) test results of OPC, EX20, and EX40 with w/b 0.3, respectively; and (d, e, f) test results of OPC, EX20, and EX40 with w/b 0.5, respectively.

Table 2.8 Critical pore entry diameter (nm)

Sample	w/b 0.3		w/b 0.5	
	Unrestrained	Restrained	Unrestrained	Restrained
OPC	28.11	24.28	35.95	33.28
EX20	30.77	26.05	33.89	33.89
EX40	28.26	26.24	48.38	40.81

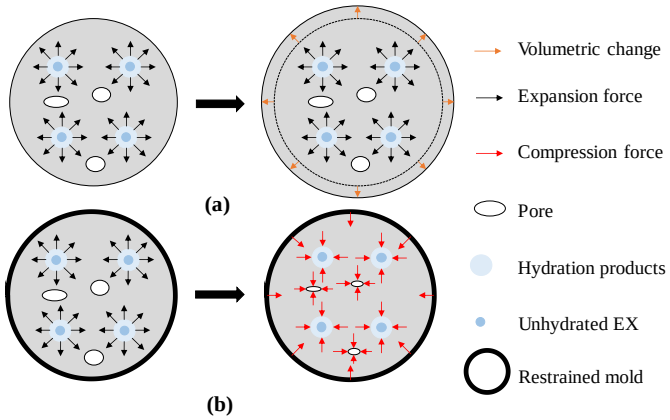

Figure 2.14 Schematic of the effect of chemical stress on the pore structure: (a) free condition and (b) triaxial restrained condition.

b) Total porosity

The under-water weighing test was used herein to determine the total porosity of concrete under the free and triaxial restrained conditions. Figure 2.15 illustrates the total porosity results for different concrete mixtures at 28 days. Consequently, the total porosity slightly increased as the amount of EX increased. This result is consistent with the findings of Choi et al. [2.21], who reported that the volume of the capillary pore increases with the increasing EX addition. The total porosity of the concrete with and without EX at the w/b ratio of 0.5 was higher than that at the w/b ratio of 0.3. The total porosity of the restrained sample at the w/b ratio of 0.5 was approximately 3% and 21% less than that of the unrestrained samples for EX20 and EX40, respectively. In other words, the pore structure of the expansive concrete was denser under the restrained condition. However, this tendency was not observed for EX40 at the w/b ratio of 0.3, which can be attributed to the higher concrete stiffness at a lower w/b ratio making the concrete expand more hardly, thereby leading to a decrease in the effect of the restrained condition. In conclusion, observing the effect of the restrained condition on the total porosity was easier with a lower stiffness in the expansive concrete.

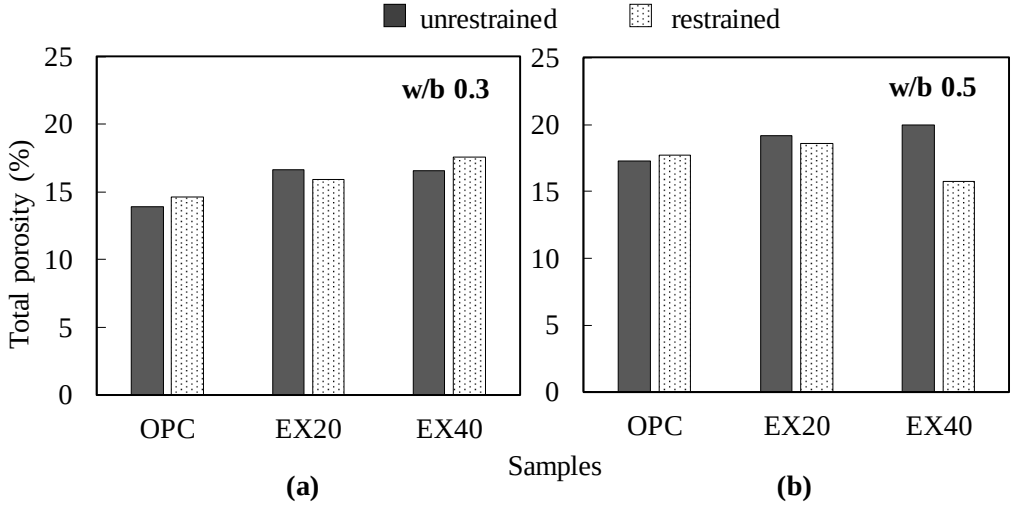

Figure 2.15 Relationship between the total porosity and EX contents under the unrestrained and triaxial restrained conditions: (a) w/b ratio of 0.3 and (b) w/b ratio of 0.5

2.5.3 Compressive Strength

2.5.3.1 Paste

Figure 2.16 shows the compressive strength test results of the cement paste with and without expansive additive with different w/b ratio of 0.3, 0.4, and 0.5. It can be seen that the compressive strength of all samples increases with increasing the curing time. It was also observed that with the lower w/b ratio gave the higher compressive strength of cement and cement-EX paste. These tendencies are consistent with the general knowledge of the compressive strength development of cement-based materials. In addition, the results indicated that the presence of EX leads to a decrease in the compressive strength of cement-EX paste when compared to that of Portland cement paste at 3, 7, 14 and 28 days. However, at 1day, the results showed an opposite trend, the compressive strength of cement-EX paste higher than that of cement paste.

This may be explained as follows: As mentioned previously, the mixture was cast into the prism steel mold and removed from the mold after 24 hours to cure under water until the day of testing (3, 7, 14, and 28 days). Meanwhile, at 1day, the compressive strength test was carried out immediately after removing the sample from the mold. In other words, the condition of the samples at 1 day and the other days were restrained and unrestrained (free) condition, respectively. Furthermore, under the restrained condition, compressive stress will be created on the inside of the specimen by the expansion of EX particle, it is known as a chemical prestressing concrete. This may be the main reason to lead to strength enhancement. Therefore, it can be concluded that the compressive strength of cement-EX paste is enhanced by the restrained condition. This conclusion is consistent with the results of previous studies [2.1], [2.1].

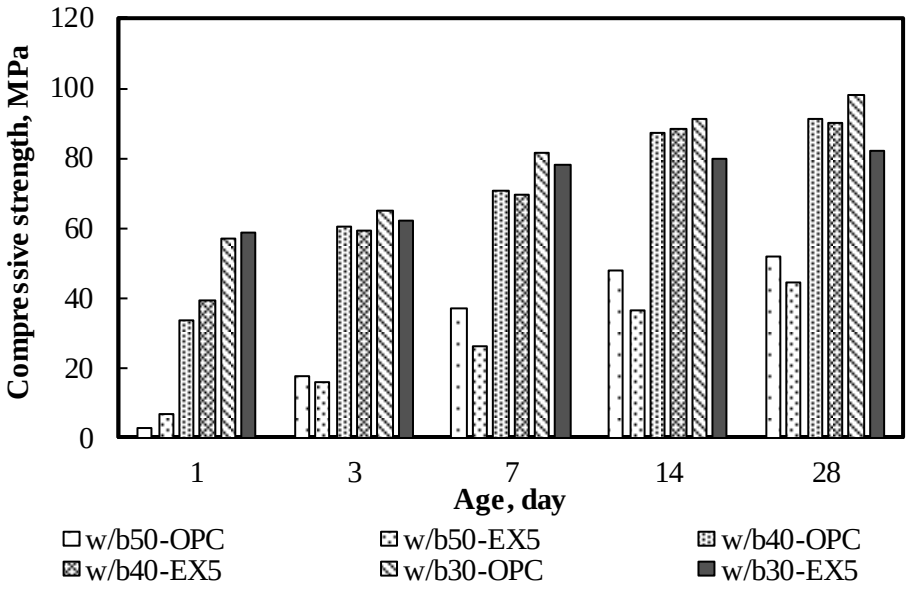

Figure 2.16 Compressive strength of Portland cement and cement-EX paste of different w/b ratio

2.5.3.2 Concrete

The compressive strengths of cement and expansive concrete were tested under the restrained and unrestrained conditions. Figure 2.17 illustrates the compressive strength results of all the concrete mixtures at ages of 3, 7, and 28 days of sealed curing age. The strength values were the average of three test samples. Figure 10 shows that the compressive strength of concrete varied between 45 MPa to 130 MPa and 20 MPa to 53 MPa for the w/b ratios of 0.3 and 0.5, respectively. The compressive strength of concrete slightly decreased with the increasing amount of EX because the total porosity increased with the increasing EX addition, which decreased the compressive strength. This result is consistent with those of the previous studies [2.21], [2.25], [2.26], which showed that the compressive strength decreases as the total porosity increases. The compressive strength of concrete at the w/b ratio of 0.3 was not enhanced by the restrained condition. This phenomenon was also found in the results of OPC and EX20 at the w/b ratio of 0.5. However, the effect of the restrained condition on the compressive strength was clearly observed for EX40 at the w/b

ratio of 0.5. The results indicate that the compressive strength of the restrained concrete was 12% larger than that of the unrestrained concrete and was approximately similar to that of EX20 at 28 days. The results also imply that at an early age of 3 days, the EX40 restrained concrete showed a larger compressive strength than both EX20 restrained and unrestrained concrete. This result is possibly caused by the decrease in the total porosity of the expansive concrete (Figure 2.15b) under the confinement condition, which led to its higher strength. These results demonstrate that the compressive strength of the expansive concrete was improved under the restrained conditions as the amount of EX increased to 40 kg/m^3. The conclusion corresponded to the results of Nagataki et al. [2.27], who studied the relations among unit expansive additive content, compressive strength, and restrained expansion rate.

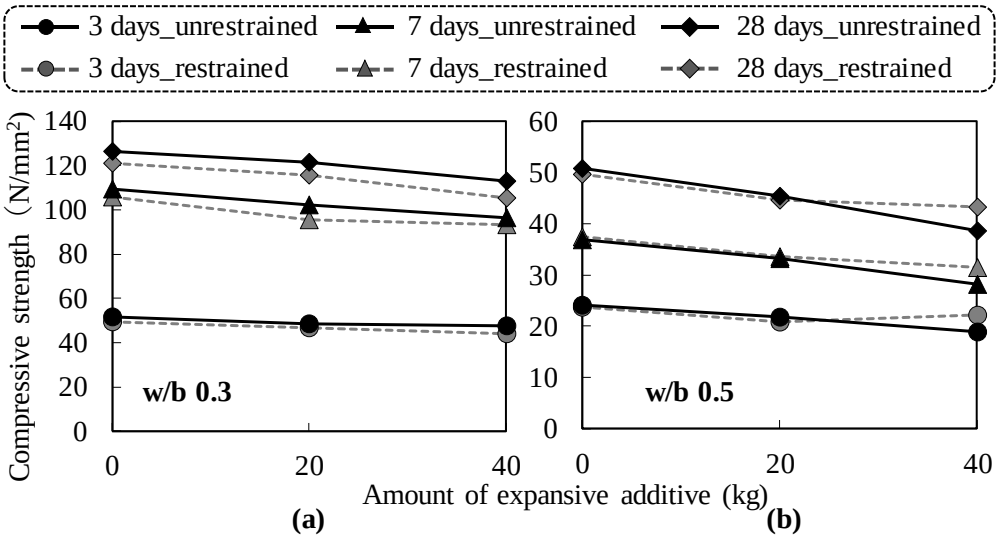

Figure 2.17 Relationship between the EX-content and compressive strength of concrete under the unrestrained and restrained conditions: (a) w/b ratio of 0.3 and (b) w/b ratio of 0.5.

2.5.4 Length Change Ratio and Expansion Strain

Figure 2.18 presents the length change ratio of the cement and expansive concrete with different w/b ratios and types of retrained conditions. In the case of w/b 0.3 (Figures 2.13a-2.13c), an insignificant effect of the restrained condition was observed on the length change ratio of both cement and expansive concrete. Moreover, these results indicate that the length change ratio increased when the expansive additive dosage was increased. These tendencies were found in the test results of w/b 0.5 (Figures 2.13d-2.13f). However, the effect of the restrained condition on the length change ratio was observed in the case of w/b 0.5, especially for EX40. The length change ratio of the restrained concrete was smaller than that of the unrestrained concrete and was clearly observed when the amount of the expansive additive reached 40 kg/m^3. When different restrained conditions were considered (free standard, JIS A 6202), the expansive concrete sample was tested following the JIS A 6202. It showed the smallest length change, which was caused by the restraint of the steel bars inside it and the two steel plates at both its ends. Meanwhile, the

expansive concrete sample was tested according to the free standard, which was restrained by reinforcement. The expansive concrete with w/b 0.3 had a smaller length change ratio compared to the expansive concrete with w/b 0.5. This result may be explained by the concrete stiffness. The concrete with w/b 0.5 had a smaller stiffness that led to a higher expansion of the concrete containing the expansive additive. This explanation is consistent with the hypothesis reported by Nguyen et al. [2.2].

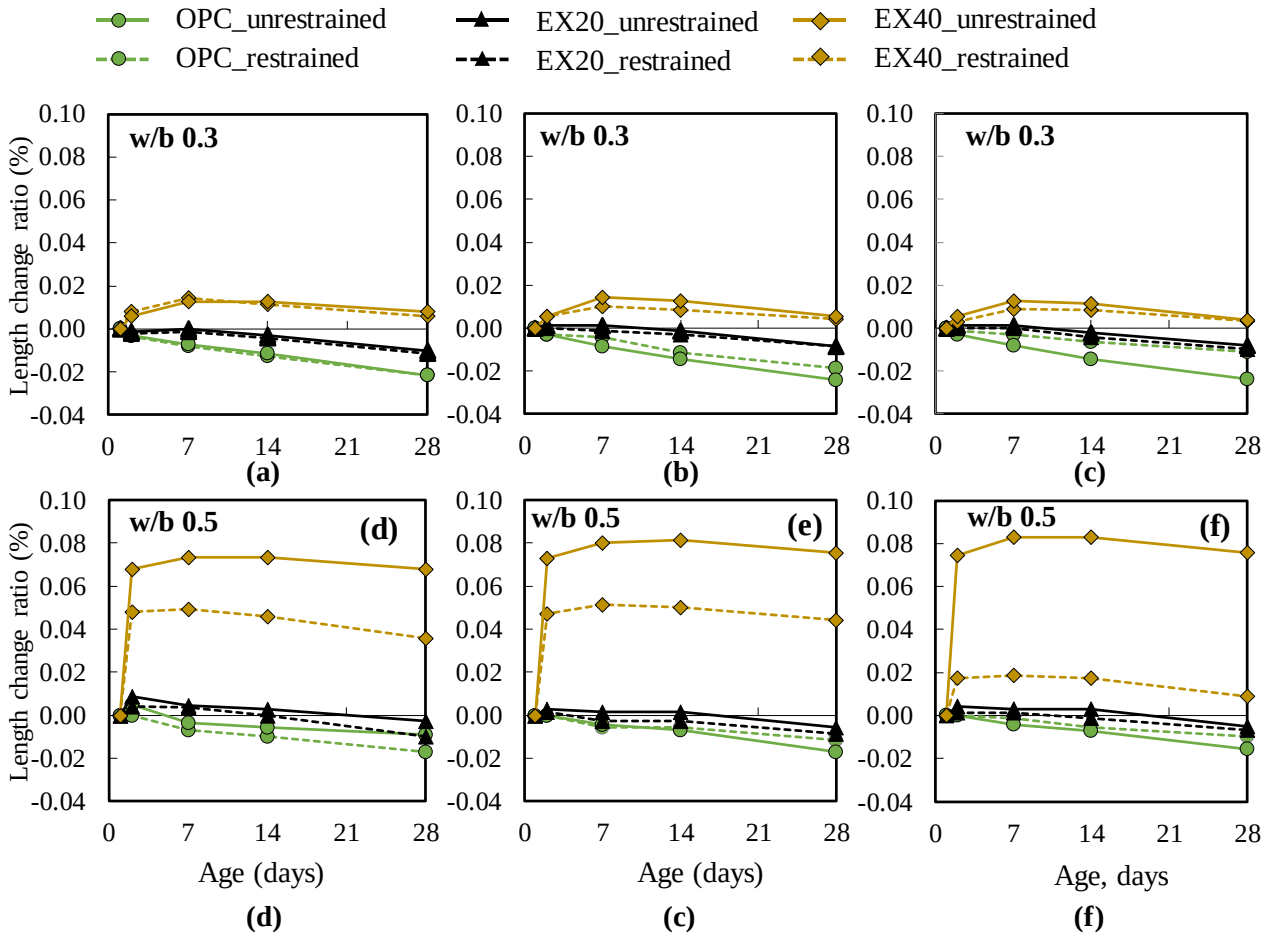

Figure 2.18 Length change ratio of concrete: (a, d) results of the sample measuring 75×75×400 mm^3; (b, e) results of the sample measuring 100×100×400 mm^3 (free standard); and (c, f) results of the sample measuring 100×100×400 mm^3 (JIS A 6202)

Figure 2.19 shows the expansion strain of the non-expansive and expansive concrete with different w/b ratios and types of restrained conditions. The expansion strain tendency was similar to the length change ratio of concrete (Figure 2.18). However, unlike in the test results of the length change ratio of concrete with w/b 0.3, the effect of the restrained condition on the expansion strain of the expansive concrete was observed, which may be attributed to the different testing positions. Meanwhile, the length change of the sample was determined by measuring the change of the whole sample. The expansion strain test was performed on the inside of a sample. Relevant to the expansion strain of EX40 with different types of restrained conditions (Figures 2.19e and 2.19f), the expansion strain of concrete restrained by the JIS A 6202 was higher than that restrained by the free standard. The higher expansion strain of EX40 by the JIS

method can be explained as follows: the expansion strain of concrete was determined by the strain gauge attached to the steel bar surface at the center of the specimen to measure the steel bar strain. In other words, the steel bar expanded (shrunk) with the expansion (or shrinking) of concrete. Therefore, when the expansive concrete was restrained by the JIS method, the effect of the expansion force on the steel bar was higher than that on the steel bar of free standard.

The results demonstrate that the expansive concrete expansion could be restrained by restraining a subject, such as a rebar. The rebar ratios and the degree of restraint could also affect the expansive concrete expansion. This study focused on a uniaxial restrained condition for the expansion strain test. Hence, studying the influence of the degree of restraint on the expansive concrete expansion will be very interesting in the future.

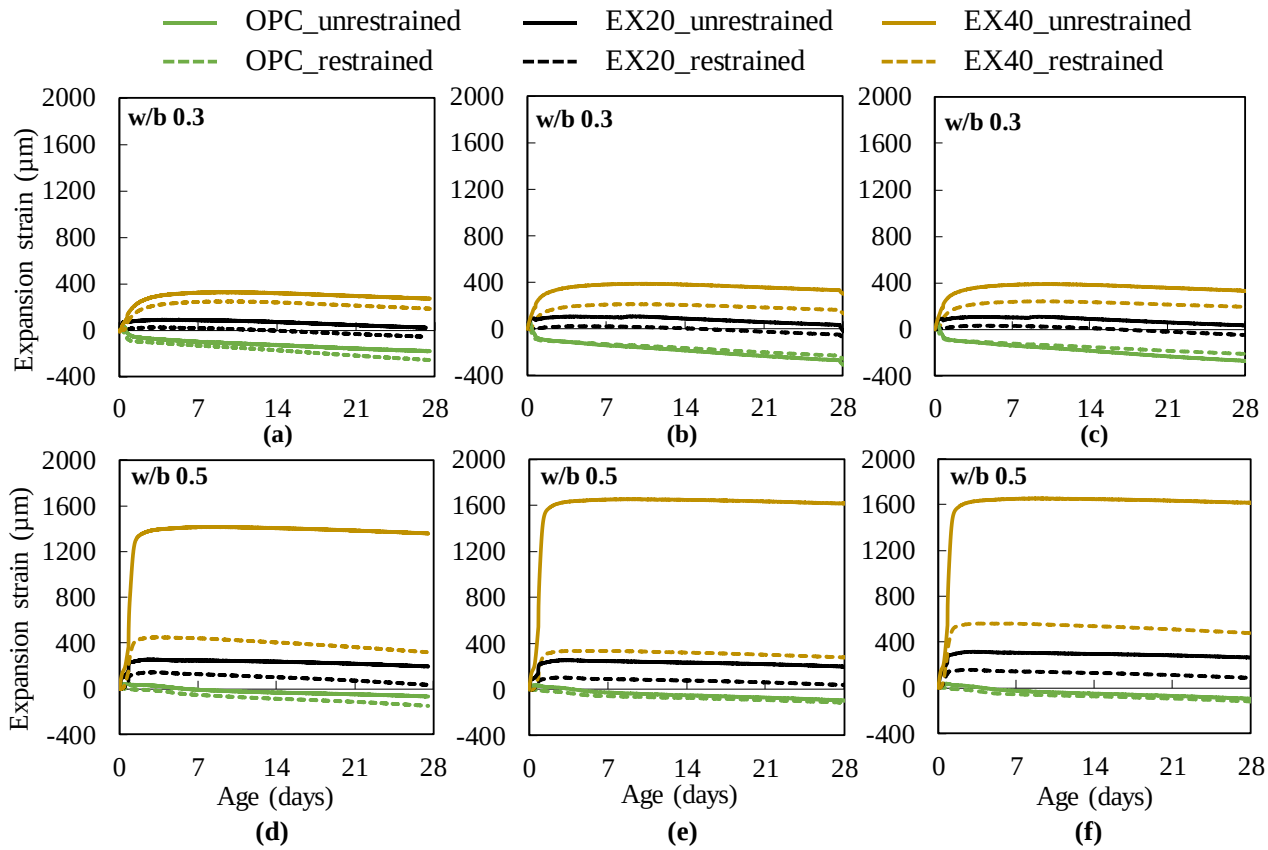

Figure 2.19 Expansion strain of concrete: (a, d) test results of the sample measuring 75×75×400 mm^3; (b, e) test results of the sample measuring 100×100×400 mm^3 (free standard); and (c, f) test results of the sample measuring 100×100×400 mm^3 (JIS A 6202)

2.5.5 Carbonation Depth

The carbonation depth of concrete with and without expansive additive at different w/b ratios was measured through the phenolphthalein test exposed in the controlled condition (temperature: 20°C; relative humidity: 60%; and CO_2 concentration: 5%) for 13 weeks (Table 2.8). The concrete carbonation depth results were

the average of 18 to 20 measurements from the exposed surface. The test results indicated that concrete was not carbonated under a w/b ratio of 0.3 compared with that under a w/b ratio of 0.5. This result may be attributed to the compact structure of the concrete at the lower w/b ratio. The concrete carbonation depth increased with the increasing w/b ratio. This observation is consistent with that reported by Singh et al. [2.28]. At the w/b ratio of 0.5, the carbonation depth increased with the addition of the expansive additive. However, comparing the different restrained conditions, the carbonation depth of the restrained condition was smaller than that of the free condition. This result can be explained by the denser structure of the restrained concrete caused by the compressed pore in the concrete by the chemical prestress effect. This phenomenon was discussed in Section *2.4.2.2*.

The results demonstrate that the carbonation resistance of the expansive concrete was enhanced by restraining. The concrete carbonation specimen was made under the uniaxial restrained condition. As mentioned, the chemical prestress effect made the pore structure of the expansive concrete denser under the restrained conditions. Nagataki et al. [2.27] also reported that the chemical prestress effect greatly depends on many factors, such as kind of cement, w/b ratio, curing method, reinforcing rebar ratio, and degree of restraint. Therefore, in the future, more investigations are necessary to find the influence of these factors on the chemical prestress effect in expansive concrete.

Table 2.9 Carbonation depth of concrete (mm)

Sample	w/b 0.3		w/b 0.5	
	Unrestrained	Restrained	Unrestrained	Restrained
OPC	0	0	1.15	0.95
EX20	0	0	2.90	1.78
EX40	0	0	3.60	2.80

2.5.6 Frost Resistance

Figure 2.15 shows a comparison of the RDMs of the Portland cement and expansive concrete under the restrained and unrestrained conditions at the w/b of 0.3 and 0.5. The values of the result were the average of two test samples.

The RDM decreased with the increasing amount of expansive additive in both the restrained and unrestrained conditions. The results demonstrate that the presence of EX led to a reduction of the frost resistance of concrete, especially for the unrestrained concrete. This result is consistent with that of the previous study [2.29] and may be explained by the formation of the micro-cracks caused by the expansion of the EX-hydration under the free conditions. When evaluating the effect of the restrained condition of the frost resistance of concrete, the results indicated that for the w/b ratio of 0.3, the restrained concretes had a higher RDM than the unrestrained concretes because the RDMs of OPC, EX20, and EX40 were approximately 80% and 87% at 300 cycles. For the w/b ratio of 0.5, observing the change of the RDM of

the OPC and EX20 was difficult. However, the expansive concrete (EX40) showed early frost damage with an RDM below 80% at 12 freezing–thawing cycles and below 60% at 100 cycles under free condition. Meanwhile, the RDM of EX40 was below 60% at 190 cycles under the restrained condition.

The results conclude that the frost resistance of the expansive concrete was enhanced by the restrained conditions at the lower w/b ratio. Furthermore, a previous study [2.7] found that under the triaxial restraint, the frost resistance of the Portland cement concrete was better than that of the uniaxial restrained concrete. According to this conclusion, the present research may be extended in the future by investigating the influence of the degree of restraint on the frost resistance of expansive concrete, especially the triaxial restraint.

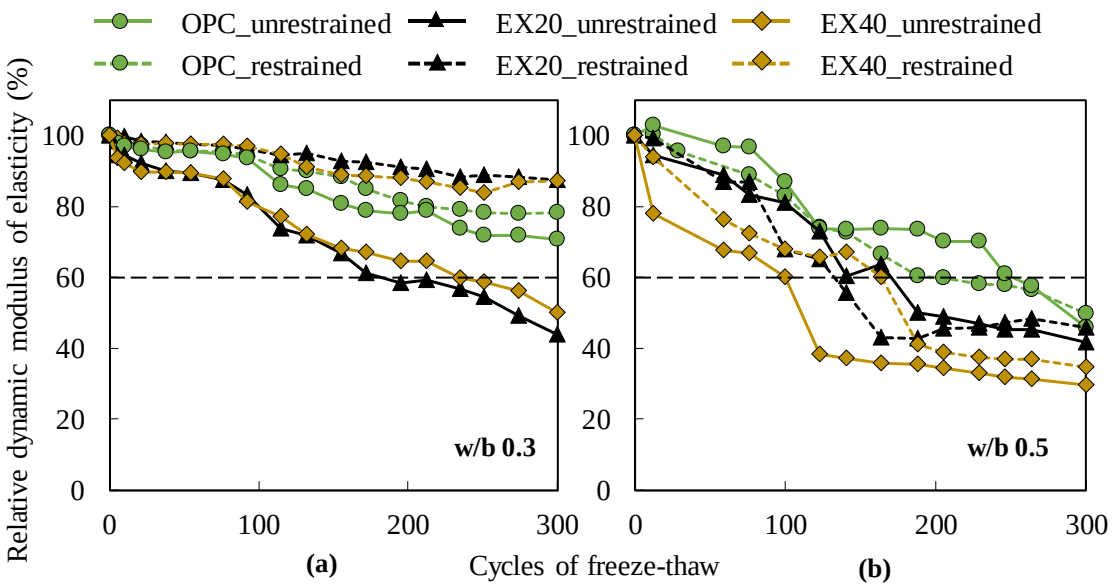

Figure 2.20 Comparison of the RDMs of cement and expansive concrete under the restrained and unrestrained conditions: (a) w/b ratio of 0.3 and (b) w/b ratio of 0.5.

2.6 Conclusion

1) The heat evolution of cement paste increases with increasing the addition of EX and increasing of curing temperature.
2) The presence of EX led to an increase in the total porosity of cement paste and concrete. However, that of expansive concrete was decreased by the restraining when the amount of EX was 40 kg/m^3 of concrete at a w/b ratio of 0.5. This is the reason why the compressive strength of the expansive concrete was enhanced under the restrained conditions when the amount of the expansive additive reached 40 kg/m^3 of concrete.
3) Under the restrained condition, the pore size distribution of the expansive mortar shifted to a smaller size.
4) The concrete expansion increased with the increasing amount of EX. The length change ratio and expansion strain of concrete with and without an expansive additive could be controlled by the restrained condition.
5) The concrete carbonation depth was not observed at the w/b ratio of 0.3. For the w/b of 0.5, the carbonation resistance of the expansive concrete was improved by restraining.
6) It is essential considering the effect of the restrained conditions in evaluating the various experimental results of the expansive concrete with a large expansive additive dosage (i.e., over 20 kg/m^3 concrete) or concrete combining EX with other cement replacement materials (e.g., fly ash and blast furnace slag).

References

[2.1] Lam N.T.; Sahamitmongkol R.; Tangtermsirikul S. Expansion and compressive strength of concrete with expansive additive", *Res. Dev. J.* 2008, *9*, 2, 40-49.

[2.2] Nguyen T.B.T.; Chatchawan R.; Saengsoy W.; Tangtermsirikul S.; Sugiyama T. Influences of different types of fly ash and confinement on performances of expansive mortars and concretes, *Constr. Build. Mater.* 2019, *209*, 176-186.

[2.3] ACI Committee 223 "Expansive cement concretes - Present state of knowledge", *ACI J.* Aug-1970, 583-610.

[2.4] Japanese Industrial Standard Committee. *Expansive additive for concrete (Amendment 1)*, JIS A 6202-2008.

[2.5] Sidney M.L. Section 5 - Calculations relating to concrete and masonry. In *Construction calculations manual*, 1st ed.; Elsevier Science: Elsevier Ltd., Netherlands, 2012; pp. 211-264.

[2.6] Tsuji Y.; Maruyama H.; A fundamental study on effect of restraint method on mechanical properties of expansive concrete. Proceedings of the 6th Annual Conference on Concrete Engineering, 1984, *86*, 341-344.

[2.7] Harada A. Influence of reinforcement restraint on the length change and frost damage during freezing-thawing action in structural concrete. Master Thesis, Muroran Institute of Technology, Japan, March-2011.

[2.8] Lobo C.; Cohen M.D. Pore structure development in type K expansive cement pastes. *Cem. Concr. Res.* 1991, *21*, issues 2-3, 229-241.

[2.9] A.M. Neville, Properties of Concrete, fifth ed., Prentice Hall, Pearson, Harlow, England.

[2.10] T. Higuchi, M. Eguchi, M. Morioka, E. Sakai, Hydration and Properties of Expansive Additive Treated High Temperature Carbonation, Cement and Concrete Research 64 (2014) 11-16.

[2.11] Shen J.; Xu Q. Effect of moisture content and porosity on compressive strength of concrete during drying at 105℃. *Constr. Build. Mater.* 2019, *195*, 19-27.

[2.12] Beaudoin J.J. Porosity measurement of some hydrated cementitious systems by high pressure mercury intrusion-microstructural limitations. *Cem. Concr. Res.* 1979, *9*, issue 6, 771-781.

[2.13] Aligizaki K.K. *Pore Structure of Cement-Based Material: Testing, Interpretation and Requirements*, 1st ed.; CRC Press: Taylor & Francis, American, 2005.

[2.14] Japanese Industrial Standard Committee. *Method of test for compressive strength of concrete*, JIS A 1108-2018.

[2.15] Japanese Industrial Standard Committee. Method of test for slump of concrete. JIS A 1101-2005.

[2.16] Japanese Industrial Standard Committee. Method of test for slump flow of concrete. JIS A 1150-2007.

[2.17] Japanese Industrial Standard Committee. Method of test for air content of fresh concrete by pressure method. JIS A 1128-2019.

[2.18] Japanese Industrial Standard Committee. Methods measurement for length change of mortar and concrete-Part 3: Method with dial gauge, JIS A 1129, 2010.

[2.19] Japanese Industrial Standard Committee. *Method of accelerated carbonation test for concrete.* JIS A 1153-2012.
[2.20] Japanese Industrial Standard Committee. Method of test for resistance of concrete of freezing and thawing, JIS A 1148-2010
[2.21] H. Choi, M. Lim, H. Choi, T. Noguchi, R. Kitagaki. Modelling of creep of concrete mixed with expansive additives. Magazine of Concrete Research, 2015, 67 (7), pp.335-348.
[2.22] I. Maruyama, Time Dependent Property of Cement-Based Materials on the Basis of Micro-Mechanics, Ph.D. Thesis, University of Tokyo, Japan, March 2003 (in Japanese).
[2.23] W. Nocun-Wczelik, A. Stok, Z. Konik, Heat evolution in hydrating expansive cement systems. J Therm Anal Calorim. 101 (2010), pp. 527-532.
[2.24] Scrivener K.; Snellings R.; Lothenbach B. *A practical guide to microstructural analysis of cementitious materials*, 1st ed.; CRC Press: Boca Raton, America, 2016.
[2.25] Van N.D., Choi H.; Hama Y. Modeling early age hydration reaction and predicting compressive strength of cement paste mixed with expansive additive. *Constr. Build. Mater.* 2019, *223*, 994-1007.
[2.26] Kim Y.Y.; Lee K.M.; Bang J.W.; Kwon S.J. Effect of w/c ratio on durability and porosity in cement mortar with constant cement amount. *Ad. Mater. Sci. Eng.* 2014, *2014*, Article ID 273460.
[2.27] Nagataki S.; Gomi H. Expansive admixtures (mainly ettringite). *Cem. Concr. Com.* 1998, *20*, 163-170.
[2.28] Singh N.; Singh S.P. Reviewing the Carbonation Resistance of Concrete. J. Mater. Eng. Struc. 2016, *3*, 35-57.
[2.29] Makoto S.; Kentoro S.; Yoshihiko H.; Ryoetsu Y. Frost Resistance of Expansive Concrete, Japan Society of Civil Engineers 67th Annual Academic Lecture, 2012 (in Japanese).

CHAPTER 3

MODELING EARLY AGE THE HYDRATION OF CEMENT PASTE MIXED WITH EXPANSIVE ADDITIVE

CHAPTER 3 MODELING EARLY AGE THE HYDRATION OF CEMENT PASTE MIXED WITH EXPANSIVE ADDITIVE

3.1 Introduction

An expansive additive (EX) is an admixture that reacts when mixed with cement and water: the expansive concrete expands due to the production of ettringite or calcium hydroxide arising from a hydration reaction [3.1]. EX is commonly used in concrete to reduce cracks resulting from drying shrinkage. There is a strong relationship between the hydration reaction of cement–expansive additive (cement–EX) blends and the heat evolution, strength development, and volumetric changes of the material, all of which lead to the cracking of hardened concrete. Therefore, it is necessary to study the hydration of cement–EX blends rigorously. However, this hydration process is more complicated than the hydration process of ordinary Portland cement (OPC) because of the co-occurrence of both OPC and EX hydration processes.

To investigate the hydration kinetics of cement, over the past few decades, a number of studies have been conducted to model cement hydration in order to grasp the time-dependent properties of cement-based materials [3.2]. In a recent study, Tomosawa [3.3] proposed a hydration model to estimate the rate of heat evolution in the hydration of OPC. The model simulates the hydration process using a single kinetic equation. Based on Tomosawa's model, a hydration model of OPC was developed by Maruyama [3.4], where the volumetric changes of cement particles, chemically bound water, and physically bound water were considered. Maekawa et al. [3.5], [3.6] proposed a multicomponent model for the heat of hydration of Portland cement. The hydration rate was controlled by evaluating the temperature dependence, hydration level, and free water consumption. However, the models proposed so far [3.2], [3.3], [3.4], [3.5], [3.6] only focus on simulating the hydration reaction of a single cement particle. Therefore, a model that could simulate both the hydration of cement and the reaction of mineral admixtures is essential.

Several models that simulate the hydration of cement taking into account the reaction of mineral admixtures have been reported. Schindler et al. [3.7] proposed a hydration model for predicting the heat evolution of cementitious materials. The proposed model focuses on the effects of the chemical composition of cement, cement fineness, mixture proportions, and supplementary cementing materials (SCMs). Riding et al. [3.8] presented an empirical model for calculating the heat evolution owing to the hydration of concrete mixtures. The model takes into account the effects of cement chemistry, aggregate type, water–cement ratio, SCMs, chemical admixture type and dosage, and temperature of hydration. Based on results of isothermal microcalorimetry experiments, De Schutter [3.9], [3.10] also proposed a general kinetic hydration model of Portland cement and slag-blended cement. Merzouki et al. [3.11] proposed a kinetic hydration model to simulate the hydration of cement paste containing blast furnace slag by considering the production of calcium hydration in cement hydration and its consumption by slag hydration. Based on an experimental study, Tanaka et al. [3.12] proposed a method for estimating the adiabatic temperature rise in concrete made with blast furnace slag-blended cement. In addition, Park et al. [3.13] designed a microstructural hydration model of Portland cement considering the reduction in the hydration rate that occurs due to the interfacial area of contact between the free water and hydration products. Furthermore, a hydration model of slag–

cement blends was proposed by Xiao-Young et al. [3.14]. In this model, the production of calcium hydroxide in cement hydration and its consumption in slag reaction were considered. Narmluk and Nawa [3.15] investigated the effects of fly ash on the hydration kinetics of cement for low water to binder fly ash–cement mixtures at different curing temperatures using a modified shrinking-core model. It should be noted that most of the general models have simulated the hydration reaction of cement paste containing blast furnace slag and fly ash. Meanwhile, information about the degree of hydration of cement containing expansive additives is still limited. Specifically, a simulation model for the hydration of cement mixed with EX has not yet been established.

In this study, therefore, a simulation model was proposed for the hydration reaction of cement paste blended with an expansive additive. The degree of hydration and rate of heat evolution of cement paste containing expansive additive was obtained from the proposed hydration model. Subsequently, the experimental and calculated results were compared to validate the proposed model. Figure 3.1 shows a flow chart representing the work undertaken.

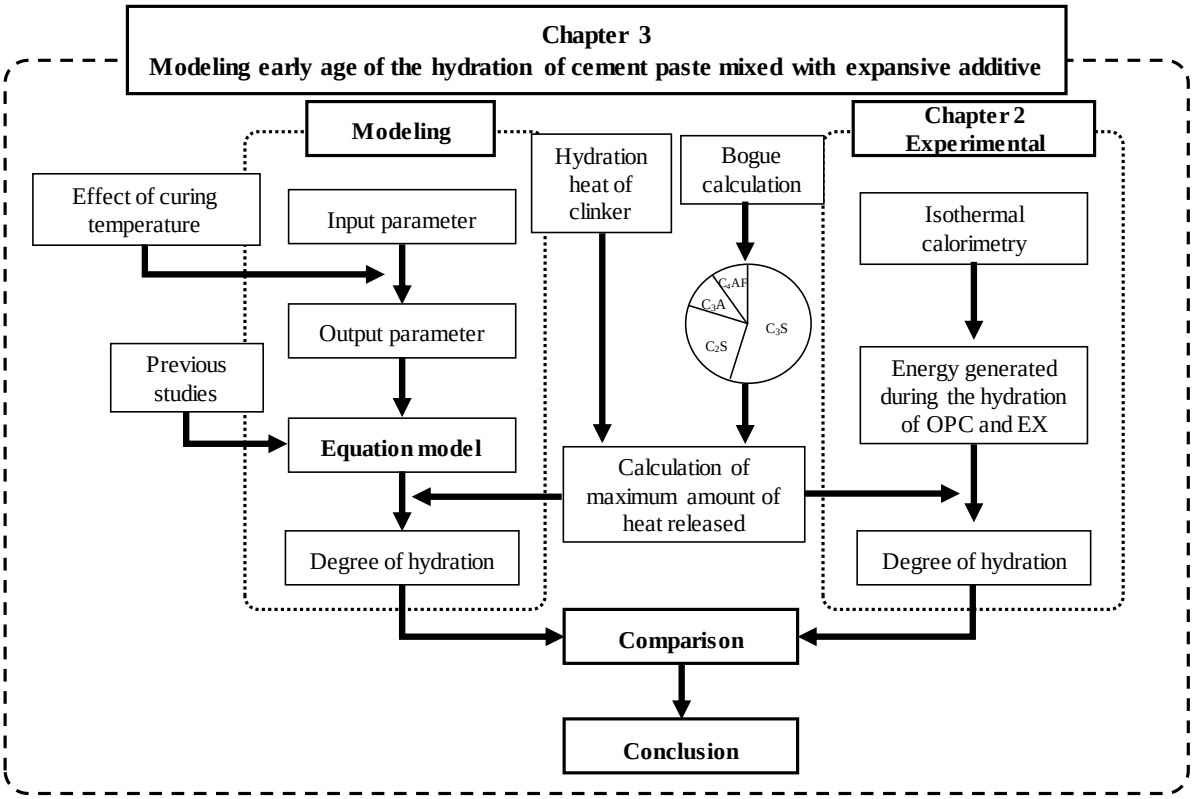

Figure 3.1 Flow chart

3.2 Hydration model

3.2.1 Model equation

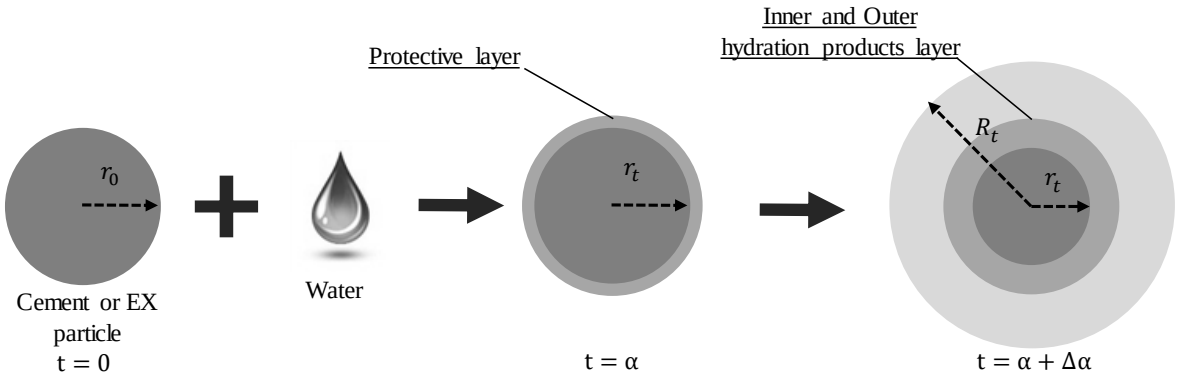

Figure 3.2 Schematic of hydration reaction of a single OPC or EX particle.

Based on the shrinking-core model, a fundamental hydration equation was proposed by Tomosawa [3.3] and developed by Maruyama [3.4] to simulate the hydration reaction of single cement particles. In the model introduced in [3.3] and [3.4], three coefficients were considered: k_d is the reaction coefficient in the induction period, D_e is the coefficient of effective diffusion of water through the hydration product layer (C–S–H gel), and k_r is the coefficient of the reaction rate of cement.

Referring to previous studies [3.2], [3.3], [3.4] that describe the hydration model of OPC, hydration of the cement–EX paste was modeled as shown in Eq. (3.1). In Eq. (3.1), we modified the calculation of some parameters to make it more suitable for simulating the hydration reaction of cement containing an expansive additive, as shown in Eq. (3), (4) (5), and (9). In order to simplify the hydration process, the cement and EX particles were simply assumed to be spherical in shape; a schematic representing the hydration reaction of a single OPC and EX particle is shown in Figure 3.2. The hydration reaction occurs immediately when water comes into contact with the OPC or EX particle and creates a protective film. After some time, the hydration product is generated. According to the shrinking-core model [3.16], the hydration reaction can be divided into three stages: (a) diffusion of water throughout the protective film surrounding the OPC or EX particle to the surface of the solid, (b) penetration and diffusion of water through the outer and inner hydration product layers to the surface of the unreacted OPC or EX particle, and (c) reaction of water with OPC or EX at this reaction surface.

$$\frac{d\alpha}{dt} = \frac{3C_{w\infty}}{(\gamma + W_{a,g})\rho_B r_0^2} \times \left(\frac{1}{\frac{1}{k_d r_0 \alpha_0^{2/3}} + \frac{\alpha_0^{-1/3} - (2-\alpha_0)^{-1/3}}{D_e} + \frac{1}{k_r r_0 \alpha_0^{2/3}}} \right) \quad \text{(Eq. 3.1)}$$

where α is the hydration degree of cement–EX blends; α_0 is the non-hydration degree; r_0 is the average radius of the initial OPC and EX particles (mm), as shown in Eq. (3.2) [3.17], [3.18]; S_B is the average specific surface area of OPC and EX (mm^2/g) as indicated in Eq. (3.3); S_{OPC} and S_{EX} are the specific surface areas of OPC and EX (mm^2/g), respectively; $(\gamma + W_{a,g})$ is the total chemically and physically

bound water in the cement–EX blends (g) as described in Eq. (3.4); γ is the average chemically bound water in cement–EX blends (g); $W_{a,g}$ is the average physically bound water in the cement–EX blends (g); ρ_B is the average specific gravity of OPC and EX; $C_{w\infty}$ is the amount of water in the outer region of the C-S-H gel (%). k_d and k_r are coefficients for the reaction (mm/h); D_e is the effective diffusion coefficient of water in the gel (mm^2/h).

$$\mathrm{r_0} = \frac{3}{\mathrm{S_B} \times \rho_\mathrm{B}} \quad \text{(Eq. 3.2)}$$

$$\mathrm{S_B} = \mathrm{S_{OPC}} \cdot \frac{\mathrm{C_0}}{\mathrm{C_0 + EX_0}} + \mathrm{S_{EX}} \cdot \frac{\mathrm{EX_0}}{\mathrm{C_0 + EX_0}} \quad \text{(Eq. 3.3)}$$

$$\left(\gamma + \mathrm{W_{a,g}}\right) = 0.42 \cdot \frac{\mathrm{C_0}}{\mathrm{C_0 + EX_0}} + 0.48 \cdot \frac{\mathrm{EX_0}}{\mathrm{C_0 + EX_0}} \quad \text{(Eq. 3.4)}$$

In Eqs. (3)–(5), C_0 and EX_0 are the mass fractions of the OPC and EX in the mixed sample, respectively. The reaction coefficient k_d [3.19], [3.20], [3.21] is assumed to be a function of the hydration degree (mm/h), as shown in Eq. (3.5), where B (mm/h) and C (mm/h) are the rate-determining coefficients; B controls the rate of protective film formation and C controls the rate of protective film decay [3.15], and r_t is the average radius of an unhydrated OPC and EX particle (mm).

$$\mathrm{k_d} = \frac{\mathrm{B}}{\alpha^{1.5}} + \mathrm{C(r_0 - r_t)^4} \quad \text{(Eq. 3.5)}$$

The effective diffusion coefficient of water D_e (mm^2/h) [3.20], [3.21], [3.22], [3.23] in the gel, assumed to be a function of the degree of hydration, is shown in Eq. (3.6). Here, D_{e0} is the initial diffusion coefficient of water in the gel (mm^2/h).

$$\mathrm{D_e} = \mathrm{D_{e0}} \ln\left(\frac{1}{\alpha}\right) \quad \text{(Eq. 3.6)}$$

The amount of water in the outer region of the C–S–H gel is expressed as a function of the degree of hydration, as shown in Eqs. (3.7) and (3.8). $C_{w\infty}$ is also described as decrease in the amount of available water in the capillary pores [3.14], [3.15]. This implies that the amount of available water will decrease when the cement and EX react with water to create the hydration product layer. In this work, therefore, it was necessary to consider the decrease in the amount of available water, caused by the cement and EX reactions. Theoretically [3.24], at complete hydration, 1 g of cement chemically binds with approximately 0.23 g of water during the cement hydration reactions and 0.19 g of physically bound gel water.
For the OPC paste, the $C_{w\infty}$ [3.14], [3.15] can be determined using the following equation:

$$\mathrm{C_{w\infty}} = \frac{\mathrm{w_0} - 0.42\mathrm{C_0}\alpha_{\mathrm{OPC}}}{\mathrm{w_0}} \quad \text{(Eq. 3.7)}$$

where 0.42 represents the total chemically and physically bound water, w_0 is the mass fraction of water in the mixed sample, and α_{OPC} is the degree of hydration of OPC.

The physically bound water is called evaporable water, which is calculated by drying the specimen in an oven at 105 °C for 24 h. The chemically bound water, also called non-evaporable water, is determined by heating the specimen at approximately 1000 °C for approximately 30 min. The loss of weight in the sample from 105 °C to approximately 1000 °C was interpreted to be the loss of chemically bond water [3.25], [3.21].

According to the experimental results, the total chemically bound water and physically bound water of EX was 0.48 g. Therefore, for cement–EX blends, the $C_{w\infty}$ is determined by the following equation:

$$\mathrm{C_{w\infty}} = \frac{\mathrm{w_0} - 0.42\mathrm{C_0}\alpha_{\mathrm{OPC}} - 0.48\mathrm{EX_0}\alpha_{\mathrm{EX}}}{\mathrm{w_0}} \quad \text{(Eq. 3.8)}$$

where α_{EX} is the degree of hydration of EX.

The effect of the curing temperature on these coefficients was assumed to follow Arrhenius' law as shown in Eqs. (9a)–(9d) [3.3], [3.4], [3.14], [3.15]:

$$\mathrm{B} = \mathrm{B_{20}}\exp\left(-\beta_1(1/\mathrm{T} - 1/293\right) \quad \text{(Eq. 3.9a)}$$

$$\mathrm{C} = \mathrm{C_{20}}\exp\left(-\beta_2(1/\mathrm{T} - 1/293\right) \quad \text{(Eq. 3.9b)}$$

$$\mathrm{D_e} = \mathrm{D_{e20}}\exp\left(-\beta_3(1/\mathrm{T} - 1/293\right) \quad \text{(Eq. 3.9c)}$$

$$\mathrm{k_r} = \mathrm{k_{r20}}\exp\left(-\mathrm{E/R}(1/\mathrm{T} - 1/293\right) \quad \text{(Eq. 3.9d)}$$

where β_1, β_2, β_3, and E/R are temperature sensitivity coefficients and B_{20} (mm/h), C_{20} (mm/h), D_{e20} (mm^2/h) , and k_{r20} (mm/h) are the values of B , C, D_e, and k_r at 20 °C (293K), respectively. In these experiments, the curing temperatures were 5, 20, and 40 °C; the values of B, C, D_e, and k_r varied for different curing temperatures.

Van Breugel [3.8], [3.26] assumed that the degree of cement hydration was proportional to the heat released, as shown in Eq. (3.10), where $\mathrm{Q_{(t)}}$ (J/g) is the heat released at time t and $\mathrm{Q_{max}}$ (J/g) is the total heat available for the blended cement hydration reaction.

$$\alpha_{(\mathrm{t})} = \frac{\mathrm{Q_{(t)}}}{\mathrm{Q_{max}}} \quad \text{(Eq. 3.10)}$$

The maximum heat released by the OPC and EX mixture at complete hydration can be determined by the following equation [3.8], [3.26]:

$$\mathrm{Q_{(OPC\ or\ EX)}} = \mathrm{q_1}.(\%\mathrm{C_3S}) + \mathrm{q_2}.(\%\mathrm{C_2S}) + \mathrm{q_3}.(\%\mathrm{C_3A}) + \mathrm{q_4}.(\%\mathrm{C_4AF}) + \mathrm{q_5}.(\%\mathrm{frC}) + \mathrm{q_6}.(\%\mathrm{MgO}) \quad \text{(Eq. 3.11)}$$

where q_1, q_2, q_3, q_4, q_5, and q_6 denote the heat evolved for each composition (J/g), predicted by Van Breugel's study [3.26] and listed in Table 4. $\%C_3S$, $\%C_2S$, $\%C_3A$, $\%C_4AF$, $\%frC$, and $\%MgO$ are the mineral compositions of cement obtained by the Bogue calculation and shown in Table 2.2 (see Chapter 2).

Table 3.1 Relative contribution of clinker compounds to heat of hydration (J/g)

Author	q_1 $\%C_3S$	q_2 $\%C_2S$	q_3 $\%C_3A$	q_4 $\%C_4AF$	q_5 %frC	q_6 %MgO
Woods [3.27]	570	260	840	125	-	-
Bogue [3.28]	500	260	866	125	-	-
Wm. Lerch et al. [3.29]	500	260	866	420	1166	850
Thorvaldson [3.30]	-	-	-	1166	-	-
Chatharin [3.31]	500	251	1340	420	1172	-
Adam [3.32]	-	-	500	170	840	-
Newkirk [3.33]	560	1360	300	-	-	-

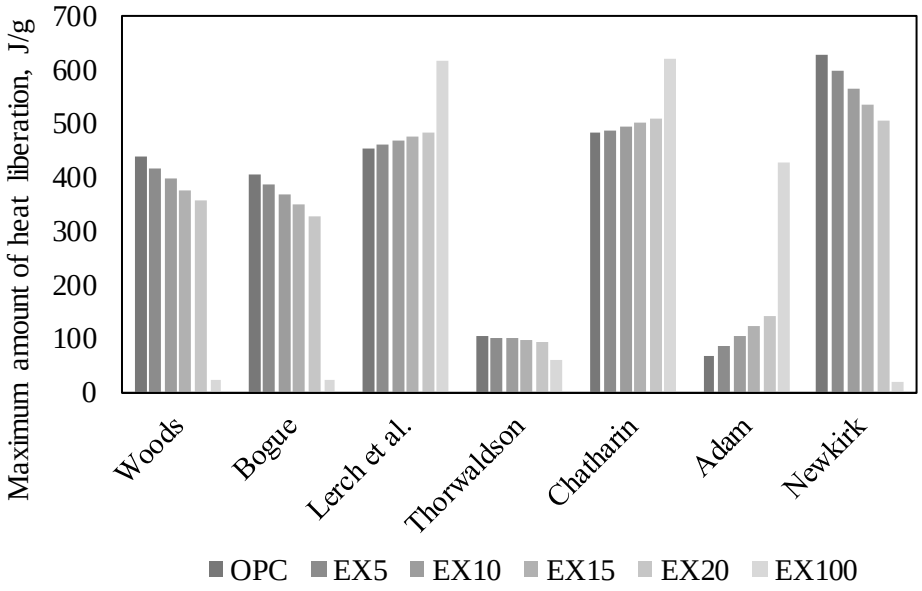

Figure 3.3 Maximum amount of heat liberated by OPC and cement–EX blends.

Based on Eq. (Eq. 3.11), the maximum heat of hydration of OPC and cement–EX blends was determined. Results are shown schematically in Figure 3.3; as can be seen, the maximum heat hydration of OPC and cement–EX blends increased with the addition of expansive additives. In order to determine the maximum amounts of heat liberated by OPC, Maruyama [3.19] has used the heat of hydration of the constituents of Woods. However, because of the expansive additive containing a large amount of free lime (frC) [3.34], [3.35], the relative contribution to the heat of hydration of the free line needed to be considered in Eq. (3.11). In this study, therefore, the heats of hydration of the constituents of Wm Lerch et al. (see Table 3.1) were used to calculate the maximum heat of hydration. Our calculated results correspond to the finding of Choi [3.36].

According to Eq. (3.10), the hydration degree of the cement–EX blends is defined as the ratio between the heat released at time *t* to the maximum amount of heat released at complete hydration. Q_t is determined using the isothermal calorimetry method and Q_{max} is calculated using the following equation:

$$Q_{(max)} = Q_{OPC} \cdot \frac{C_0}{C_0 + EX_0} + Q_{EX} \cdot \frac{EX_0}{C_0 + EX_0} \quad \text{(Eq. 3.12)}$$

where Q_{OPC} and Q_{EX} are the maximum amounts of heat released by the OPC and EX (J/g), respectively. Note that Q_{OPC} and Q_{EX} are calculated from Eq. (3.11).

3.2.2 Effect of mineral composition on the model parameters

Previous studies [3.4], [3.37] reported a relationship between the model parameters B, D, C, and k_r and the cement component (C_3S, C_3A, and C_2S). However, the detailed reasons for explaining these relationships were not established. Therefore, in this section, the relationship between the mineral composition and model parameters was deduced on the basis of the degree of hydration of the composition and the least-squares method. In addition, we have also discussed why the model parameters have a relation with the mineral composition of the cement.

Odler [3.38] determined the hydration degree of the mineral composition as a function of hydration time (see Figure 3.4), demonstrating that the hydration of C_3A and C_4AF began immediately after the initial contact of the OPC or EX with water. The hydration of C_3S started after approximately 2 h, and that of C_2S started at around 30 h. In addition, Jansen [3.39] suggested a typical calorimetric curve for the rate of heat evolution of cement-based materials (see Figure 3.5). In this figure, the hydration process comprised four periods: the initial period, induction period (also called the dormant period), acceleration period, and deceleration period. In the initial period, C_3A and C_4AF began to undergo the reaction; during the induction and acceleration periods, the hydration of C_3S occurred; finally, during the deceleration period, C_2S began to undergo its reaction and the C_3A reaction speed increased. Furthermore, in this study, the least-squares method was used to determine the value of model parameters. Fitting the experimental results to the model using the least-squares method showed that B_{20} and D_{20} had an effect on the induction period and deceleration period, respectively. On the other hand, k_{r20} had an effect on both the acceleration and deceleration periods.

From this information, the relationship between the mineral composition and the model parameters was deduced. The parameters B, D, and k_r showed a relationship with the C_3S, ($C_3A + C_2S$), and ($C_3S + C_3A$) phase, respectively. In other words, the model parameters can be represented as a function of the components of the cement.

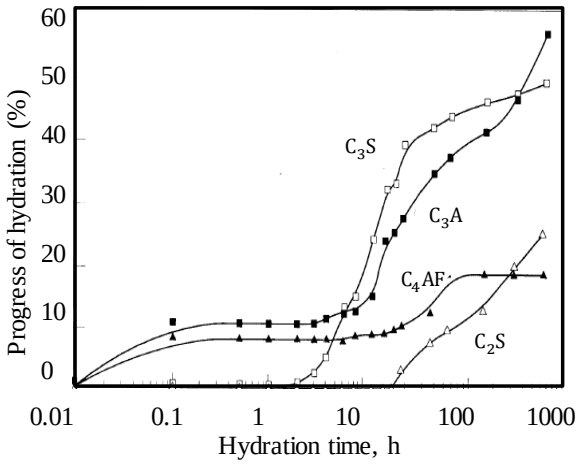

Figure 3.4 Hydration degree of mineral compositions [3.38].

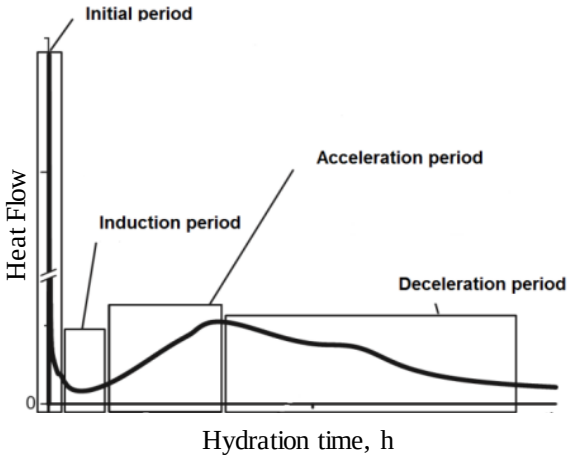

Figure 3.5 Changes detected in phase composition of the OPC paste at different periods of OPC hydration [3.39].

3.3 Results and Discussion

3.3.1 Relationship between mineral composition and model parameters

Model parameters determined using the least-squares method are shown in Table 3.2 for a w/b of 0.3 and 0.5 at 20 ℃. C_{20} is 1×10^9 for the OPC paste without expansive additive replacements and 5×10^8 for 5, 10, 15, and 20% expansive additive replacement contents. For EX100, the C_{20} are 5×10^{11} at w/b 0.3 and 0.5, respectively. The other model parameters varied with the EX replacement content: B and D increased and k_r decreased with the addition of the expansive additive. In addition, the dependence of model parameters B, D, and k_r on the mineral compositions of cement at different curing temperature is shown in Figure 3.6 and Figure 3.7 for w/b 0.3 and w/b 0.5, respectively. B and D decreased and k_r increased with increasing mineral content. However, an effect of the curing temperature on the tendency noted for these relationships was not observed. The results showed that the relationship between the model parameters and the mineral composition was approximately linear with a good correlation (approximately 0.9).

Table 3.2 Model parameters of Eqs. (3.9a)–(3.9d) at 20 ℃

w/b	Sample	B_{20}	C_{20}	D_{20}	k_{r20}	R^2
0.3	OPC100	3.6E-11	1.0E+9	2.5E-11	6.6E-8	0.96
	EX5	8.0E-11	5.0E+8	5.8E-11	6.3E-8	0.89
	EX10	1.3E-10	5.0E+8	8.5E-11	5.8E-8	0.96
	EX15	1.7E-10	5.0E+8	1.2E-10	5.7E-8	0.95
	EX20	2.4E-10	5.0E+8	1.7E-10	5.6E-8	0.87
	EX100	1.2E-12	5E+11	8.00E-7	8.85E-8	0.71
0.5	OPC100	3.6E-11	1.0E+9	2.5E-11	6.8E-8	0.89
	EX5	1.0E-10	5.0E+8	5.8E-11	6.0E-8	0.92
	EX10	1.5E-10	5.0E+8	1.0E-10	5.0E-8	0.93
	EX15	2.0E-10	5.0E+8	1.8E-10	5.2E-8	0.97
	EX20	2.6E-10	5.0E+8	3.0E-10	5.0E-8	0.96
	EX100	3.6E-8	5.0E+11	3.0E-10	1.25E-7	0.94

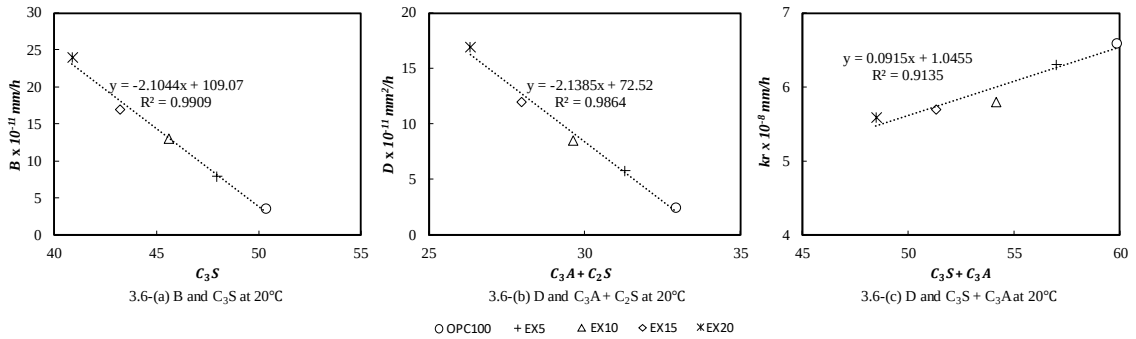

3.6-(a) B and C_3S at 20℃ 3.6-(b) D and C_3A+C_2S at 20℃ 3.6-(c) D and C_3S+C_3A at 20℃

Figure 3.6 Relationship between mineral composition and model parameters at w/b 0.3: (a) relationship between B and C_3S, (b) relationship between D and (C_3A + C_2S), and (c) relationship between k_r and (C_3S + C_3A) at 20℃, respectively.

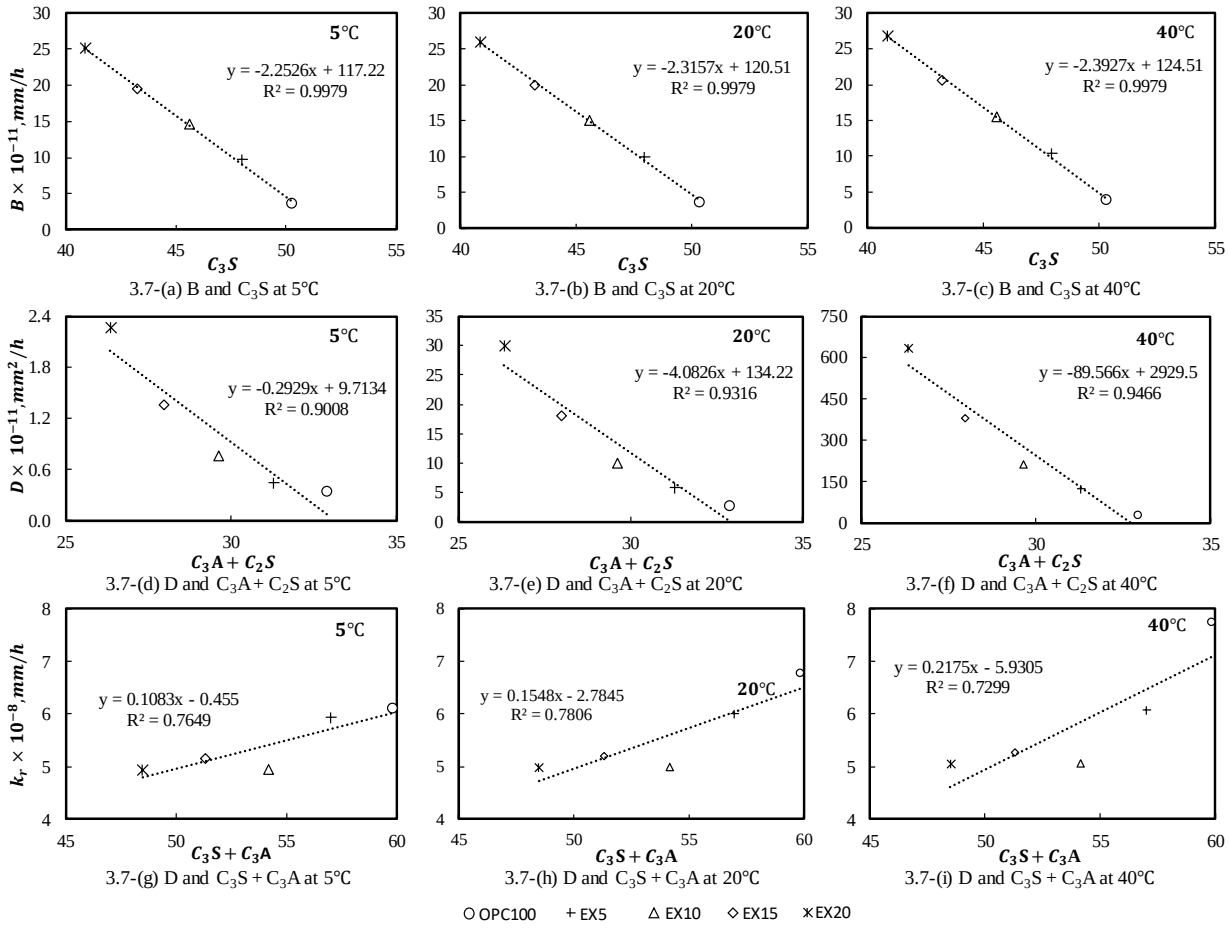

Figure 3.7 Relationship between mineral composition and model parameters at w/b 0.5: (a), (b), and (c) relationship between B and C_3S at 5℃, 20℃, and 40℃, respectively; (d), (c), and (e) relationship between D and (C_3A + C_2S) at 5℃, 20℃, and 40℃, respectively; (g), (h), and (i) relationship between k_r and (C_3S + C_3A) at 5℃, 20℃, and 40℃, respectively.

The results reported here demonstrate that the proposed suggestion can effectively explain the relationship between the model parameters and the mineral compositions, as explained in Section 3.3.2. Based on Eqs. (9a)–(9d), these relationships as a function of the mineral composition are shown in Table 3.3. Maruyama [3.4] suggested the parameters D and k_r to be functions of C_3S and $(C_3S + C_3A)$, respectively. These relationships were also proposed in a previous work reported by Wang [3.44], who reported that B, C, D, and k_r show a relationship with $(C_3S + C_3A)$, C_3S, C_2S, and C_3S, respectively. However, unlike in previous studies [4,44], in this study, B, D, and k_r were seen to be functions of C_3S, $(C_3A + C_2S)$, and $(C_3S + C_3A)$, respectively. The difference between previous studies [3.4] and [3.44] and our investigation arises from several factors. One factor is the materials used in the current study. Another factor may be the method to determine the model parameters and the experimental method. As shown in Table 3.3, the parameter C was not dependent on the cement component. The results also indicated that the value of C increased on increasing the curing temperature. A previous study [3.15] reported that C controls the rate of protective film decay. Therefore, it can be concluded that increasing the curing temperature leads to the rate of

protective film decay becoming faster. In other words, the higher curing temperature leads to a faster hydration reaction of cement and cement–EX paste. This conclusion is consistent with our results.

Table 3.3 Equations showing relationship between mineral composition and model parameters

Temperature		Equations	
5 ℃		$B = (-2.25 \times (C_3S\% + 117.2) \times 10^{-11}$	(22a)
		$D = (-0.29 \times (C_3A\% + C_2S\%) + 9.7) \times 10^{-11}$	(22b)
		$k_r = (0.11 \times (C_3S\% + C_3A\%) - 0.45) \times 10^{-8}$	(22c)
		OPC case: C = 2.0E+8; EX case: C = 0.5E+8	
20 ℃	w/b 0.3	$B = (-2.10 \times C_3S\% + 109.1) \times 10^{-11}$	(23a)
		$D = (-3.14 \times (C_3A\% + C_2S\%) + 72.5) \times 10^{-11}$	(23b)
		$k_r = (0.09 \times (C_3S\% + C_3A\%) - 1.04) \times 10^{-8}$	(23c)
		OPC case: C = 1.0E+9; EX case: C = 5.0E+8; (EX100: C = 5E+11)	
	w/b 0.5	$B = (-2.32 \times (C_3S\% + 120.5) \times 10^{-11}$	(24a)
		$D = (-4.08 \times (C_3A\% + C_2S\%) + 134.2) \times 10^{-11}$	(24b)
		$k_r = (0.15 \times (C_3S\% + C_3A\%) - 2.7) \times 10^{-8}$	(24c)
		OPC case: C = 1.0E+9; EX case: C = 5.0E+8; (EX100: C = 5E+11)	
40 ℃		$B = (-2.39 \times (C_3S\% + 124.5) \times 10^{-11}$	(25a)
		$D = (-89.57 \times (C_3A\% + C_2S\%) + 2929.5) \times 10^{-11}$	(25b)
		$k_r = (0.21 \times (C_3S\% + C_3A\%) - 5.9) \times 10^{-8}$	(25c)
		OPC case: C = 67E+8; EX case: C = 68E+8	

3.3.2 Verification of hydration model

As mentioned previously, the aim of this study was to propose a simulation model for the hydration reaction of cement–EX blends. In this section, therefore, first, to verify the heat evolution using the proposed model, experiments were performed using isothermal calorimetry at a curing temperature of 20 ℃. A comparison of the measured and the calculated rate of heat evolution for OPC100 and cement–EX pastes (EX5, EX10, EX15, and EX20) at w/b 0.5 is illustrated in Figure 3.8. The figure shows that the calculated and experimental results were in good agreement for all the samples. Furthermore, to verify the applicability of the proposed model and the effectiveness of Eqs. 3.9(a)-3.9(d), we measured and predicted the degrees of hydration for OPC100, EX5, and EX10 at different curing temperatures of 5 ℃, 20 ℃, and 40 ℃ with a w/b of 0.5, as illustrated in Figure 3.9. As shown in Figure 3.9, a higher curing temperature led to an accelerated degree of hydration. At the same curing temperature, the hydration degree increased with the addition of the EX replacement ratio at 72 h. The values of the temperature sensitivity coefficients for Arrhenius' law were obtained and are listed in Table 3.4. Good agreement between the calculated results and the measured results is evident here, as well. Finally, to evaluate the applicability of our model, a total comparison of the calculated and measured hydration degrees of all samples with a w/b of 0.3 and 0.5 at

curing temperatures of 5 ℃, 20 ℃, and 40 ℃ is shown in Figure 3.10. Most of the points fall within the accuracy limit lines.

Based on the results of the verification of the proposed model, we confirmed that our model shows good applicability for cement–EX blends and a wide range of curing temperatures. In addition, previous studies [3.4], [3.26], and [3.37] have shown that the hydration reaction of cement-based materials shows a relationship with properties of concrete such as its compressive strength, chemical shrinkage, volumetric change, and carbonation depth. Therefore, it is very useful to use our model to predict the mechanical properties and durability of expansive concrete. In order to prove our suggestion, in this study, the compressive strength of expansive concrete was predicted using our model through the gel/space ratio, which will be discussed next chapter.

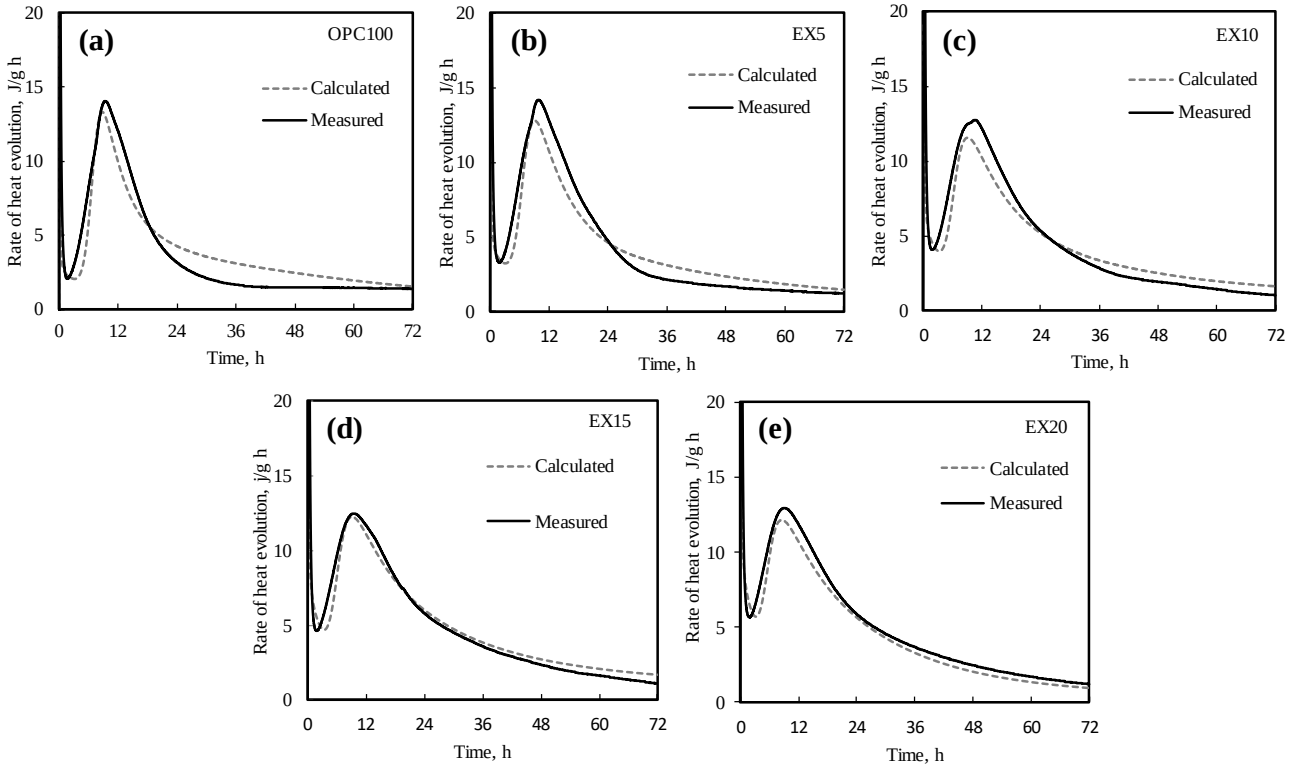

Figure 3.8 Comparison of calculated and measured rates of heat evolution at 20 ℃: (a) OPC100, (b) EX5, (c) EX10, (d) EX15, and (e) EX20.

Table 3.4 Coefficients for Arrhenius' law

Sample	β_1 (K)	β_2 (K)	β_3 (K)	E/R (K)
OPC100	150	8700	11000	600
EX5	150	12000	14000	60
EX10	150	12000	14000	60

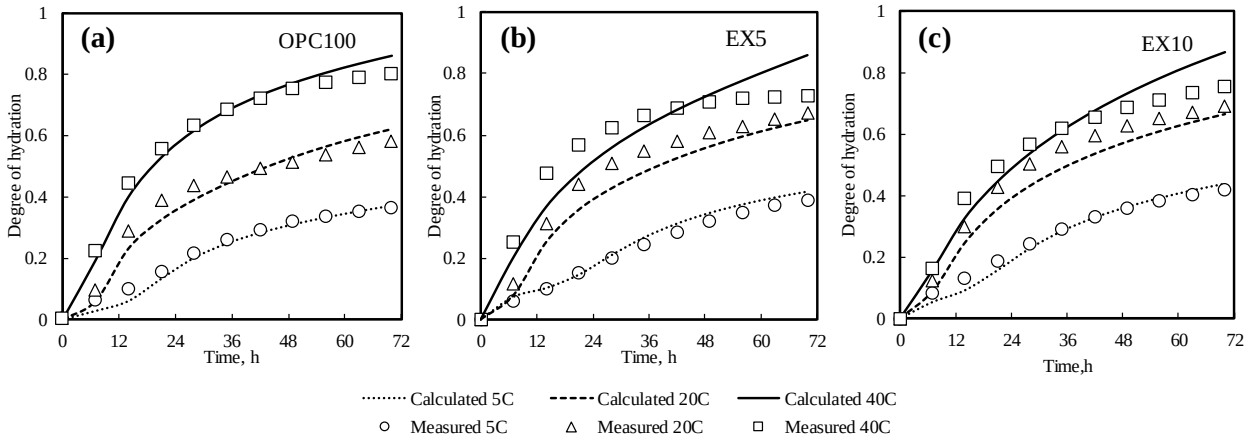

Figure 3.9 Calculated and measured hydration degrees of cement with and without EX at 5℃, 20℃, and 40 ℃ at w/b 0.5: (a) OPC100, (b) EX5, and EX10.

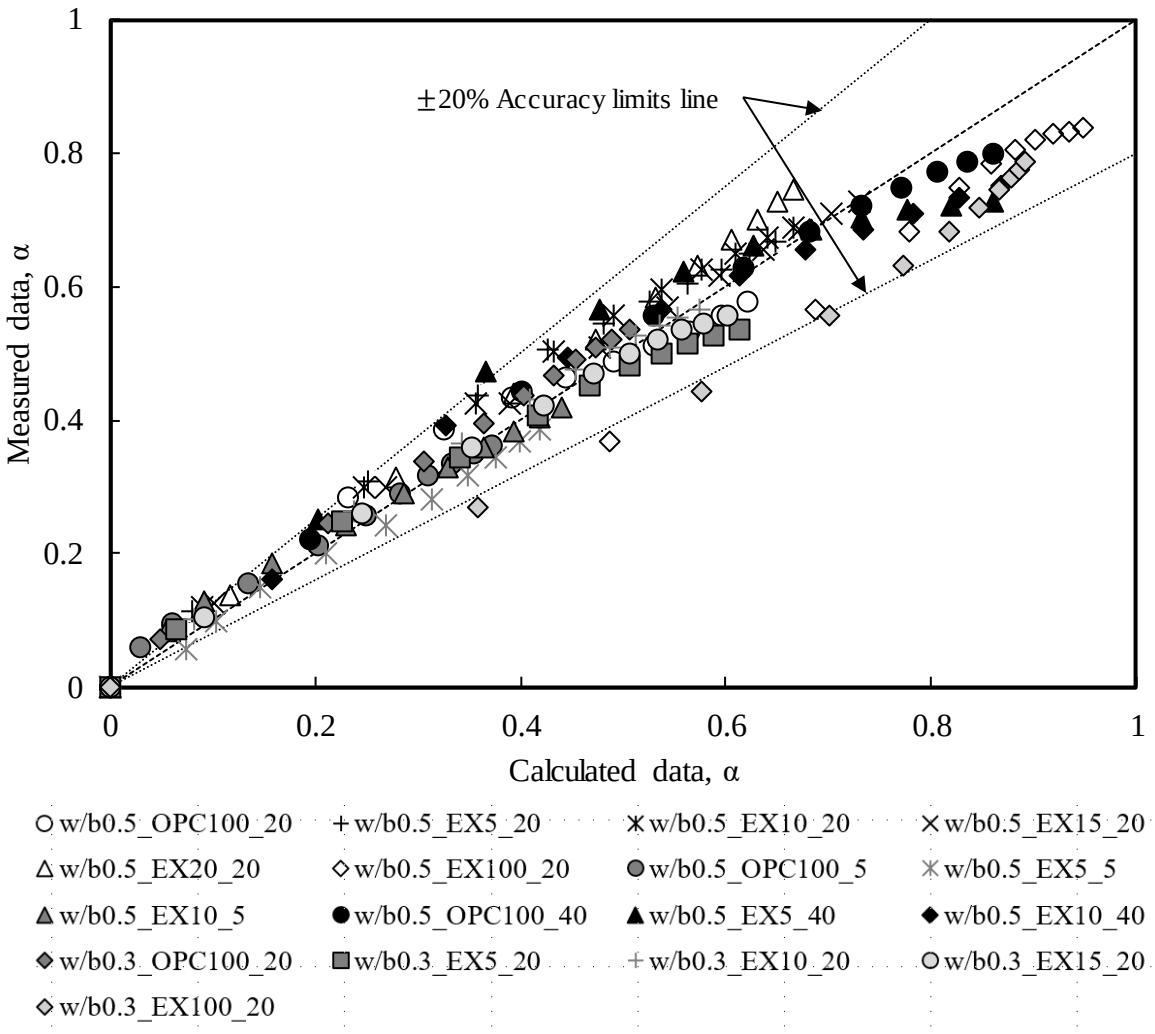

Figure 3.10 Total comparison of calculated and measured hydration degrees.

3.4 Conclusion

A numerical model is proposed to simulate the hydration reaction of cement paste containing expansive additive at an early age. In order to test the accuracy of the proposed model, the predicted results from the model for cement–EX blends were compared with experimental results. The results from the proposed model were in good agreement with experimental results and so the model proposed here can be applied to the simulation of the hydration reaction of cement containing an expansive additive. Furthermore, the present study found that the hydration parameters B, D, and k_r have a relationship with the C_3S, ($C_3A + C_2S$), and ($C_3S + C_3A$) phase, respectively.

References

[3.1] Recommended Practice for Expansive Concrete, Concrete Library of JSCE No.23, June 1994.

[3.2] I. Maruyama, T. Matsushita, T. Noguchi, 2008. Numerical modeling of Portland cement hydration, International RILEM Symposium on Concrete Modeling-CONMOD'08 26-28 May 2008, Delft, The Netherlands.

[3.3] F. Tomasawa, Development of a kinetic model for hydration of cement, in Proceeding of the 10th International Congress Chemistry of Cement, Gothenburg, Sweden, 2-6 June 1997; Chandra, S., Ed.; pp. 51-58.

[3.4] I. Maruyama, Time Dependent Property of Cement-Based Materials on the Basis of Micro-Mechanics, Ph.D. Thesis, University of Tokyo, Japan, March 2003 (in Japanese).

[3.5] K. Maekawa, R. Chaube, T. Kishi, Modeling of Concrete Performance: Hydration, Microstructure Formation and Mass Transport. London, New York: Routledge; 1998.

[3.6] K. Maekawa, T. Ishida, Modeling of structural performances under coupled environmental and weather actions. Materials and Structures. 35 (2002) pp. 591–602.

[3.7] K.A. Schindler, J.K. Folliard, Heat of hydration models for cementitious materials. ACI Materials Journal. 102 (1) (2005), pp. 24–22.

[3.8] K.A. Riding, J.L. Poole, K.J. Folliard, M.C.G. Juenger, A.K. Schindeler, Modeling hydration of cementitious systems. ACI Materials Journal. 109 (2) (2012), pp. 225–234.

[3.9] G. De Schutter, Hydration and temperature development of concrete made with blast-furnace slag cement. Cement and Concrete Research. 29 (1) (1999), pp. 143–149.

[3.10] G. De Schutter, Fundamental study of early age concrete behavior as a basis for durable concrete structures. Materials and Structures. 35 (2002), pp. 15–21.

[3.11] T. Merzouki, M. Bouasker, N. El H. Khalifa, P. Mounanga, Contribution to the modeling of hydration and chemical shrinkage of slag-blended cement at early age. Construction and Building Materials. 44 (2013), pp. 368–380.

[3.12] S. Tanaka, K. Inoue, Y. Shioyama, R. Tomita, Methods of estimating heat of hydration and temperature rise in blast furnace slag blended cement. ACI Materials Journal. 92 (1995), pp. 429–436.

[3.13] K.B. Park, N.Y. Jee, I.S. Yoon, H.S. Lee, Prediction of temperature distribution in high-strength concrete using hydration model. ACI Materials Journal. 105 (2008), pp. 180–186.

[3.14] X.Y. Wang, H.S. Lee, K.B. Park, J.J. Kim, J.S. Golden, A multi-phase kinetic model to simulate hydration of slag-cement blends. Cement and Concrete Composite. 32 (2010), pp. 468–477.

[3.15] M. Narmluuk, T. Nawa, Effect of fly ash on the kinetics of Portland cement hydration at different curing temperatures. Cement and Concrete Research. 41 (2011), pp. 579–589.

[3.16] O. Levenspiel, Chemical Reaction Engineering, Third Edition. John Wiley & Sons, Inc. (1999).

[3.17] K.B. Park, T. Noguchi, J. Plawsky, Modeling of hydration reaction using neural networks to predict the average properties of cement paste. Cement and Concrete Research. 35 (2005), pp. 1676-1684. https://doi.org/10.1016/j.cemconres.2004.08.004.

[3.18] H. Sugiyama, Y. Masuda, Prediction of temperature rise of concrete member using mathematical model for cement hydration and microstructure formation. J. Struct. Constr. Eng., AIJ. 73 (623) (2008), pp.
[3.19] I. Maruyama, T. Noguchi, T. Matsushita, Hydration model of Portland cement. J. Struct. Constr. Eng., AIJ. (593) (2005), pp. 1–8 (in Japanese). https://doi.org/10.3130/aijs.70.1_7.
[3.20] X.Y. Wang, H.S. Lee, Simulation of a temperature rise in concrete incorporating fly ash or slag. Materials and Structures. 43 (2010), pp. 737–754. https://doi.org/10.1617/s11527-009-9525-8.
[3.21] X.Y. Wang, H.S. Lee, Modeling of hydration kinetic in cement based materials considering the effects of curing temperature and applied pressure. Construction and Building Materials. 28 (2012), pp. 1–13.
[3.22] H.S. Lee, X.Y. Wang, L.N. Zhang, K.T. Koh, Analysis of the optimum usage of slag for the compressive strength of concrete. Materials. 8 (2015), pp. 1213–1229. https://doi.org/10.3390/ma8031213.
[3.23] W.J. Fan, X.Y. Wang, K.B. Park, Evaluation of the chemical and mechanical properties of hardening high-calcium fly ash blended concrete. Materials. 8 (2015), pp. 5933–5952. https://doi.org/10.3390/ma8095282.
[3.24] K.K. Aligizaki, Pore structure of cement-based materials: testing, interpretation and requirements. Modern Concrete Technology. Taylor & Francis (2006).
[3.25] L. Lam, Y.L. Wong, C.S. Poon, Degree of hydration and gel/space ratio of high-volume fly ash/cement systems. Cement and Concrete Research. 30 (2000), pp. 747–756.
[3.26] K. van Breugel, Simulation of Hydration and Formation of Structure in Hardening Cement-Based Materials, Ph.D. Thesis, Delft, The Netherlands (1991).
[3.27] H. Woods, H.H. Steinour, and H.R. Starke. Effect of composition of Portland cement on heat evolved during hardening. Industrial & Engineering Chemisty. 24 (11) (1932) pp. 1207-1214. https://doi:10.1021/ie50275a002.
[3.28] R.H. Bouge. Calculation of the compounds in Portland cement. Industrial & Engineering Chemistry Analytical Edition. 1 (4) (1929), pp. 192-197. https://doi:10.1021/ac50068a006.
[3.29] Wm. Lerch and R.H. Bogue, Heat of hydration of Portland cement pastes. Part of Bureau of Standards Journal of Research. 12 (1934), pp. 645-664.
https://nvlpubs.nist.gov/nistpubs/jres/12/jresv12n5p645_A2b.pdf.
[3.30] T. Thorvaldson, W. G. Brown, C.R.Peaker, Studies on the thermochemistry of the compounds occurring in the system CaO-Al_2O_3-SiO_2. IV. The heat of solution of tricalcium aluminate and its hydrates in hydrochloric acid. (1930), pp. 3927-3936. https://doi:10.1021/ja01373a024.
[3.31] P. Catharin, Heat of hydration and strength development. BETONWERK+ FERTIGTEIL-TECHNIK. 99 (1978), p.539-544.
[3.32] L.D. Adam, The measurement of very early hydration reactions of portland cement clinker by a thermoelectric conduction calorimeter. Cement and Concrete Research 6 (1976), pp. 293-307. https://doi.org/10.1016/0008-8846(76)90127-7.
[3.33] T.F. Newkirk, in 3rd ISCC, London (1952), pp 151-168.

[3.34] A. Hori, M. Takahashi, Y. Tsuzi, M. Harada, Fundamental properties of concrete using low added expansive additive. Proceeding of the Japan Concrete Institute. 24 (1) (2002) (in Japanese).
[3.35] T. Higuchi, M. Eguchi, M. Morioka, E. Sakai, Hydration and properties of expansive additive treated high temperature carbonation. Cement and Concrete Research. 64 (2014), pp.11-16.
[3.36] H. Choi, T. Noguchi, Modeling of mechanical properties of concrete mixed with expansive additive, International Journal of Concrete Structures and Materials. 9 (4) (2015), pp. 391–399.
[3.37] X.Y. Wang, Modeling of hydration, compressive strength, and carbonation of Portland-Limestone Cement (PLC) concrete. Materials. 10 (2017), pp. 115.
[3.38] I. Odler (1998). Hydration, setting and hardening of portland cement, in P. Hewlett (ed.), Lea's chemistry of cement and concrete, 4th edn, Arnold, London, U.K., pp. 241–297.
[3.39] D. Jansen, F. Goetz-Neunhoeffer, C. Stabler, J. Neubauer, A remastered external standard method applied to the quantification of early OPC hydration. Cement and Concrete Research. 41 (2011), pp. 602–608.

CHAPTER 4

PREDICTING THE COMPESSIVE STRENGTH OF EXPANSIVE CONCRETE BASED ON THE HYDRATION MODEL

CHAPTER 4 PREDICTING THE COMPESSIVE STRENGTH OF EXPANSIVE CONCRETE BASED ON THE HYDRATION MODEL

4.1 Introduction

Concrete is widely used in the world as a building material with many outstanding features such as high strength and durability, low cost, and so on. Although there are many kinds of strength (compressive strength, flexural strength, etc.), compressive strength is commonly considered to evaluate the quality of concrete because strength is directly related to the structure of hydrated cement paste [4.1]. It is well-known that the water-cement (w/c) ratio has affected the compressive strength. However, at any w/c ratio, the strength depends on the hydration degree of cement and its chemical and physical properties [4.1]. Therefore, the hydration process of cement or cement-based material has a relationship with the development of compressive strength of concrete. The other words, the compressive strength development could be predicted through the hydration reaction of cementitious systems.

In order to predict the compressive strength of concrete, many studies [4.2], [4.3], [4.4], and [4.5] have reported a relationship between the compressive strength and the pore volume and predicted the compressive strength through these relations. Choi et al. [4.6] modeled the compressive strength and elastic modulus of a hardened cement paste mixed with expansive additives and validated the model by considering the pore structure of a hardened cement paste based on the hydration. Furthermore, Powers [4.7] found that the compressive strength was related to the gel/space ratio and suggested a compressive strength equation as a function of the gel/space ratio. Lam et al. [4.8] introduced a model to describe the relationship between the gel/space ratio and the compressive strength. The results showed that the gel/space ratio of the fly ash–cement paste was consistent with that of the OPC paste in terms of the relationship with the compressive strength. In addition, considering the gel/space ratio, Wang [4.9] evaluated the development of the compressive strength of ultra-high-performance concrete using a blended cement hydration model employing Powers' strength theory. The abovementioned studies [4.2], [4.3-4.9] indicated that it is possible to predict the development of the compressive strength of concrete through Powers' strength theory considering the gel/space ratio. However, these studies have mostly focused on the mechanical properties of Portland cement, fly ash–cement, and slag–cement blends; few investigations have studied the properties of expansive concrete. Moreover, applying the hydration model to predict the mechanical properties and durability of expansive concrete has not been studied specifically.

As mentioned above, Powers [20] suggested a strength theory that determined a relationship between the compressive strength of Portland cement concrete and gel/space ratio through experimental data. The analysis herein is also based on the theory suggested above but we apply it to expansive concrete considering the contribution of cement hydration and expansive additive reaction. In this case, the compressive strength of expansive concrete was predicted from the strength of cement paste and the characteristics of aggregates, and the gel/space ratio was obtained from the proposed hydration model.

Figure 4.1 shows a flow chart representing the work undertaken. In order to predict the compressive strength, using Powers' Strength theory, the relationship between the gel/space ratio and the compressive strength

of paste was deduced. Then, a relationship between the gel/space ratio and compressive strength of concrete was suggested.

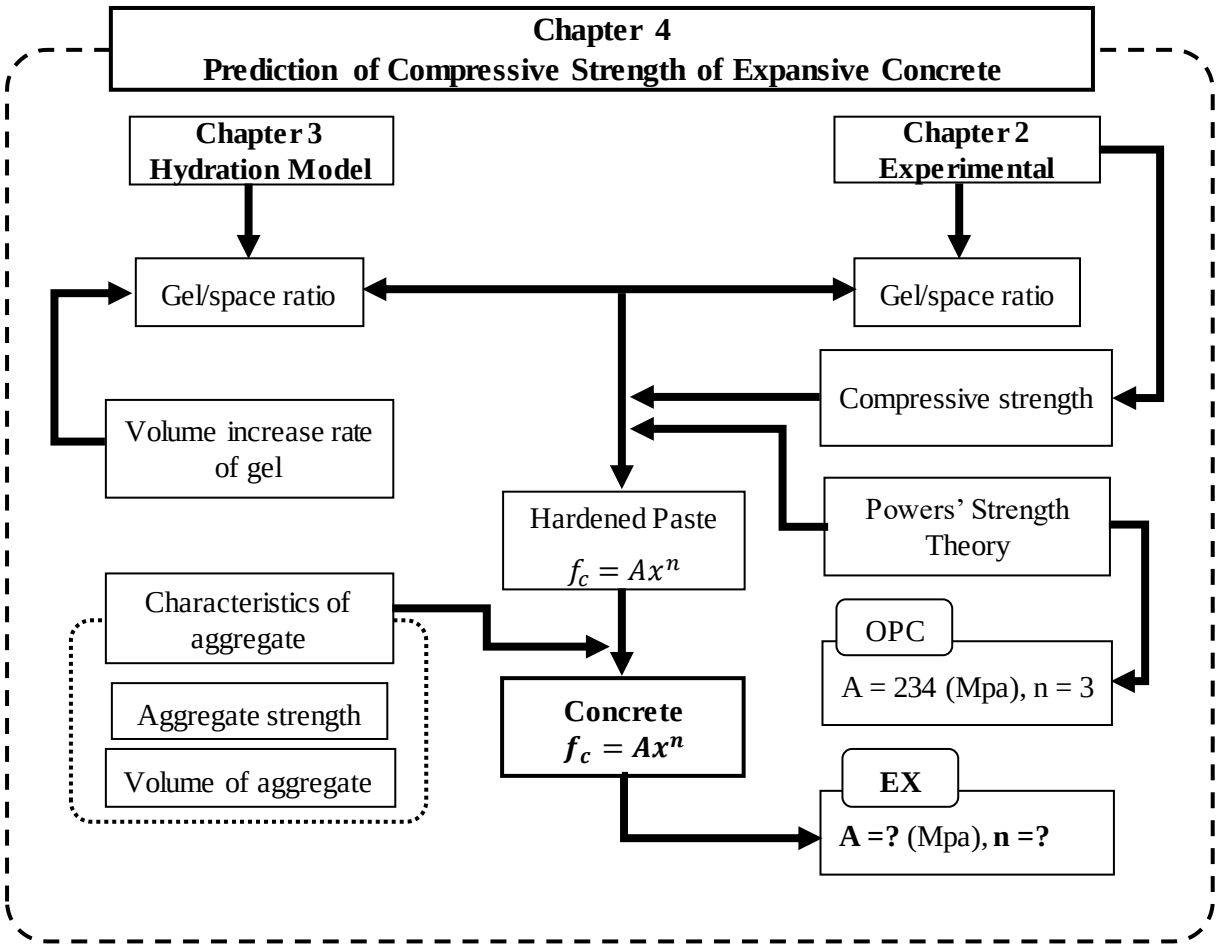

Figure 4.1 Flow chart

4.2 Predicting the compressive strength

4.2.1 Gel/space ratio

In general, there exists a fundamental inverse relationship between the porosity and the strength of solids [4.1047]. Choi et al. [4.6] assumed that the strength development of a cement paste mixed with an expansive additive is closely related to the pore volume based on the results of existing studies. Wang [4.11] reported that the compressive strength depends on the gel/space ratio determined from the cement hydration and w/b ratio. A gel/space ratio is defined as the ratio of the volume of the hydrated cement paste to the sum of the volumes of the hydrated cement and the capillary pore. This ratio is also called the amount of solid fraction in the system and is therefore equal to 1-porosity [4.10].

In this section, we describe the relationship between the concrete strength and the gel/space ratio for concrete with a 5% EX replacement content. The concrete strength was investigated by considering the cement paste strength, the characteristics of the aggregate, and an original coefficient ω. Gel/space ratio was calculated from the proposed model.

The gel/space ratio of Portland cement paste x_c [4.1] can be described by the following expression:

$$x_C = \frac{2.06(1/\rho_C)\alpha_C C_0}{(1/\rho_C)\alpha_C C_0 + W_0} \quad \text{Eq. (4.1)}$$

where ρ_C is the specific gravity of cement; 2.06 is the volume increase rate of the OPC paste based on the understanding that 1 mL of hydrated cement occupies 2.06 mL of volume [4.1], [4.10]; and α_C is the degree of hydration of the OPC paste.

For the Portland cement paste, Powers [4.1] found that the 28-day compressive strength f_c of three different mixtures was related to the gel/space ratio, as shown in Eq. (4.2):

$$f_c = Ax_C^n \quad \text{Eq. (4.2)}$$

where x_c is the gel/space ratio; A is the intrinsic strength of materials at zero porosity (MPa); and n is an exponent.

For the compressive strength of concrete, Powers [4.1] found the values of A and n to be 234 MPa and 3, respectively.

For the cement–EX paste, the compressive strength can be predicted using Powers' Strength theory as follows:

$$f_{C-EX} = Ax_{C-EX}^n \quad \text{Eq. (4.3)}$$

where $f_{C\text{-}EX}$ is compressive strength of the cement–EX blend; A is the intrinsic strength of the cement–EX blend at zero porosity (MPa); and n is an exponent.

In Eq. (4.3), x_{C-EX} is the gel/space ratio, which can be calculated using Eq. (4.4). Choi et al. [4.6] proposed a volume increase rate of 3.34 for the EX paste. Therefore, the gel/space ratio of the EX paste must be adjusted as follows:

$$x_{C-EX} = \frac{2.06(1/\rho_c)\alpha_c C_0 + 3.34(1/\rho_{EX})\alpha_{EX} EX_0}{(1/\rho_c)\alpha_c C_0 + (1/\rho_{EX})\alpha_{EX} EX_0 + W_0} \quad \text{Eq. (4.4)}$$

where $x_{C\text{-}EX}$ is the gel/space ratio of the cement–EX paste; ρ_{EX} is the specific gravity of EX; and 3.34 is the volume increase rate of the EX paste [4.6].

4.2.2 Relationship between cement paste strength and concrete strength

The relationship between the cement paste and concrete strength was investigated through a model developed by Upendra [4.12]. In this model, the author considered a unit volume of concrete in the form of a prism (or cylinder) as shown in Figure 4.2. The cylinder of concrete has a unit area of cross-section as shown in Figure 4.3. Assuming that the volume of the cylinder of the aggregate is V_a, the deformation behavior of such a model can be determined by assuming the following:

- The stress applied to the concrete cylinder does not vary along the depth of the layer AA_1D_1D or BB_1C_1C;
- For the combined material (aggregate and matrix) BB_1C_1C, the strain in the direction of application of stress is the same as the strains in the aggregate and in the matrix.

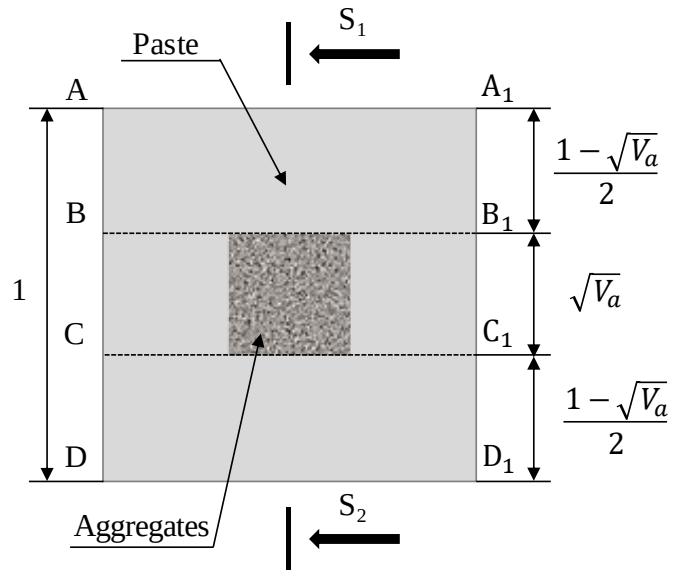

Figure 4.2 Unit volume of concrete [4.12].

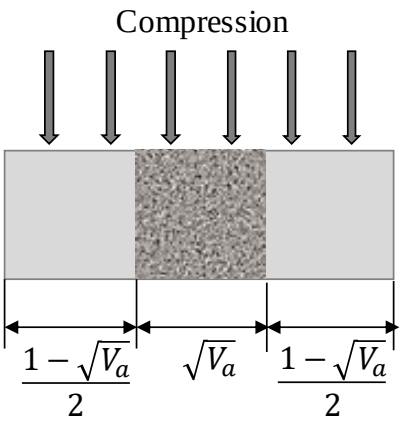

Figure 4.3 Cross section S_1-S_2 [4.12].

The elastic strain of concrete [48] is

$$\varepsilon_c = \varepsilon_p\left(1 - \sqrt{V_a}\right) + \varepsilon_a.\sqrt{V_a} \quad \text{Eq. (4.5)}$$

where ε_c, ε_p, and ε_a (N/mm^2) are given by

$$\varepsilon_c = \frac{f_c}{E_c}; \varepsilon_p = \frac{f_c}{E_p};\ \varepsilon_a = \frac{f_c}{E_a} \quad \text{Eq. (4.6-a)}$$

$$\frac{f_c}{E_c} = \frac{f_p}{E_p} = \frac{f_a}{E_a} \qquad \text{Eq. (4.6-b)}$$

Combining Eqs. (4.5) and (4.6-a, b), the compressive strength of concrete is expressed as

$$f_c = f_p\left(1 - \sqrt{V_a}\right) + f_a.\sqrt{V_a} \qquad \text{Eq. (4.7)}$$

where f_c, f_p, and f_a are the compressive strengths of the concrete, paste, and aggregate (MPa), respectively; V_a is the volume of aggregate (%).

Based on Eq. (4.7), however, the aggregate strength has a strong effect on the compressive strength of concrete. This means that the compressive strength of concrete mainly depends upon the compressive strength of aggregates; the strength deterioration of concrete is more than or equal to that of the aggregates. In fact, however, there are two damaged concrete cases, as the compressive strength test is carried out as shown in Figure 4.4. In the first case, the compressive strength of cement paste is less than that of aggregates and the damage only occurs in the cement paste. In the second case, the compressive strength of the cement paste is more than or equal to that of the aggregates and the damage would occur in the cement pastes as well as in the aggregates.

Therefore, to determine a satisfactory value for the predicted result that is consistent with the results in this study, a coefficient should be deduced, which can be written as ω.

The prediction equation can be rewritten as:

$$f_c = \left\{f_p\left(1 - \sqrt{V_a}\right) + f_a.\sqrt{V_a}\right\} \cdot \omega \qquad \text{Eq. (4.8)}$$

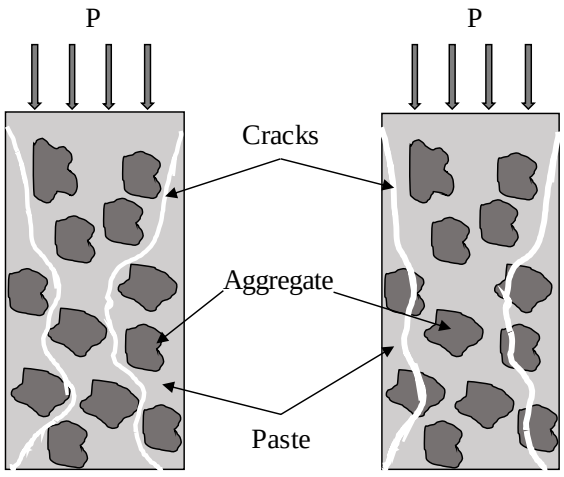

4.4-(a) Damage of normal concrete 4.4-(b) Damage of high strength concrete

f_p: Compressive strength of cement paste
f_a: Compressive strength of aggregates

Figure 4.4 Schematic of damage of concrete: (a) normal concrete, (b) high strength concrete

4.3 Results and Discussion

4.3.1 Relationship between compressive strength of cement paste and gel/space ratio

In this section, to predict the compressive strength of expansive concrete, the dependence of compressive strength of cement paste on the gel/space ratio with and without EX was determined. The relationship between the gel/space ratio and the compressive strength of OPC and EX pastes are shown in Figure 4.5. The gel/space ratio correlates with the compressive strength for coefficient correlations of 0.72 and 0.82 for the OPC and EX5 samples, respectively. According to Eq. (4.2) and the results, the compressive strength can be expressed as:

For OPC paste: $f_c = 250x^{3.16}$ Eq. (4.9)

For EX paste: $f_{EX} = 454x^{3.99}$ Eq. (4.10)

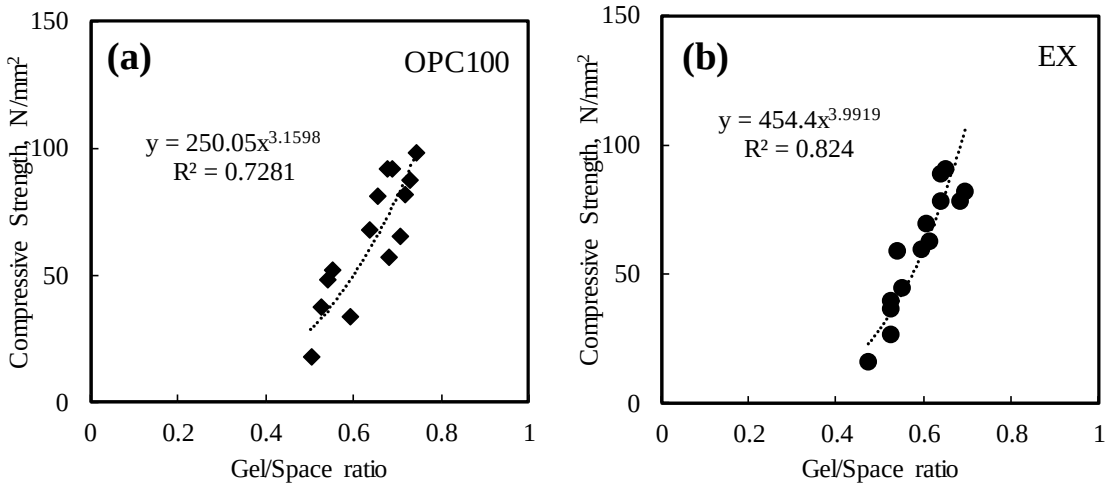

Figure 4.5 Gel/space ratio and compressive strength of OPC and EX pastes: (a) Portland cement paste, (b) Cement-EX paste.

According to the results, for a given gel/space ratio, the cement–EX paste shows higher compressive strength than that of the cement paste. This is possibly due to the effect of the pore structure of the cement–EX paste on the strength enhancement. The formation of ettringite crystals will fill the pores in the cement–EX paste matrix, which leads to a denser pore structure. This result is in agreement with the previous finding of Nguyen. et al [4.13], who studied the effect of expansive additive on the total porosity of mortars. They found that the total porosity of expansive mortar is smaller than that of non-expansive mortar. This is the reason for the higher intrinsic strength of the cement–EX paste at zero porosity when compared to that of cement paste (see Eqs. (4.9), (4.10)).

4.3.2 Relationship between conversion coefficient and gel/space ratio

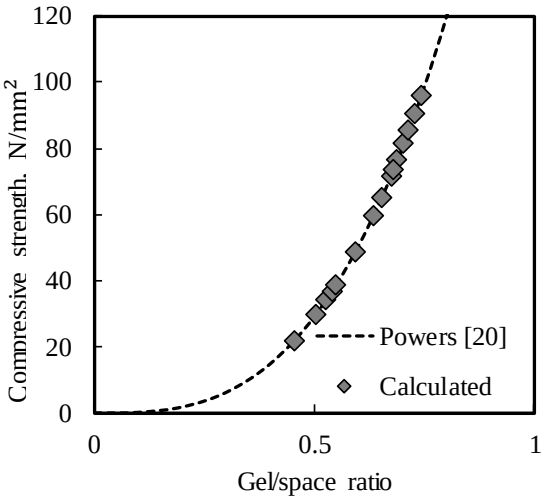

Figure 4.6 Fitting the calculated data to the Powers [20] data.

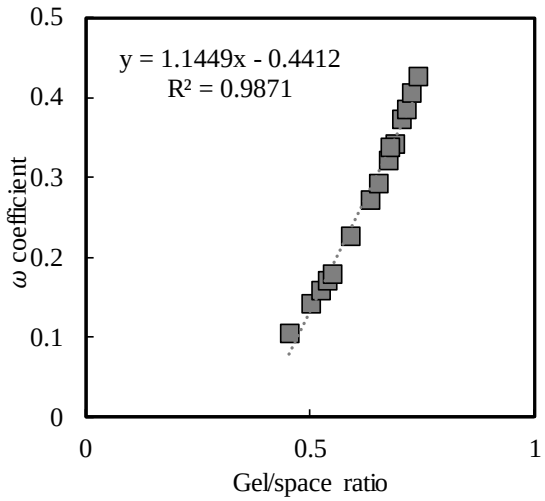

Figure 4.7 Relationship between ω and gel/space ratio.

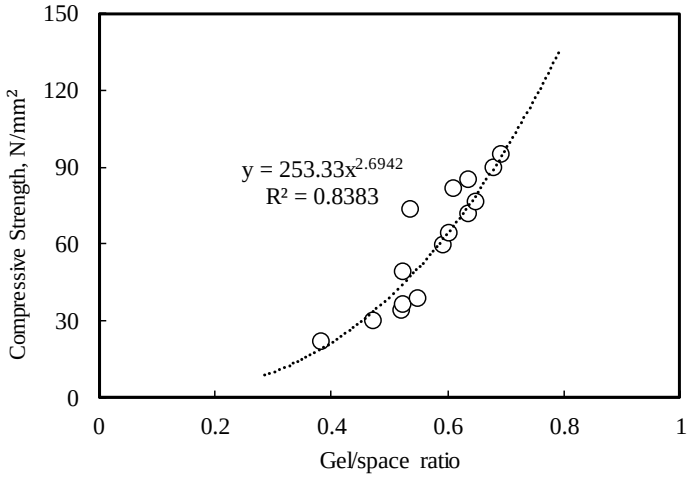

Figure 4.8 Relationship between compressive strength and gel/space ratio of expansive concrete.

In this part of the study, the compressive strength of expansive concrete was calculated from the strength of the cement–EX paste, characteristics of the aggregate, and the value of ω using Eq. (4.8), as presented in Section 4.2.2. The gel/space ratio was calculated from the proposed model through Eq. (4.4).

By fitting the calculated data to the Powers [4.1], [4.7], [4.10] data using the least-squares method, the value of the ω coefficient could be calculated. Figure 4.6 shows the fitting results. Furthermore, the relationship between the value of the coefficient ω and the gel/space ratio was also evaluated, as shown in Figure 4.7. The ω coefficient correlated linearly with the gel/space ratio with a high correlation coefficient of 0.98 (see Figure 4.7). It was also evident that the ω coefficient can be represented as a function of the gel/space ratio and is given by

$$\omega = 1.1449x - 0.4412 \qquad \text{Eq. (4.11)}$$

where x is the gel/space ratio.

Combining the value of the ω coefficient and Eq. (21), the relationship between the compressive strength of concrete and the gel/space ratio was evaluated for wEX5, as shown in Figure 4.8. The figure shows that the gel/space ratio data correlates with the predicted compressive strength. As mentioned above, Powers [4.1], [4.7], [4.10] suggested a relationship, given by f_c=$234x^3$, between the compressive strength of concrete and the gel/space ratio for OPC. Similar to the suggestion of Powers, we suggest a relationship between the compressive strength of expansive concrete and the gel/space ratio, which can be given as:

$$f_{C-EX}=253x_{C-EX}^{2.69} \qquad \text{Eq. (4.12)}$$

In Eq. (28), the value of intrinsic strength A is 253 MPa and n is 2.69 for expansive concrete. As shown in Figure 4.8, give a certain gel/space ratio, the compressive strength of expansive concrete is higher than that of Portland cement concrete. This result is consistent with the experimental results reported previously [4.14]. Thus, the proposed model has been proven to be able to estimate the gel/space ratio of cement–EX pastes and capable of modeling the compressive strength of expansive concrete. However, our prediction is only applicable for expansive concrete with 5% of expansive additive, which is known as a standard amount (20kg/m^3) of expansive additive for expansive concrete in Japan. In fact, we have considered a wide range of expansive additives such as 10%, 15%, and 20% expansive additive replacement by weight. However, experimental results indicated that a large amount of expansive additive will increase the volumetric change of sample under unconfined conditions, which causes many internal and surface cracks. This strongly affects the total porosity and compressive strength of the cement–EX paste. In other words, the total porosity increases for a larger amount of expansive additive under unconfined conditions. This tendency was also found in the study reported by Choi et al. [4.6].

4.4 Conclusions

1) The gel/space ratio of cement–EX blends was calculated by applying the proposed model. An original ω coefficient was deduced to find a satisfactory value for predicted results, called the conversion coefficient.
2) The compressive strength of expansive concrete was predicted by considering the cement–EX paste strength, characteristics of the aggregate, and the conversion coefficient. Using Powers' strength theory, an equation showing dependence of the compressive strength of expansive concrete on the gel/space ratio of expansive additive was deduced with A = 253 and n = 2.69.

References

[4.1] A.M. Neville, Properties of Concrete, 5th ed. Harlow, England: Prentice Hall, Pearson.

[4.2] F. Tomasawa, Development of a kinetic model for hydration of cement, in Proceeding of the 10th International Congress Chemistry of Cement, Gothenburg, Sweden, 2-6 June 1997; Chandra, S., Ed.; pp. 51-58.

[4.3] E. Ryshkewithch, Composition and strength of porous sintered alumina and zirconia. Journal of the American Ceramic Society. 36 (1953), pp. 65–68.

[4.4] K.K. Schiller, Mechanical properties of non-metallic materials. London, UK: Butterworths. (1958) pp. 35–50.

[4.5] C. Lian, Y. Zhuge, S. Beecham, The relationship between porosity and strength for porous concrete. Construction and Building Materials. 25 (2011), pp. 4294–4298.

[4.6] H. Choi, T. Noguchi, Modeling of mechanical properties of concrete mixed with expansive additive, International Journal of Concrete Structures and Materials. 9 (4) (2015), pp. 391–399.

[4.7] T.C. Powers, Structure and physical properties of hardened Portland cement paste. Journal American Ceramic Society. 41 (1958), pp.1–6.

[4.8] L. Lam, Y.L. Wong, C.S. Poon, Degree of hydration and gel/space ratio of high-volume fly ash/cement systems. Cement and Concrete Research. 30 (2000), pp. 747–756.

[4.9] X.Y. Wang. Properties prediction of ultra-high performance concrete using blended cement hydration model. Construction and Building Materials.

[47] [4.10] P.K. Mehta, P.J.M. Monteiro, Concrete: Microstructure, Properties, and Materials, Fourth Edition. New York: McGraw-Hill Education.

[44] [4.11] X.Y. Wang, Modeling of hydration, compressive strength, and carbonation of Portland-Limestone Cement (PLC) concrete. Materials. 10 (2017), pp. 115.

[48] [4.12] J.C. Upendra, The effect of the elastic modulus of the aggregate on the elastic modulus, creep and creep recovery of concrete. Magazine of Concrete Research. 16 (48) (1964), pp 129-138.

[51] [4.13] T.B.T. Nguyen, R. Chatchawan, W. Saengsoy, S. Tangtermsirikul, T. Sugiyama. Influences of different types of fly ash and confinement of performances of expansive mortars and concrete. Construction and Building Material 209 (2019) pp.176-186.

[52] [4.14] D.T. Nguyen, R. Sahamitmogkol, L.N. Trong, S. Tongaroonsri, S. Tangtermsirikul. Prediction of shrinkage cracking age of concrete with and without expansive additive. Songklanakarin J. Sci. Technol. 32 (5), pp469-480, Sep-Oct. 2010.

CHAPTER 5

PREDICTING CARBONATION DEPTH OF EXPANSIVE CONCRETE BASED ON HYDRATION REACTION MODEL

CHAPTER 5 PREDICTING CARBONATION DEPTH OF EXPANSIVE CONCRETE BASED ON HYDRATION REACTION MODEL

5.1 Introduction

Expansive concrete has been used as an efficient way to prevent and minimize cracking caused by drying shrinkage in concrete structures such as slabs, pavements, etc. [5.1, 5.2]. The expansion is generated by the production of ettringite and calcium hydroxide (CH) from the hydration reaction of expansive additive with water [5.2]. Concrete mixed with expansive additive (EX) that will expand in the first few days of its life, and a prestress is induced in concrete to offset or reduce tensile stress caused by drying shrinkage when the expansion of expansive concrete has been restrained by a restraining object such as embedded steel reinforcement.

It is well-known that the steel reinforcement in concrete is protected from corrosion by a thin oxide layer forms on the steel and prevents metal atoms from dissolving due to the alkaline environment of concrete with high pH (pH of 12 to 13). One of the factors that enhance the corrosion of the steel embedded is cracking [5.3]. As the cracks in the surface of concrete or mortar are present, the CO2 gaseous from the atmosphere may move towards the inner zones of concrete, then neutralize the alkalinity of concrete, which leads to the pH of the pore water in a concrete decrease to a low value of 9. The passive layer on the steel surface is no longer stable and corrosion can take place [5.3, 5.4]. Therefore, the effect of the carbonation on the service like time of concrete structure with or without supplement cementing materials (SCM) such as fly ash, blast-furnace slag, and expansive additive (EX) as well must be considered.

Several experimental researches [5.5, 5.6] were studied to investigate the influence of carbonation on the properties and microstructure of expansive concrete. Sakai et al. [5.5] reported that no differences were found in the carbonation depth and the compressive strength between expansive concrete and cement concrete. However, Tu Liuqing et al. [5.6] also reported that replacing Portland cement with fly ash and expansive additive increases the carbonation rate of concrete. This result is not consistent with the finding of Sakai et al. [5.5]. Meanwhile, Papadakis [5.7-5.9] was the first to propose and develop a fundamental mathematical model for the physicochemical process involved in the carbonation of Portland cement concrete and concrete containing SCM. This model considered both concrete composition and environmental factors. However, in this model [1], the calculating equation of parameters did not consider the hydration dependence of cement. Because the production of calcium hydroxide (CH) and calcium silicate hydroxide (C-S-H) depends on the hydration degree of cement and SCM. Therefore, a mathematical model that could predict the carbonation depth of concrete considering the hydration dependence of cement is essential. Wang and Lee [5.10] have proposed a numerical model for predicting the carbonation depth of concrete containing the low-calcium fly ash. The hydration reaction of cement compounds was considered in this model.

It notes that the above studies [5.5-5.10] have a deal with the carbonation of expansive concrete in experimental and predicting the carbonation depth of cement concrete and concrete mixed with the SCM; there is no research that proposed a numerical model for predicting the carbonation of expansive additive.

In this study, therefore, the mathematic model was proposed and developed to predict the carbonation depth of concrete mixed with expansive additive. The parameters such as CH, C-S-H content, and porosity of concrete were calculated by considering the hydration dependence of both Portland cement and EX. Subsequently, the measured data and calculated data were compared to validate the proposed model. Figure 5.1 shows a flow chart representing the work undertaken.

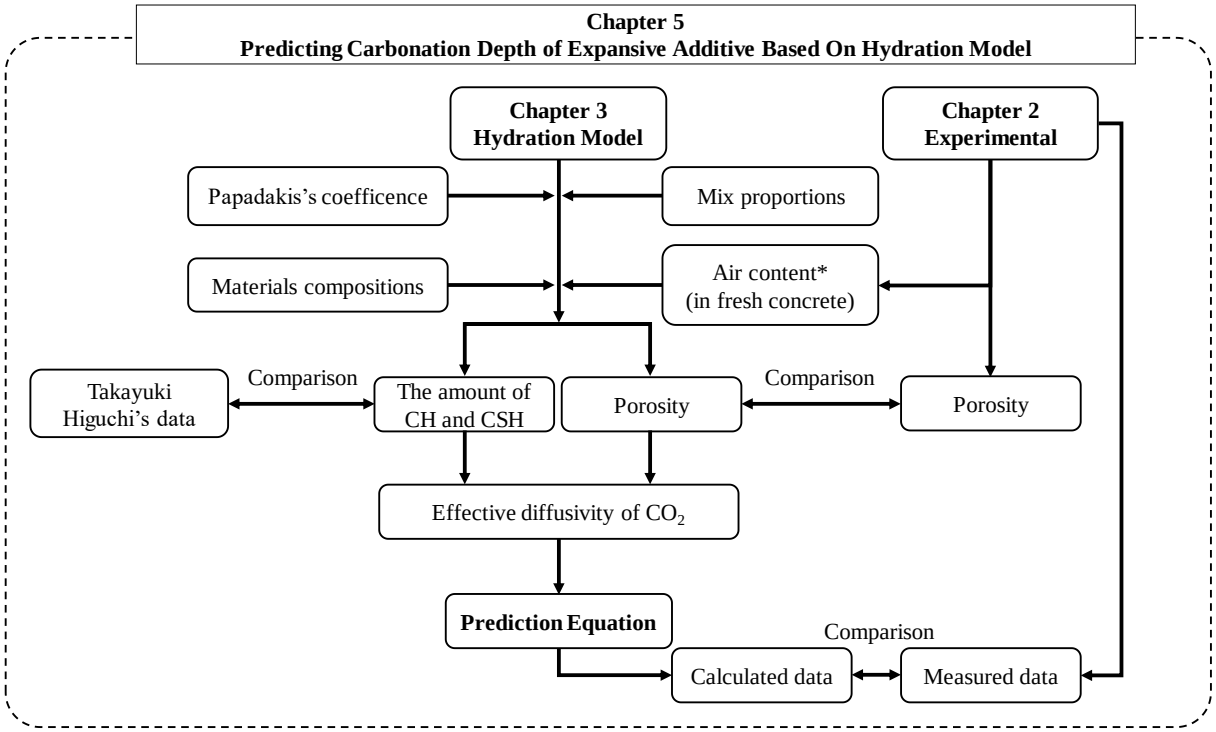

Figure 5.1 Flow chart

5.2 Predicting carbonation depth

The main carbonation reaction in concrete or mortar is usually described by the carbonated of calcium hydroxide as shown in the Eq. (5.1a). Besides $Ca(OH)_2$, the carbonation of C-S-H is also possible [5.3] [5.9], [5.10], [5.11], [5.12], [5.13], 5.14] (see Eq. 5.1b).

$$Ca(OH)_2 + CO_2 \rightarrow CaCO_3 + H_2O \quad \text{Eq. (5.1a)}$$

$$3CaO.2SiO_2.3H_2O + 3CO_2 \rightarrow (3CaCO_3.2SiO_2.3H_2O) \quad \text{Eq. (5.1b)}$$

For predicting the carbonation depth of concrete, a fundamental and comprehensive reaction engineering model of the process of the concrete carbonation was developed and experimentally verified by Papadakis et al. [5.7], [5.15], as shown in Eq. (5.2). This model considered the diffusion of CO_2 in a gaseous phase into concrete pore, its dissolution in the aqueous film of these pores, the dissolution of solid $Ca(OH)_2$ in pore water, its ultimate reaction with the dissolved CO_2, and the reaction of CO_2 with C-S-H and with some unhydrated phases of cement.

$$x_c = \sqrt{\frac{2D_{e,CO_2}[CO_2]^0}{[CH] + 3[CSH]}} \cdot \sqrt{t} \quad \text{Eq. (5.2)}$$

where,

x_c (cm) is the carbonation depth;

t (week) is the time to expose specimen in carbonation condition;

D_{e,CO_2} (m^2/s) is the effective diffusivity of CO_2 in carbonated concrete;

$[CO_2]^0$ (%) is the CO_2 content in the ambient air at the concrete surface, $[CO_2]^0$ = 5%;

$[CH]$ and $[CSH]$ (mol) are the molar concentrations of Portlandite and Calcium silicate hydrate.

In this study, the carbonation depth of expansive concrete is predicted by using Eq. (5.2). However, some parameters in Eq. (5.2) are modified to make it more suitable for predicting the carbonation depth of concrete mixed with expansive additive, as described in the next parts in detail.

In Eq. 5.1, the calcium hydroxide reacting is produced by hydration of the calcium silicate compounds of the cement [5.3], [5.11]. In this study, concrete was mixed with an expansive additive as a replacement material. Therefore, the calcium hydroxide reacting here is also produced by the hydration of free-CaO and the calcium silicate compounds of the expansive additive. Similar to the production of the calcium hydroxide, the production of the calcium silicate hydroxide reacting in Eq. (5.2) is not only from the hydration cement but also from the hydration of expansive additive.

The hydration of Portland cement is a series of complex reactions of the cement compounds. In this study, however, the hydration reactions of ordinary Portland cement are described by the Eqs. (5.3-5.6) [5.9], [5.9] [5.13], [5.14].

$$2C_3S + 6H \rightarrow C_3S_2H_3 + 3CH \quad \text{Eq. (5.3)}$$

$$2C_2S + 4H \rightarrow C_3S_2H_3 + CH \quad \text{Eq. (5.4)}$$

$$2C_3A + C\bar{S}H_2 + 10H \rightarrow C_4A\bar{S}H_{12} \quad \text{Eq. (5.5)}$$

$$C_4AF + 2CH + 10H \rightarrow C_6AFH_{12} \quad \text{Eq. (5.6)}$$

Meanwhile, the hydration reactions of the expansive additive are described by Eqs. (5.7-5.10) [5.16], [5.17].

$$C + H \rightarrow CH \quad \text{Eq. (5.7)}$$

$$6CH + C_4A_3\bar{S} + 8CaSO_4 + 90H \rightarrow (3CaO.Al_2O_3 3.CaSO_4.32H_2O) \quad \text{Eq. (5.8)}$$

$$2C_2S + 4H \rightarrow C_3S_2H_3 + CH \quad \text{Eq. (5.9)}$$

$$C_4AF + 2CH + 10H \rightarrow C_6AFH_{12} \quad \text{Eq. (5.10)}$$

In order to calculate the amount of CH and C-S-H, the method of calculating the molar mass of an element in chemistry is performed using the equation as shown in Eq. (5.11).

$$n = \frac{m}{M} \quad \text{Eq. (5.11)}$$

where,

n is the molar mass of an element (mol);

m is the amount of an element (g);

M is the relative formula mass.

An example was carried out to explain the method. Example: Calculating the amount of CaO from 4g Ca? Firstly, the reaction of Ca and oxygen are described by following equation:

$$2Ca + O_2 \rightarrow 2CaO \quad \text{Eq. (5.12)}$$

From reaction Eq. (5.12), with 1 mol of Ca create 1mol CaO. According to Eq. (5.11), the number of moles of Ca equal to the amount of Ca divided by the relative formula mass of Ca, which is 0.1 mol. Therefore, the number of moles of CaO is 0.1. The amount of CaO is $m_{CaO} = n_{CaO} \times M_{CaO} = 0.1 \times 56 = 5.6$ (g).

5.2.1 Calcium hydroxide

In this study, the CH content is calculated by considering the production and consumption of CH from the hydration reaction of cement and expansive additive through the Eqs. (5.3-5.10). From the Eqs. (5.3-5.10), the number of moles of CH is

$$n_{CH} = n_{CH[Eq.\ (5.3)]} + n_{CH[Eq.\ (5.4)]} - n_{CH[Eq.\ (5.6)]} + n_{CH[Eq.\ (5.7)]} - n_{CH[Eq.\ (5.8)]} + n_{CH[Eq.\ (5.9)]} - n_{CH[Eq.\ (5.10)]} \quad \text{Eq. (5.13)}$$

$$m_{CH} = n_{CH} \times M_{CH} \quad \text{Eq. (5.14)}$$

$$n_{Eq.\ (5.3)} = \frac{3}{2}\frac{f_{C_3S}^{OPC}}{M_{C_3S}} \times C \quad \text{Eq. (5.15a)}$$

$$n_{Eq.\ (5.4)} = \frac{1}{2}\frac{f_{C_2S}^{OPC}}{M_{C_2S}} \times C \quad \text{Eq. (5.15b)}$$

$$n_{Eq.\ (5.6)} = 2\frac{f_{C_4AF}^{OPC}}{M_{C_4AF}} \times C \quad \text{Eq. (5.15c)}$$

$$n_{Eq.\ (5.7)} = \frac{f_{CaO}^{EX}}{M_{CaO}} \times EX \quad \text{Eq. (5.15d)}$$

$$n_{\text{Eq. (5.8)}} = 6\frac{f^{EX}_{Ye'el.}}{M_{Ye'el.}} \times EX \quad \text{Eq. (5.15e)}$$

$$n_{\text{Eq. (5.9)}} = \frac{1}{2}\frac{f^{EX}_{C_2S}}{M_{C_2S}} \times EX \quad \text{Eq. (5.15f)}$$

$$n_{\text{Eq. (5.10)}} = 2\frac{f^{EX}_{C_4AF}}{M_{C_4AF}} \times EX \quad \text{Eq. (5.15g)}$$

where,

n_{CH} is the number moles of calcium hydroxide (mol);

$n_{\text{Eq. (5.3)}}, n_{\text{Eq. (5.4)}}, n_{\text{Eq. (5.6)}}, n_{\text{Eq. (5.7)}}, n_{\text{Eq. (5.8)}}, n_{\text{Eq. (5.9)}}$ and $n_{\text{Eq. (5.10)}}$ are the number of moles of calcium hydroxide according to the chemical equation (5.3), (5.4), (5.6), (5.7), (5.8), (5.9), and (5.10), respectively, as indicated in Eq. (5.15a-5.15g);

m_{CH} is the amount of calcium hydroxide (g);

M_{CH} , M_{C_3S}, M_{C_2S}, M_{C_4AF}, M_{CaO} and $M_{Ye'el.}$ are the relative formula mass of CH, cement and expansive additive compound, respectively. The values are given in Table 5.1;

C and EX are the weigth of cement and expansive additive in the mix proportion.

Table 5.1 Molar weight and molar volume of the main compounds found in Portland cement and Portland-based binders.

Compound	Molar weight 10^3 (kg/mol)	Density 10^{-3} (kg/m^3)	Molar volume 10^6 (m^3/gmol)
C_3S	228.30	3.20	71.34
C_2S	172.22	3.30	52.19
C_3A	270.18	3.03	89.17
C_4AF	485.96	3.77	128.90
$C\bar{S}H_2$	172.17	2.32	74.21
H	18.02	1.00	18.02
CH	74.10	2.24	33.08
$C_3S_2H_3$	342.41	2.28	150
$C_4A\bar{S}H_{12}$	622.51	1.95	319.24
C_4AH_{13}	560.47	2.06	272.07
$C_3A \cdot 3C\bar{S} \cdot H_{32}$	1255.13	1.78	705.13
C_6AFH_{12}	814.31	2.65	307.87
$C_8AF\bar{S}_2H_{24}$	1302.44	2.3	560
C_8AFH_{26}	1178.29	2.3	500
Ye'elimite ($C_4A_3\bar{S}$)	610	-	-

$C\bar{C}$	100.09	2.71	36.93
C	56.08	3.32	16.89
S	60.08	2.20	27.28
A	101.96	4.00	25.49
F	159.69	5.24	30.48
$\bar{S}$	80.07	-	-

However, the presented equations of number moles and amount of CH (see Eq. (5.13) and Eq. (5.14)) are the values when the hydration degree of cement (or cement-EX blend) is equal to 1 (α_{max} = 1). To evaluate time dependent on the production of CH, the hydration degree of cement and expansive additive is considered. The degree of hydration of cement and cement-EX blend was modeled by the numerical model, which was discussed in Chapter 3. The number moles of CH are rewritten

$$n_{CH}^{t} = (n_{CH[Eq.\ (5.3)]} + n_{CH[Eq.\ (5.4)]} - n_{CH[Eq.\ (5.6)]}) \times \alpha_{OPC} + (n_{CH[Eq.\ (5.7)]} - n_{CH[Eq.\ (5.8)]} + n_{CH[Eq.\ (5.9)]} - n_{CH[Eq.\ (5.10)]}) \times \alpha_{EX} \quad \text{Eq. (5.16)}$$

$$m_{CH}^{t} = n_{CH}^{t} \times M_{CH} \quad \text{Eq. (5.17)}$$

where,

n_{CH}^{t} (mol) and m_{CH}^{t} (g) are the number moles and the amount of CH at time t, respectively;

α_{OPC} and α_{EX} are the hydration degree of cement and expansive additive.

5.2.2 Calcium Silicate hydroxide

Similar to the method of calculating the amount of CH, the amount of C-S-H is also calculated by balancing the production and consumption of CH in the hydration reactions of cement and expansive additive (see Eqs. (5.3-5.10). According to Eqs. (5.3-5.10), the number moles of C-S-H is

$$n_{CSH} = n_{CSH[Eq.\ (5.3)]} + n_{CSH[Eq.\ (5.4)]} + n_{CSH[Eq.\ (5.9)]} \quad \text{Eq. (5.18)}$$

$$n_{CSH[Eq.\ (5.3)]} = \frac{1}{2}\frac{f_{C_3S}^{OPC}}{M_{C_3S}} \times C \quad \text{Eq. (5.19a)}$$

$$n_{CSH[Eq.\ (5.4)]} = \frac{1}{2}\frac{f_{C_2S}^{OPC}}{M_{C_2S}} \times C \quad \text{Eq. (5.19b)}$$

$$n_{CSH[Eq.\ (5.9)]} = \frac{1}{2}\frac{f_{C_2S}^{EX}}{M_{C_2S}} \times EX \quad \text{Eq. (5.19c)}$$

where,

n_{CSH} is the total number moles of C-S-H;

$n_{CSH[Eq.\ (5.3)]}$, $n_{CSH[Eq.\ (5.4)]}$, and $n_{CSH[Eq.\ (5.9)]}$ (mol) are the number moles of C-S-S according to Eq. (5.3), (5.4), and (5.9), respectively, as shown in Eqs. (5.19a-5.19b)

The amount of C-S-H is

$$m_{CSH} = n_{CSH} \times M_{CSH} \quad \text{Eq. (5.20)}$$

where,

m_{CSH} (g) is the amount of C-S-H;

M_{CSH} (g) is the relative formula mass of C-S-H (see Table 5.1).

At time t, the total number moles and amount of C-S-H is written

$$n_{CSH}^{t} = (n_{CSH[Eq.\ (5.3)]} + n_{CSH[Eq.\ (5.4)]}) \times \alpha_{OPC} + n_{CSH[Eq.\ (5.9)]} \times \alpha_{EX} \quad \text{Eq. (5.21)}$$

$$m_{CSH}^{t} = n_{CSH}^{t} \times M_{CSH} \quad \text{Eq. (5.22)}$$

n_{CSH}^{t} (mol) and m_{CSH}^{t} (g) are the number moles and the amount of C-S-H at time t, respectively.

5.2.3 Effective diffusion of CO_2 in concrete and porosity of concrete

Papadakis et al. [5.17] reported that the effective diffusivity of CO_2 depends on the volume, the structure, and the degree of saturation of the pores in concrete (or mortar). It has been measured using a Wick-Kallenbach type of apparatus [5.8] and represented as a function of porosity, the composition of concrete, and the ambient relative humidity, as shown in Eq. (5.23).

$$D_{e,CO_2} = A\left(\frac{\varepsilon_c}{\frac{C}{\rho_c} + \frac{P}{\rho_p} + \frac{W}{\rho_w}}\right)^{a}\left(1 - \frac{RH}{100}\right)^{b} \quad \text{Eq. (5.23)}$$

where,

D_{e,CO_2} (m^2/s) is the effective diffusivity of CO_2;

RH (%) is the ambient relative humidity;

ρ_c, ρ_p, and ρ_w (kg/m^3) are the density of cement, supplementary cementing materials, and water, respectively;

C, P, and W is the cement, supplementary cementing materials (silica fume or fly ash) and water content in 1 m^3 of fresh concrete;

ε_c (%) is the porosity of concrete as shown in Eq. (5.24) [5.9].

$$\varepsilon_c = \varepsilon_{air} + \frac{W}{\rho_w} - \varepsilon_h - \varepsilon_p - \varepsilon_{car} \quad \text{Eq. (5.24)}$$

where,

ε_{air} (%) is the volume fraction of entrapped or entrained air in concrete;

ε_h, ε_p, and ε_{car} are the porosity reductions due to hydration of Portland cement, pozzolanic activity, and carbonation, respectively. Papadakis suggested that the porosity reduction due to pozzolanic activity is almost zero [5.9]. The ε_h and ε_{car} are given by Eqs. (5.25) and (5.26), respectively [5.5], [5.11]:

$$\varepsilon_h = f_{C_3S}\Delta\overline{V_{C_3S}} + f_{C_2S}\Delta\overline{V_{C_2S}} + f_{C_3A}\Delta\overline{V_{C_3A}} + f_{C_4AF}\Delta\overline{V_{C_4AF}} \quad \text{Eq. (5.25)}$$

$$\varepsilon_{car} = n_{CH}\Delta\overline{V_{CH}} + n_{CSH}\Delta\overline{V_{CSH}} \quad \text{Eq. (5.26)}$$

where,

$\Delta\overline{V_{C_3S}}$, $\Delta\overline{V_{C_2S}}$, $\Delta\overline{V_{C_3A}}$, $\Delta\overline{V_{C_4AF}}$, $\Delta\overline{V_{CH}}$, and $\Delta\overline{V_{CSH}}$ and are differences in volumes between the solid reactants and solid products, respectively (see Table 5.2) (m^3/mol).

n_{CH} and n_{CSH} are the molar volume of CH and C-S-H.

Table 5.2 Molar volume differences [5.8]

Unit	C_3S	C_2S	C_3A	C_4AF	CH	C-S-H
$\Delta\overline{V}$ x 10^{-6}, m^3/mol	53.28	39.35	155.86	220	3.85	15.39

The parameters A, a, and b are $1.64*10^{-6}$, 1.8, and 2.2 respectively, obtained from regression analysis of experimental data for 0.5<w/c<0.8 [5.11]. Papadakis [5.11] also reported that the diffusion parameter values were changed by the w/b ratios.

Based on Papadakis's equation, the effective diffusivity of CO_2 in concrete mixed with expansive additive is described in Eq. 5.27.

$$D_{e,CO_2} = A\left(\frac{\varepsilon_c}{\frac{C}{\rho_c}+\frac{E}{\rho_{EX}}+\frac{W}{\rho_w}}\right)^a\left(1-\frac{RH}{100}\right)^b \quad \text{Eq. (5.27)}$$

where,

E (kg/m^3) is the expansive additive content in 1 m^3 of fresh concrete;

ρ_{EX} (kg/m^3) is the expansive additive density;

The parameter A, a, and b are obtained by fitting data in this study.

In this study, the porosity of cement concrete and expansive concrete is calculated by considering the time dependent of hydration reaction, are given in Eqs. (28) and (29):

$$\varepsilon_h = \left(f_{C_3S}\Delta\overline{V_{C_3S}} + f_{C_2S}\Delta\overline{V_{C_2S}} + f_{C_3A}\Delta\overline{V_{C_3A}} + f_{C_4AF}\Delta\overline{V_{C_4AF}}\right)\times\alpha_{OPC} + \left(f_{C_3S}\Delta\overline{V_{C_3S}} + f_{C_4AF}\Delta\overline{V_{C_4AF}}\right)EX\alpha_{ex} \quad \text{Eq. (5.25)}$$

$$\varepsilon_{car} = n_{CH}^t\Delta\overline{V_{CH}} + n_{CSH}^t\Delta\overline{V_{CSH}} \quad \text{Eq. (5.26)}$$

where,

n_{CH}^t and n_{CSH}^t are the molar volume of CH and C-S-H at time t, as described in Eqs. (5.16) and (5.21).

5.3 Results and Discussion

5.3.1 Amount of calcium hydroxide and calcium silicate hydroxide

As mentioned above, the aim of this chapter is to predict the carbonation depth of cement concrete and expansive concrete. It is known that the main reactions of the carbonation process in concrete are the reaction of calcium hydroxide (CH) and CaO in the calcium silicate hydroxide (C-S-H) compound of hardened cement with CO_2 into calcium carbonate. Hence, it is very important to calculate the amount of CH and C-S-H. Therefore, to verify the present equation, a comparison between the predicted results and experimental results is shown in Figure 5.2. The present equation was validated using data from Takayuki [5.18] and Zhang [5.19]. For experimental results, the CH content of these studies was obtained by determining the mass loss in the temperature range of 350-500℃ using the TG-DTA and TGA apparatus. It can be seen in Figure 5.2 that the experimental results and predicted results have a good relationship due to most of the data are within the confidence limits line (±10%). The results of verification suggest that the present equation is useful for predicting the CH and C-S-H content from the hydration of OPC and EX.

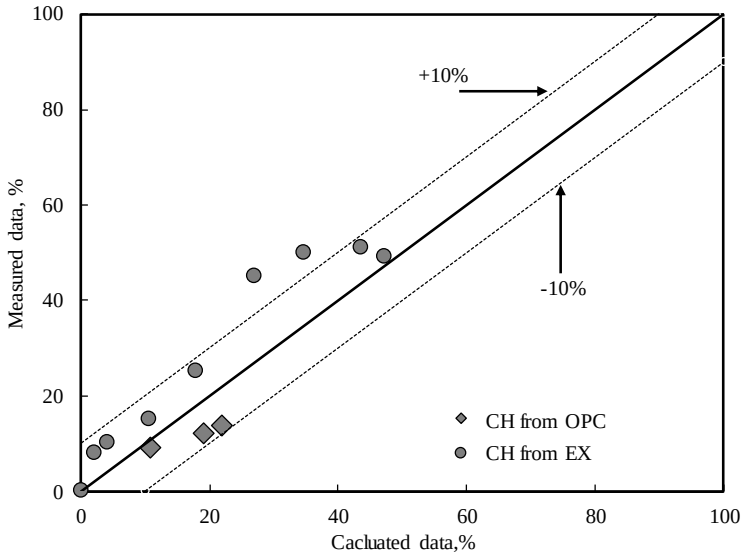

Figure 5.2 Comparison of calculated data and measured data of the amount of CH from OPC and EX

The prediction results of the calcium hydroxide contents are shown in Figure 5.3 at different w/b ratios. The CH content of all samples increases with time for both w/b ratios. Results showed that the CH content increases with the addition of the expansive additive. It is well-known that the production of CH from the hydration of EX is the hydration reaction of free-CaO and from the hydration of OPC is the hydration reaction of cement composition (C_3S and C_2S). In this study, the amount of free CaO is about 45.4 % of the mass (see Chapter 2). Therefore, this is due to the high content of free CaO in expansive additive, which directly related to the production of CH. The CH content are approximately 98, 105 and 112 kg/m^3, and 70, 78, and 85 kg/m^3 at w/b 0.3 and w/b 0.5, respectively. The value of CH content herein is calculated by using the present equation combining the mix proportion of concrete. The results also indicated that the CH

content of samples at lower w/b ratio is large than that of samples at higher w/b ratio. This may be explained by the amount of cement at w/b of 0.3. According to the mix proportions (see chapter 2), the amount of cement is 583 kg/m^3 and 370 kg/m^3 at w/b of 0.3 and 0.5, respectively. Therefore, the higher amount of cement is the reason why the CH content of the sample at w/b 0.3 larger than that of the sample at w/b 0.5.

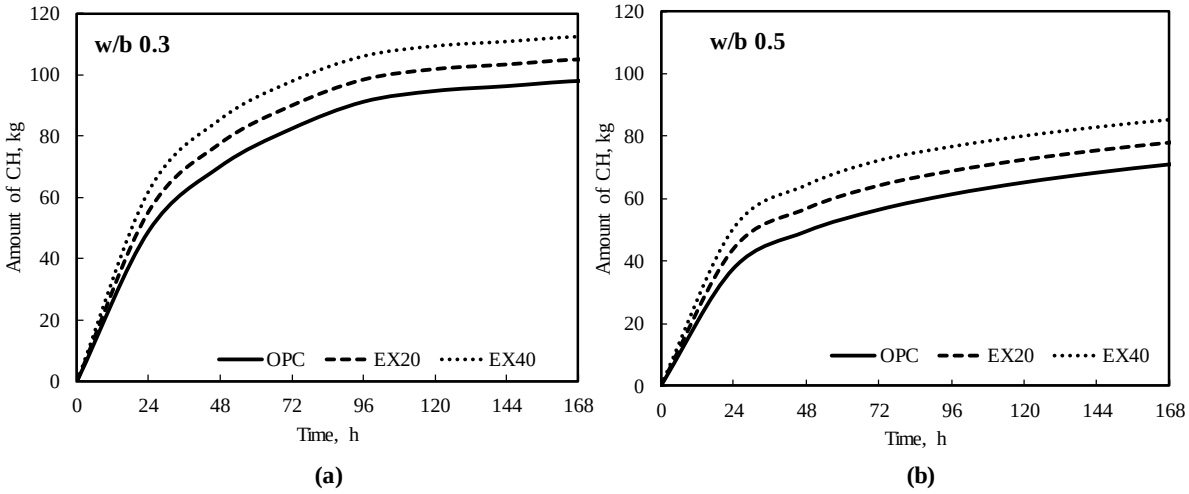

Figure 5.3 Amount of calcium hydroxide

Figure 5.4 shows the predicted data of the amount of calcium silicate hydroxide of cement and expansive concrete at different w/b ratios. With the time of hydration, the amount of C-S-H tendency was similar to the CH content of concrete. However, unlike in the predicted data of the CH content, the amount of C-S-H decreased when the expansive additive dosage was increased. These tendencies were found in both w/b ratios of 0.3 and 0.5. The C-S-H is the main hydration product of the hydration process of cement, the production of C-S-H depends on the cement content in 1 cubic meter of concrete. Therefore, when the expansive additive addition increased, the amount of cement was decreased. The decrease in cement dosage leads to a decrease in the amount of C-S-H. This is explaining the tendency that was reported above.

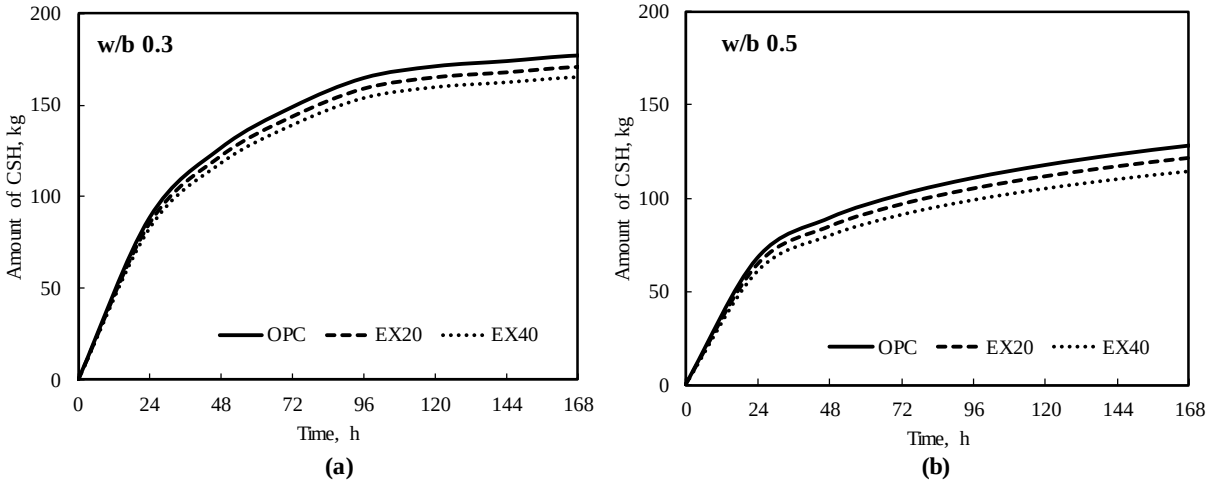

Figure 5.4 Amount of calcium silicate hydroxide

5.3.2 Porosity of concrete

One of the important factors to predict the carbonation depth of concrete is porosity (total porosity). The same as other parameters, to verify the predicting equation for calculating the porosity content, a comparison between measured data and predicted data of porosity of concrete and cement paste is illustrated in Figure 5.5. For experiment data, the porosity of concrete and cement paste with and without expansive additive was determined by under-water weighing (discussion in Chapter 2). The testing times are 28-day and 1-day, 3-day, 7day, 14-day, and 28 days for concrete and cement paste, respectively. The results showed that most of the data are within in confidence limit line ($\pm$10). It concludes that the present equation here can be applied to predicting the porosity of concrete and cement paste mixed with expansive additive.

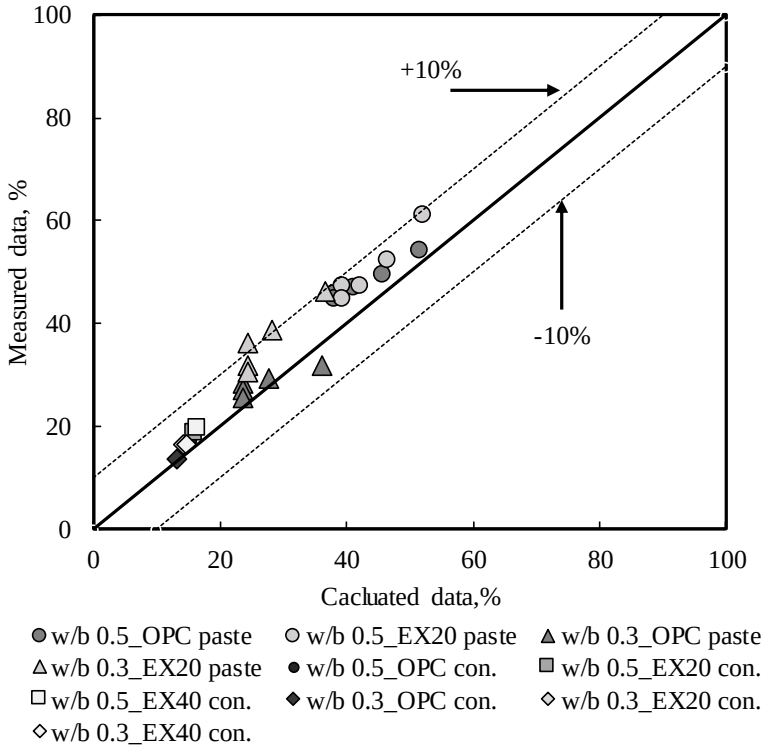

Figure 5.5 Comparison of calculated data and measured data of concrete porosity and paste

5.3.3 Verification of prediction equation.

The value of coefficients in Eq. (5.27) is given in Table 5.1. The coefficients A and c increased with the addition of the expansive additive, which leads to the value of the effective diffusivity of CO_2 in carbonated concrete (D_{e,CO_2}) increased. In other words, the diffusion of CO_2 gas through concrete becomes easier. This is maybe explained the hydration of expansive additive in concrete generates the capillary pore more than that of Portland cement. The effect of the dosage of the expansive additive on the capillary pore was discussed in chapter 2. This result is in agreement with the previous finding of Papadakis [5.11], who reported that the addition of supplementary cementing materials may further promote the pore

disconnection. The results have also shown that the decrease in A and c when the w/b ratio was lower. This is due to the development of a disconnected pore system, which will lead to low transport rates [5.20]. According to Eq. (5.27), the coefficient d directly related to the environment humidity of the testing condition (unchanged 60%). Unlike coefficients A and a, therefore, the value of coefficient b is not changed with different w/b ratios and the addition of EX. These results also consistent with the previous results [5.11]. Finally, the comparison between the prediction results and experimental results is shown in Figure 5.6. As shown in Figure 5.6, the prediction results are in agreement with the experiment results. It concluded that the present equation is useful for predicting the carbonation depth of expansive concrete.

As mentioned above, combining the hydration reaction equation and the hydration model the hydration products were calculated. It means from this way the amount of ettringite is also calculated. It is well-known that the production of ettringite and calcium hydroxide are directly related to the expansion of expansive concrete. In other words, the expansion of expansive concrete could be predicted by calculating the production process of ettringite and calcium hydroxide. This will be discussed in the next chapter.

Table 5.3 Coefficient of predicting equation

Sample	w/b	A	a	b	RH, %	CO_2, %
OPC	0.3	3.5E-06	1.6	2.2	60	5
EX		6.70E-06	3.2	2.2		
OPC	0.5	4.95E-06	1.8	2.2		
EX		6.50E-04	2.5	2.2		

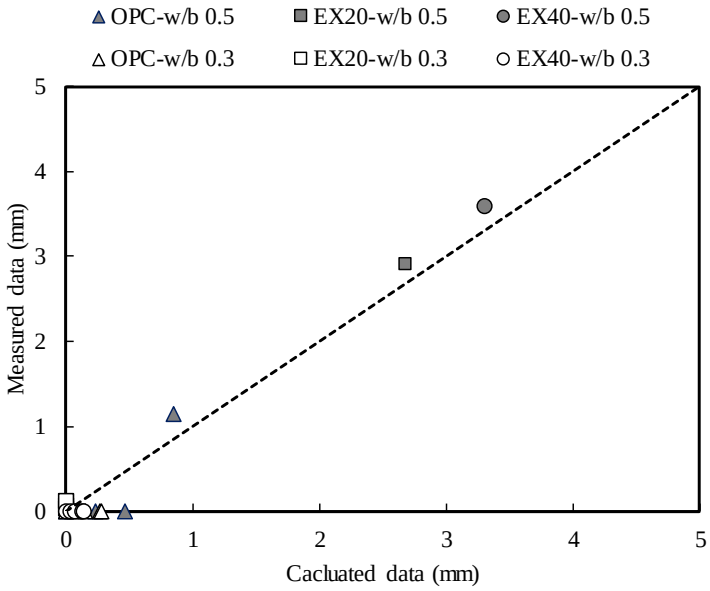

Figure 5.6 Comparison of calculated data and measured data of carbonation depth of concrete

5.4 Conclusions

This study proposed a numerical model for predicting the carbonation depth of concrete mixed with expansive additive. The amount of CH, C-S-H, and total porosity of concrete were calculated with the time of hydration reaction of cement and expansive additive based on the hydration model. In order to test the accuracy of the proposed model, the prediction results and experiment results were compared. The results indicated that prediction results were in good agreement with experimental results and so the model proposed here can be applied to calculate the CH, C-S-H content, porosity, and the carbonation depth of expansive concrete.

References

[5.1] J.J. Brooks, Chapter 6 shrinkage of concrete, Concrete and Masonry Movements (2015) pp 137-185.

[5.2] Recommended practice for expansive concrete, Concrete library of JSCE No.23 (1994).

[5.3] A.M. Neville, Properties of Concrete, 5th ed. Harlow, England: Prentice Hall, Pearson.

[5.4] M. Criado, Chapter 13-The corrosion behavior of reinforced steel embedded in alkali-activated mortar. Handbook of Alkali-Activated Cement, Mortars and Concrete (2015) pp333-372.

[5.5] E. Sakai, K. Kosuge, S. Teramura, K. Nakagawa, Carbonation of Expansive Concrete and Change of Hydration Products, ACI symposium paper 126 (1991) 989-1000.

[5.6] T. Liuqing, S. Zhonghe, C. Wei, X. Wenbing, M. Juntao, Effect of carbonation on the microstructure of concrete containing fly ash and expansive admixture. Advanced Materials Research Vol. 347-353 (2011) pp 4074-4080.

[5.7] V.G. Papadakis, C.G. Vayenas, M.N. Fardis, Fundamental modeling and experimental investigation of concrete carbonation, ACI Mater J 88 (1991) pp 363–373.

[5.8] V.G. Paparakis, C.G. Vayenas, M.N. Fardis, Physical and chemical characteristics affecting the durability of concrete. ACI materials journal, Technical paper, title no. 88-M24 (1991) pp 186-196.

[5.9] V.G. Papadakis, Experimental investigation and theoretical modeling of silica fume activity in concrete. Cement and Concrete Research 29 (1) (1999) pp 79–86.

[5.10] X.Y. Wang, H.S. Lee, A model for predicting the carbonation depth of concrete containing low-calcium fly ash. Construction and Building Materials 23 (2009) pp 725-733.

[5.11] V. G. Papadakis, Effect of supplementary cementing materials on concrete resistance against carbonation a chloride ingress. Cement and Concrete Research Volume 30, (2000) pp 291-299.

[5.12] M.A. Peter, A. Muntean, S.A Meier, M. Bohm, Competition of several carbonation reactions in concrete: A parametric study. Cement and Concrete Research 38 (2008) pp 1385-1393.

[5.13] V.G. Papadakis, Effect of fly ash on Portland cement systems. Part I: lowcalcium fly ash. Cement and Concrete Research 29 (11) (1999) pp 1727–36.

[5.14] V.G. Papadakis, Effect of fly ash on Portland cement systems. Part II: high calcium fly ash. Cement and Concrete Research 30 (10) (2000) pp 1647–54.

[5.15] V.G. Papadakis, M.N. Fardis, C.G. Vayenas, Effect of composition, environmental factors and cement-lime mortar coating on concrete carbonation. Materials and Structures 25 (1992) pp 293-304.

[5.16] H. Choi, A study on the macro prediction of shrinkage-reduction behavior in concrete using expansive additive. Doctoral thesis, the university of Tokyo 2013.

[5.17] M. Morioka, H. Hagiwara, E. Sakai, M. Daimon, Hydration reaction of the calciumsulphoaluminate-type expansive additive. Cement Science and Concrete Technology, No.52 1998 pp 2-7.

[5.18] T. Higuichi, M. Eguchi, M. Morioka, E. Sakai. Hydration and properties of expansive additive treated high temperature carbonation. *Cement and Concrete Research* 64 (2014) pp 11-16.

[5.19] Zh. Y. Rong, K. X. Ming, L. Z. Chen, L. Z. Bao, Z. Qing, D. B. Qin, X. Feng, Influence of triethanolmine on the hydration product of portlandite in cement paste and the mechanism. Cement and Concrete Research 87 (2016) pp 64-76.

[5.11] V. G. Papadakis, Effect of supplementary cementing materials on concrete resistance against carbonation an chloride ingress. Cement and Concrete Research Volume 30, (2000) pp 291-299.

[5.20] F. Young, Sulfate attack, Concrete International 20 (1998) 7.

CHAPTER 6

PREDICTING EXPANSION STRAIN OF EXPANSIVE CONCRETE BASED ON HYDRATION REACTION MODEL

CHAPTER 6 PREDICTING EXPANSION STRAIN OF EXPANSIVE CONCRETE BASED ON HYDRATION REACTION MODEL

6.1 Introduction

In concrete structures, Portland cement is used as a binder that binds the other materials together. The shrinkage of cement caused by the loss of water from the concrete during environmental exposure, leading to cracks in concrete. Because these cracks will directly affect the durability and strength of concrete, minimizing their formation to guarantee the serviceability of concrete structure is essential [6.1-6.2]. To address this problem, the application of the expansive additive is well-known as an effective way to reduce shrinkage and can enhance the density of cement concrete structures [6.3]. Thus, it has been widely applied to many kinds of concrete structures (slab, pavement, etc.) [6.4].

The expansive additive can increase the volume of concrete by the expansion of ettringite and calcium hydroxide generated in cement paste in the hydration process. To model the volumetric change of expansive concrete, Choi et al. [6.5] suggested a method that takes into account the balance between the shrinkage of cement and the expansion of expansive additive. In this modeling, the expansion of EX was modeled by considering an increase in the outermost radius of the EX-particles of the hydration products. The shrinkage of cement was modeled by considering the pore diameter distribution and the thermodynamic equilibrium state of the moisture. Miyazawa [6.6] also reported that the expansion strain of expansive concrete is the balance of the expansion strain of expansive additive and the autogenous shrinkage of cement.

The aim of this chapter is to model the expansion strain of expansive concrete, which also considers the expansion of EX and shrinkage of cement. The expansion of expansive concrete was calculated by considering the production of CH and ettringite in expansive concrete. A parameter that describes the effect of the shrinkage of cement was deduced by considering the relationship between the calculated data and experimental data. Because the model was built for expansive concrete under the unrestrained condition, a coefficient was proposed to find predicted data for expansive concrete under the restrained condition. Figure 6.1 shows a flow chart of this chapter.

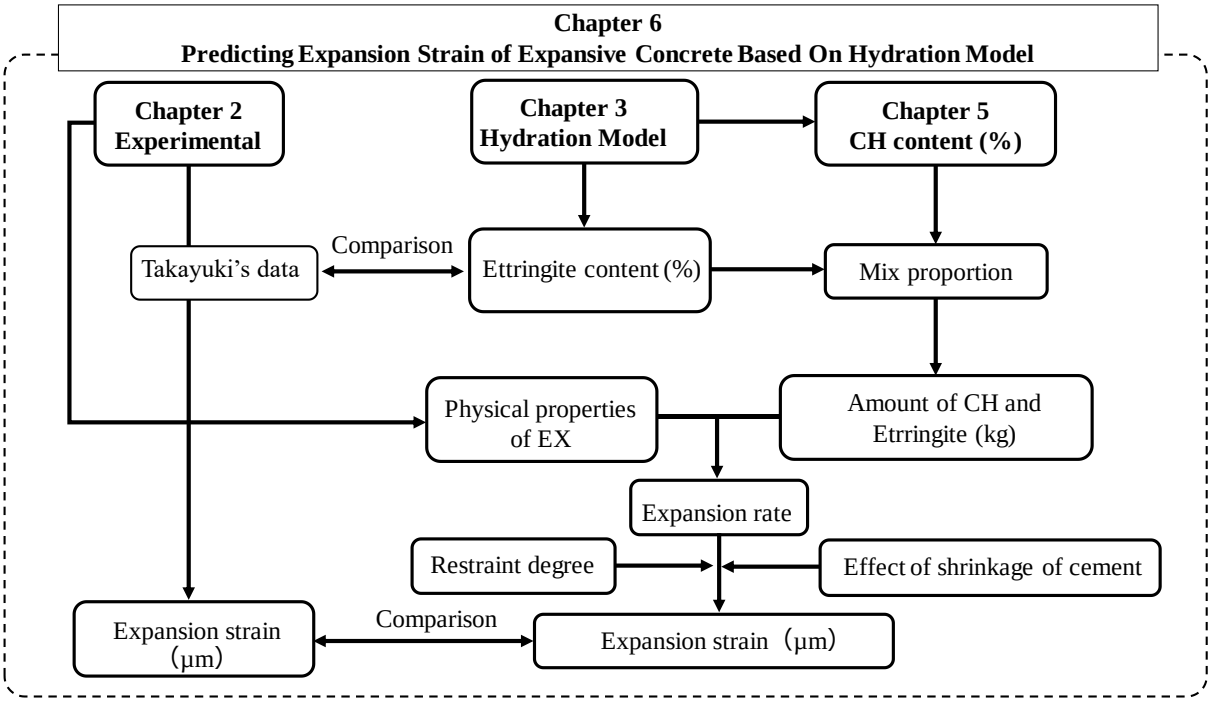

Figure 6.1 Flow chart

6.2 Predicting expansion strain

6.2.1 Production of ettringite

As discussed in Chapter 5 that the hydration products of expansive additive are the CH and ettringite. The reaction of expansive additive with water is described by Eqs. (5.7-5.10) in chapter 5. However, Morioka et al. [6.7] found that the hydration products of expansive additive are not only CH and ettringite but also gypsum ($C\bar{S}H_2$) and monosulfate ($C_4A\bar{S}H_{10}$) using the XRD quantitative analysis. The gypsum was generated from the hydration of anhydrite, as shown in Eq. (6.5). Nagataki et al. [6.8] reported that the ettringite and monosulfate were generated as the SO_3/Al_2O_3 ratio was about 3 and 1, respectively. And in previous research [6.7], the authors explained that the formation of the monosulfate is due to the SO_3/Al_2O_3 ratio was 2.18. It concludes that the formation of the monosulfate depends entirely on the SO_3/Al_2O_3 ratio. In this study, the SO_3/Al_2O_3 ratio is over 3 (see Table 2.1 in Chapter 2), therefore, there is no the monosulfate in the hydration products of EX. Additionally, Higuchi et al. [6.9] also found the C_2S and C_4AF in the composition of EX. For these reasons, the hydration of expansive are shown as follows:

$$C + H \rightarrow CH \quad \text{Eq. (6.1)}$$

$$6CH + C_4A_3\bar{S} + 8CaSO_4 + 90H \rightarrow 3(CaO.Al_2O_3 3.CaSO_4.32H_2O) \quad \text{Eq. (6.2)}$$

$$2C_2S + 4H \rightarrow C_3S_2H_3 + CH \quad \text{Eq. (6.3)}$$

$$C_4AF + 2CH + 10H \rightarrow C_6AFH_{12} \quad \text{Eq. (6.4)}$$

$$C\bar{S} + 2H \rightarrow C\bar{S}H_2 \quad \text{Eq. (6.5)}$$

As shown in Eqs. (6.1-6.5), the reaction of CH, ye'elimite, and anhydrite is related to the formation of ettringite. However, the CH and anhydrite are also involved in other reactions (see Eq. (6.4) and Eq. (6.5). Therefore, in this case, the formation of ettringite is closely related to the hydration of ye'elimite. The other words, the amount of ettringite will be calculated by considering the hydration of ye'elimite based on the hydration reaction of expansive additive. It notes that the ettringite is also produced from the hydration reaction of cement, but produced ettringite will convert to the monosulfate at an early age. Furthermore, Yamamoto et al. [6.10] reported that the formation of CH and ettringite from cement hydration, which was not a role play in the expansion. Therefore, in this study, the ettringite was formed from the hydration of cement, which is not considered as a factor of the expansion of expansive concrete.

Similar to calculating method of CH and CSH content in Chapter 5, the number moles and ettringite content are calculated, as shown in Eq. (6.6) and Eq. (6.7):

$$n_{Ett}^{t} = 3\frac{f_{Ye'el.} \times EX \times \alpha_{EX}}{M_{Ye'el.}} \quad \text{Eq. (6.6)}$$

$$m_{Ett}^{t} = n_{Ett}^{t} \times M_{Ett} \quad \text{Eq. (6.7)}$$

where,

$f_{Ye'el.}$ (%) is the mass fraction of ye'elimite;

α_{EX} is the hydration degree of EX;

EX (kg) is the dosage of EX;

$M_{Ye'el.}$ (g/mol) is the relative formula mass of ye'elimite;

n_{Ett}^{t} (mol) is the moles of ettringite;

m_{Ett}^{t} (g) is the amount of ettringite.

6.2.2 Modeling of expansion strain

To model the expansion strain of expansive concrete, it is important to identify the volume change of concrete. The volume change of concrete is caused by an increase in the formation of CH and ettringite with the time of hydration. In this study, by assuming that the concrete mixed with the expansive additive will be expanded with the directions (x-y-z) under free condition, as described in Figure 6.2. From this assumption, the volume of concrete the expansive additive is

$$V_0 = 1\ (m^3) \qquad \text{Eq. (6.8)}$$

$$V_{0+\alpha} = (1 + 2x)^3 (m^3) \qquad \text{Eq. (6.9)}$$

where,

V_0 and $V_{0+\alpha}$ (m^3) are the volume of concrete at t = 0 and t = α ;

x is the expansion strain (μm).

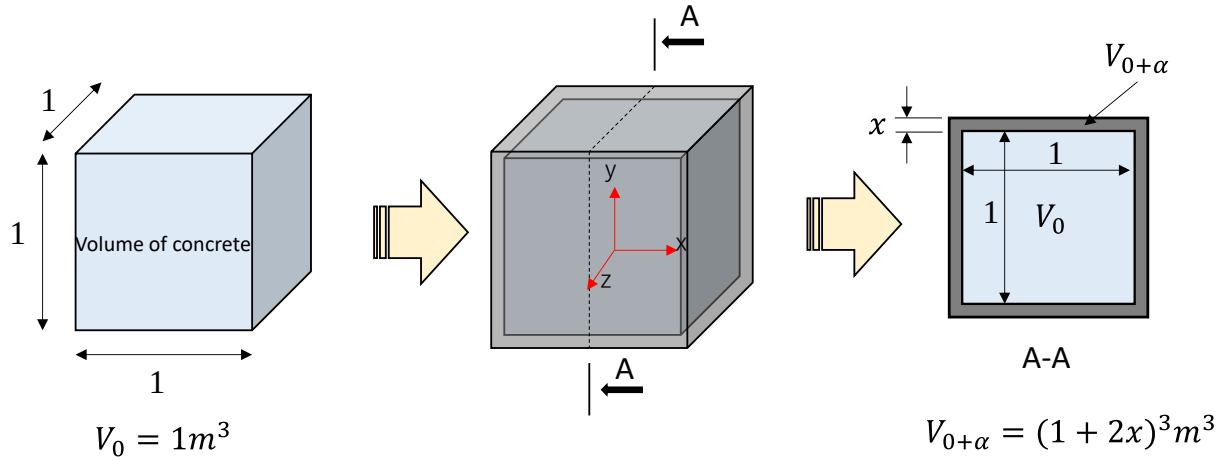

Figure 6.2 Schematic of volumetric change of expansive concrete

The volumetric change of expansive additive is also the volume of CH and ettringite generated in the hardened paste, as indicated in Eq. (6.10)

$$V_{Ettringte+CH} = V_{0+\alpha} - V_0 = (1 + 2x)^3 - 1 \quad \text{Eq. (6.10)}$$

$$V_{Ettringte+CH} = \frac{m_{ettringite}}{\rho_{ettringite}} + \frac{m_{CH}}{\rho_{CH}} \quad \text{Eq. (6.11)}$$

where,

$V_{Ettringte+CH}$ is the volume of etrringite and CH, as described in Eq. (6.11).

$\rho_{ettringite}$ and ρ_{CH} (g/cm^3) are the density of ettringite (1.7 g/cm^3) and CH (2.24 g/m^3).

Thus, expansion strain is

$$x = \frac{\sqrt[3]{V_{Ettringte+CH} + 1} - 1}{2} \quad \text{Eq. (6.12)}$$

In this study, the author is only focusing on the expansion strain of expansive concrete by calculating the volume of CH and ettringite. However, the shrinkage of cement also occurs in expansive concrete. This is discussed in Chapter 1. Therefore, to find a satisfactory value for predicted results, a coefficient is deduced, called β the coefficient of shrinkage effect. The value of β is calculated by considering the relationship between predicted data and the experimental data [6.11]. So, the β can be represented as a function of time. The expansion strain is

$$x = \frac{\sqrt[3]{V_{Ettringte+CH} + 1} - 1}{2} \times \beta \quad \text{Eq. (6.13)}$$

As mentioned above that the present model here is applied for concrete without restrained condition effect. In this study, despite the expansion strain of expansive concrete was measured immediately after the concrete is cast into the mold, the experimental sample was removed from the mold after one day. At the same time, the expansion also begins when EX mixed with cement and water. Therefore, during that one day, the expansive concrete will be affected by the restraint caused by the mold. On the other hand, for expansive concrete, the experimental measurement of expansion strain is performed under restrained conditions according to JIS A 6202 [6.12]. To address this problem, a coefficient that expresses the effect of restrained condition on the expansion strain of expansive concrete is needed, called δ the restraint degree coefficient. The δ coefficient is obtained by comparing the restrained and unrestrained expansion strain, which will be discussed in the next section in detail.

Thus, now the expansion strain is:

$$x = \frac{\sqrt[3]{V_{Ettringte+CH} + 1} - 1}{2} \times \beta \times \delta \quad \text{Eq. (6.14)}$$

6.3 Results and Discussion

6.3.1 Amount of ettringite

To verify the calculating equation of ettringite content, a comparison between the predicted data and measured data was performed, as shown in Figure 6.3. In this Figure, the calculated data was obtained by combining Eq. (6.6) and (6.7), the measured data was obtained by Rietveld analysis of the XRD patterns [6.9]. The figure shows that the calculated and experimental data were in good agreement. It demonstrates that the proposed equation is effective in calculating the ettringite content was generated by the hydration of EX. Furthermore, this also confirms that the hypothesis about the relationship between the content of ettringite generated and the reaction of ye'elimite is correct.

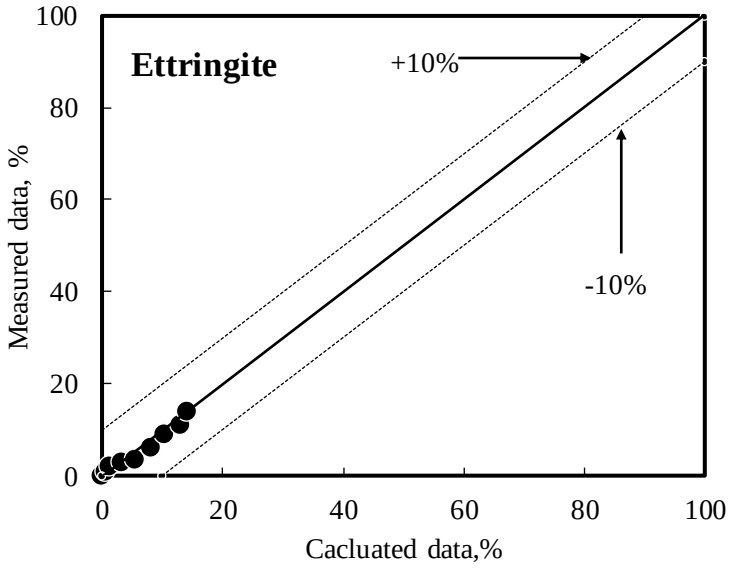

Figure 6.3 Comparison of predicted data and measured data of ettringite content

The actual ettringite is obtained by the mix proportion of concrete (see Chapter 2), as indicated in Figure 6.4. As can be seen, the amount of ettringite in the EX40 sample was higher than that of EX20 at all ages. At 7 days, the ettringite amounts were approximately 2.2 and 5 kg in 1 m^3 of concrete. This may be explained by the dosage of EX used in 1 m^3 of concrete, it means the amount of ettringite increased when the dosage of EX increased. As mentioned above, in this study, the author did not consider the formation of ettringite from the hydration of cement. Therefore, there was only the ettringite amount that was generated by the hydration of EX.

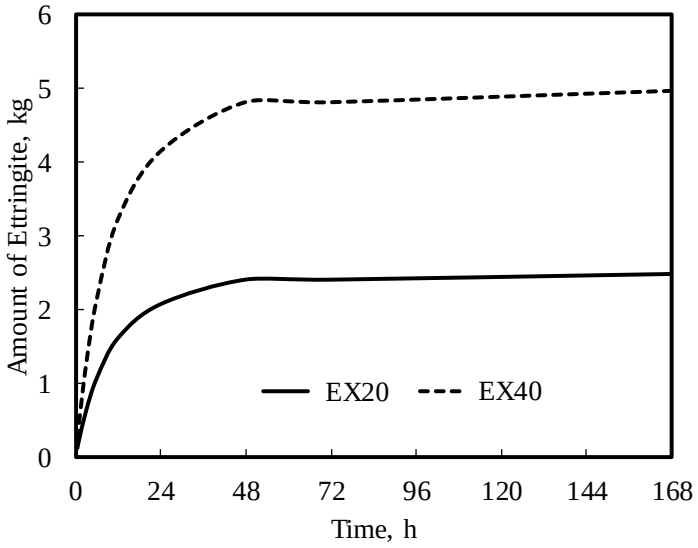

Figure 6.4 Actual amount of ettringite

6.3.2 Verification of prediction equation

The β coefficient was determined by considering the relationship between the experimental results [6.11] and the calculated data from Eq. (6.12). The comparison of experimental results and calculated data is shown in Figure 6.5.

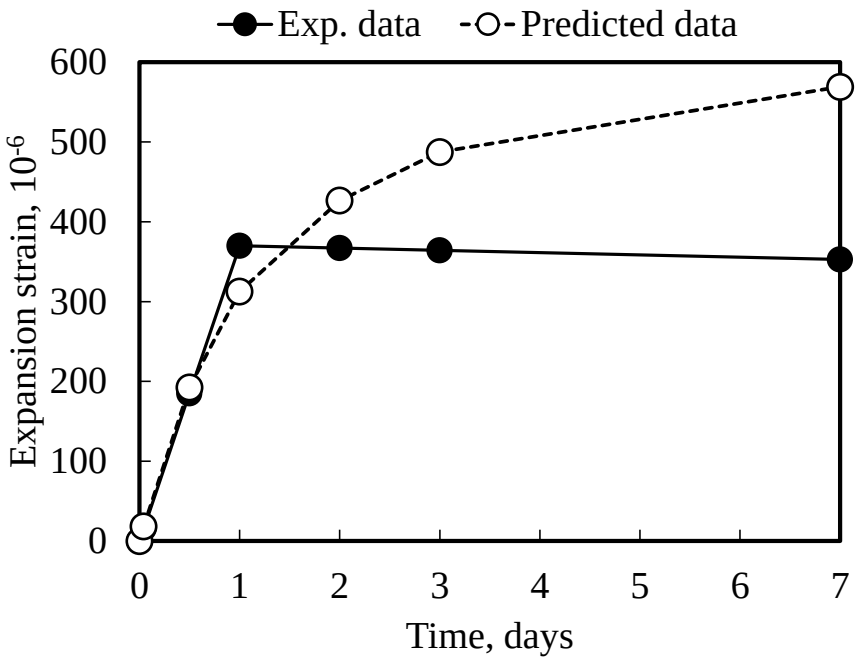

Figure 6.5 Comparison of experimental data [6.11] and calculated data (according to Eq. 6.12).

Figure 6.6 shows the relationship between the value of the β coefficient and time. The β coefficient correlated with the time with a high correlation coefficient of 0.96. Thus, the β coefficient can be represented as a function of time and is given by:

$$\beta = 0.9881e^{-0.067t} \quad (0.6 \leq \beta \leq 1 \text{ and } 0 \leq t \leq 7) \qquad \text{Eq. (6.14)}$$

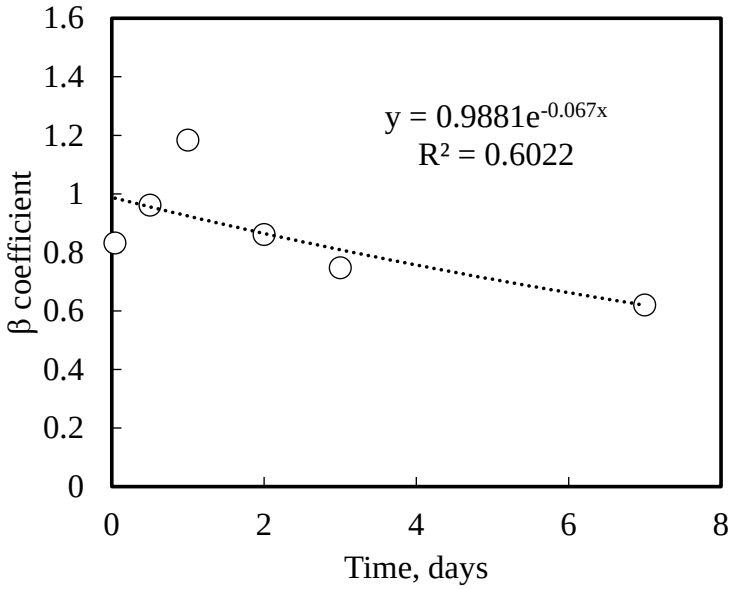

Figure 6.6 Time-dependent β coefficient

While the β was a time-dependent coefficient, δ was a constant. The value of δ coefficient was obtained by comparing the previous results [6.11] and the results of this study (see chapter 2), as shown in Figure 6.7. According to this figure, the value of the δ coefficient was approximately 0.42.

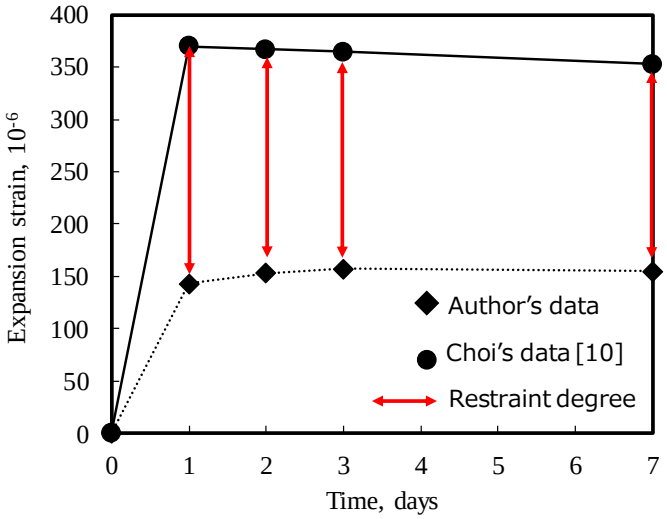

Figure 6.7 Comparison of author's data (under restrained condition) and Choi's data [6.11] (unrestrained condition)

Thus, the expansion strain of expansive additive can be written as follows:

$$x = \frac{\sqrt[3]{V_{Ettringte+CH}+1}-1}{2} \times 0.9881e^{-0.067t} \times 0.42 \ (0 \leq t \leq 7) \qquad \text{Eq. (6.15)}$$

From Eq. (6.15), the expansion strain of expansive concrete under restrained conditions was calculated and compared with measured results (JIS A 6202) as shown in Figure 6.8. The results show that the predicted data was approximately equal to the experimental results. The results reported here demonstrate that the proposed equation is effective and useful in predicting the expansion strain of expansive concrete under the restrained conditions with w/b 0.5 and the dosage of EX is 20 kg/m^3 of concrete. However, the Eq (6.15) was built from fitting the experimental data and model data to obtain the value and time-dependent equation of β and δ is perhaps the biggest limitation to accurately model. Therefore, in the future, in order to address these limitations, a behavior mechanism of cement shrinkage should be proposed to explain the present expansion model of expansive concrete in detail. Furthermore, the experiments of expansive concrete under different restrained conditions need to carry out to find the excellent value of the δ coefficient.

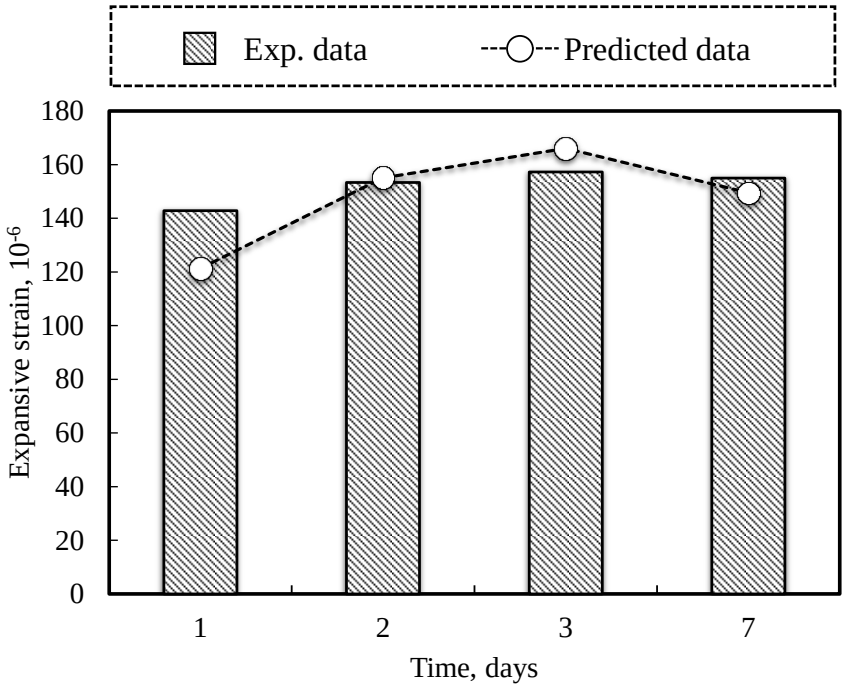

Figure 6.8 Comparison of predicted data and measured data

6.4 Conclusions

A hypothesis supporting the expansion of expansive concrete under free conditions was described. An equation was proposed to predict the expansion strain of expansive concrete under restrained conditions by considering the formation of ettringite from hydration reaction of expansive additive, shrinkage of cement, and restraining factor. Especially, the ettringite was calculated based on the hydration reaction model. A comparison between calculated data and experimental data of expansion strain was performed that showed the agreement. It demonstrates that the proposed equation is useful for predicting the expansion strain of expansive concrete under restraining.

References

[6.1] Architectural Institute of Japan (AIJ), Recommendations for practice of crack control in reinforced concrete buildings (design and construction); 2006.

[6.2] Japan Concrete Institute (JCI), Research committee report on shrinkage of concrete; 2010.

[6.3] Chapter 4-Cement, Building materials in civil engineering. Woodhead publishing series in civil and structural engineering (2011) pp 46-80.

[6.4] J.J. Brooks, Chapter 6-Shrinkage of concrete, Concrete and Masonry Movements (2015) pp 137-185.

[6.5] H. Choi, H. Choi, M. Lim, T. Noguchi, R. Kitagaki, Modeling of volume changes of concrete mixed with expansive additives, Construction and Building Materials 75 (2015), pp 266-274.

[6.6] Shingo Miyazawa, JCI-RILEM International Workshop, Concrack5, April 24-26, 2017, Japan.

[6.7] M. Morioka, H. Hagiwara, E. Sakai, and M. Daimon, Hydration reaction of the calciumsulphoaluminate-type expansive additive. Cement Science and Concrete Technology, No.52,1998.

[6.8] Nagataki S., Gomi H., Expansive admixtures (mainly etrringite), Cement and Concrete Composites, 20, pp 163-170, 1998.

[6.9] T. Higuchi, M. Eguchi, M. Morioka, E. Sakai, Hydration and properties of expansive additive treated high temperature carbonation. Cement and Concrete Research. 64 (2014), pp.11-16.

[6.10] K. Yamamoto, M. Morioka, E. Sakai and M. Daimon, Expansion mechanism of cement added with expansive additive. Concrete Research and Technology, Vol.14, No.3, Sep. 2003.

[6.11] Hyeonggil Choi, A study on the macro prediction of shrinkage-reduction behavior in concrete using expansive additive, Doctoral Thesis, University of Tokyo, 2013.

[6.12] Japanese Industrial Standard Committee. *Expansive additive for concrete (Amendment 1)*, JIS A 6202-2008.

CHAPTER 7

CONCLUSIONS AND FUTURE WORKS

CHAPTER 7 CONCLUSIONS AND FUTURE WORK

7.1 Conclusions

In this study, by using a mathematical equation the hydration reaction of cement pastes containing the expansive additive was modeled. Based on the hydration reaction model, the compressive strength, carbonation depth, and expansion strain of expansive concrete were predicted. In order to verify the model and predicted data, several experiments on the properties and durability of expansive concrete were carried out. Especially, the influence of restrained conditions on these properties was also experimentally investigated in this study. There are some conclusions obtained from the results in this study as follows:

1. Under the restrained condition, the compressive strength, frost resistance, carbonation resistance of expansive concrete was improved. This phenomenon is observed when the dosage of expansive additives used reached about 40 kg/m^3.
2. By considering three processes: Diffusion of water through the protective layer surrounding the particle to the surface of the cement; Penetration and diffusion of water through the blanket of hydration product to the surface of the unreacted core; And the reaction of water with cement or EX at this reaction surface, a numerical model was proposed to simulate the hydration reaction of cement paste containing expansive additive at an early age.
3. The gel/space ratio of cement-EX paste was calculated by considering the hydration of cement and expansive additive based on the hydration reaction model. Using Powers' strength theory, an equation showing the dependence of the compressive strength of expansive concrete on the gel/space ratio of cement-EX paste was proposed with the value of A and n are 253 and 2.69, respectively.
4. The amount of CH and CSH generated from the hydration of cement and EX were calculated based on the hydration reaction model. A mathematical equation describing the carbonation of expansive concrete was proposed to predict the carbonation depth.
5. A hypothesis describing the expansion of concrete containing the expansive concrete was deduced. By considering the balance of expansion of expansive and shrinkage of cement and restraining factor, a mathematical equation was proposed to predict the expansion strain of expansive concrete under restrained conditions.

7.2 Future Works

1. As mentioned in the Introduction chapter, the hydration reaction of cement (or cement-based materials) is related to many properties of concrete, in addition to the properties described in the study, there are also other properties such as pore structure and so on. Therefore, it is interesting to find out the relationship between pore structure and hydration reaction of cement. From there, it is possible to model the pore structure of cement concrete as well as expansive concrete.
2. Regarding the hydration reaction model and predicting carbonation depth, the model parameters were calculated by the last-squared method that is also known as a fitting method. Therefore, to be more persuasive, it is necessary to study and use other methods in calculating the coefficients such as machine learning.
3. One of the important factors that directly affect the quality and durability of concrete is the curing conditions such as temperature and humidity. In this study, the effect of temperature on the hydration of the cement and expansive additive was considered. It is therefore interesting to extend the research to predict the properties of concrete based on the hydration model and take into account the effects of the curing conditions on these properties.
4. Regarding predicting the expansion strain, the effect of shrinkage of cement was investigated by comparison of experimental data and calculated data. Using the hydration reaction model to predict the shrinkage of cement is interesting in the next study. It is essential to find the effect of the w/b ratio on the parameter in order to extend the predicting equation.

ACKNOWLEDGMENTS

I wish to express my sincere appreciation to those who have contributed to this thesis and supported me in one way or the other during this amazing journey.

My deep gratitude goes first to Prof. Yukio Hama, my supervisor for his patience, motivation, caring, and immense knowledge. He has been always there to help, guide me in all the time of research, writing of journal, and this thesis as well. I am very grateful to him for his comments and plans to solve problems encountered in doing research through the Lab's seminars and discussions.

My sincere thanks also go to Assoc. Prof. Hyeonggil Choi who is my co-advisor. The door to Assoc. Prof. Choi's office was always open whenever I ran into a trouble spot or had a hard question not only about my master thesis but also my doctoral thesis. I have always felt motivated to continue solving research problems after having long discussions with him.

My gratitude extends to Dr. Jihoon Kim who has given helpful advice, discussions, suggestions, guidance, and encouragement during the seminar presentations in our laboratory.

Besides my advisor, I would like to thank the rest of my thesis committee: Prof. Mitsuo Mizoguchi, Assoc. Prof. Noriyuki Sugata, Assoc. Prof. Yuya Takase, for their insightful comments, encouragement, and constructive suggestions which have helped me significantly to improve the quality of my research.
A big "Thank you!" also goes out to all the students in my laboratory, who are always willing to help me in the process of doing experiments as well as responsible for organizing activities for the laboratory. Thanks also go to Ms. Matsumura, Mr. Takai, and Ms. Kuroiwa, who were my partner for providing me with unfailing support. In particular, I am grateful to Dr. Kim Junho and Dr. Nguyen Xuan Quy for helping and enlightening me on how to write and review a scientific paper. Without their precious support, it would not be possible to conduct this research.

As an international student, I would like to thank all the members of the Office of the Center for International Relations for their full support not only for me but also for my family to help me achieve my goals. In particular, I must show my gratitude to Mr. Inoya and his family for their whole-hearted support while we are living in Muroran as our friends.

I would also like to thank my Vietnamese friends and all international friends for their friendship and for sharing with me their best wishes. In particular, I am also very grateful to Dr. Tran Vinh Ha in the Nihonshu team who always willing to give me a lot of advice not only in scientific research but also in everyday life.

Last but not the least, I would like to extend my heartfelt thanks and love to my whole family for providing me with unfailing support throughout my years of study and through the process of researching. I am deeply grateful to my parents, my parents in law, and my brother for trusting and encouraging me to achieve my goals in my research career. And finally, I would like to acknowledge the most important persons in my life – my wife, Luong Thi Mui, and my daughter, Nguyen Mai Khanh Vy for always being there for me, encouraging me, and always being my motivation to get through the toughest times during the Ph.D course.

Muroran, March 2021

Nguyen Duc Van